NACA RM L51H16

NACA

RESEARCH MEMORANDUM

INVESTIGATION OF THE EFFECT OF A NACELLE AT VARIOUS CHORDWISE AND VERTICAL POSITIONS ON THE AERODYNAMIC CHARACTERISTICS AT HIGH SUBSONIC SPEEDS OF A 45° SWEPTBACK WING WITH AND WITHOUT A FUSELAGE

By H. Norman Silvers, Thomas J. King, Jr., and
Thomas B. Pasteur, Jr.

Langley Aeronautical Laboratory
Langley Field, Va.

NATIONAL ADVISORY COMMITTEE
FOR AERONAUTICS

WASHINGTON
September 24, 1951

NACA RM L51H16

NATIONAL ADVISORY COMMITTEE FOR AERONAUTICS

RESEARCH MEMORANDUM

INVESTIGATION OF THE EFFECT OF A NACELLE AT VARIOUS CHORDWISE AND VERTICAL POSITIONS ON THE AERODYNAMIC CHARACTERISTICS AT HIGH SUBSONIC SPEEDS OF A 45° SWEPTBACK WING WITH AND WITHOUT A FUSELAGE

By H. Norman Silvers, Thomas J. King, Jr., and
Thomas B. Pasteur, Jr.

SUMMARY

A nacelle was investigated at various chordwise positions and vertical locations on a semispan model of a wing with and without a fuselage through a Mach number range from 0.4 to 0.9. The nacelle was a body of revolution of fineness ratio 5.0 with a modified NACA 65-series profile shape. The investigation was made to determine the interference characteristics between the nacelle and the model and to determine the effect of the fuselage on nacelle interference.

The results showed that the nacelle reduced the drag rise Mach number of the model. The reduction appeared to be due to flow conditions over the nacelle which were in general little affected by changes in interference due to changes in nacelle position. Appreciable reduction in nacelle interference drag accompanied rearward chordwise movement of the nacelle in both an underwing and a symmetrical vertical location below force break. An overwing nacelle location showed increased nacelle interference drag as well as appreciable reductions in drag-rise Mach number. In contrast to the nacelle interference drag coefficient the static-pressure distributions in the nacelle junctures showed that the incremental section pressure drag coefficients increased with rearward chordwise movement of the nacelle and that a rearward movement of the peak minimum pressure in the nacelle junctures accompanied rearward movement of the nacelle.

The nacelle reduced the lift-curve slope of the wing-fuselage model with the largest reductions occurring for the rearward chordwise position of the nacelle. The nacelle produced an increase, however, in the lift-curve slope of the wing alone. In addition to giving evidence of appreciable effects on the stability of the model at the higher lift

coefficients, the various nacelle positions showed that forward chordwise locations in either an underwing or a symmetrical vertical position produced a destabilizing change in the aerodynamic-center location of the model at a low lift coefficient; whereas a stabilizing change was obtained with rearward nacelle locations. Stabilizing changes were, however, evident for both forward and rearward nacelle locations in an overwing position.

Although the addition of the fuselage resulted in reductions in the drag break Mach numbers of the model with nacelle, it appeared to have only negligible effect on the interference drag coefficients in this speed range. Below force break the fuselage had little effect on nacelle interference drag coefficients. The fuselage was responsible for abrupt changes in the aerodynamic-center locations, lift-curve slopes, and angles of zero lift at force break.

INTRODUCTION

It has been shown (references 1 and 2) that combining a swept wing with fuselages and engine housings can result in interference phenomenon that tend to destroy the advantages of the swept wing. As a part of a general program of research at transonic speeds, the National Advisory Committee for Aeronautics is conducting investigations to develop engine nacelles for use on aircraft employing swept wings. As a phase of this program, the present paper presents results obtained from an investigation conducted at high subsonic speeds to determine the effect of a nacelle-like body of revolution at several chordwise and vertical positions and one spanwise location on the aerodynamic characteristics of a 45° sweptback wing alone and of the wing combined with a fuselage. The results include measurements of lift, drag, and pitching moments and static-pressure measurements at two spanwise stations on the wing corresponding to the inboard and outboard junctures of the wing with the nacelle.

SYMBOLS

C_L lift coefficient (Twice semispan lift/qS)

C_D drag coefficient (Twice semispan drag/qS)

C_{D_I} interference drag coefficient $\left[C_{D_{model+nacelle}} - \left(C_{D_{model}} + 2C_{D_{nacelle}}\right)\right]$

C_m pitching-moment coefficient referred to $0.25\bar{c}$ of wing and $0.635l$ of nacelle, which corresponds to a nacelle location of $\frac{x_c}{c} = -0.40$ on the wing (Twice semispan pitching moment/$qS\bar{c}$)

c_n section normal-force coefficient (Section normal force/qc)

c_c section chord-force coefficient (Section chord force/qc)

c_d section pressure-drag coefficient ($c_c \cos \alpha + c_n \sin \alpha$)

P pressure coefficient $\left(\frac{p_l - p}{q}\right)$

q free-stream dynamic pressure, pounds per square foot $\left(\frac{1}{2}\rho V^2\right)$

p free-stream static pressure, pounds per square foot

S twice wing area of semispan model, 2.356 square feet

$\bar{c}$ mean aerodynamic chord of wing, 0.640 foot, $\left(\frac{2}{S}\int_0^{b/2} c^2 dy \text{(using the theoretical tip)}\right)$

c local wing chord, feet

b twice span of semispan model, 3.76 feet

d diameter, feet

x longitudinal distance from local-chord leading edge (positive rearward), feet

l length of body of revolution, inches

y perpendicular distance from plane of symmetry along semispan, feet

z perpendicular distance from wing-chord plane to nacelle center line (positive upward), feet

V free-stream air velocity, feet per second

a free-stream velocity of sound, feet per second

M free-stream Mach number (V/a)

M_B drag-break Mach number, free-stream Mach number at which $\frac{\partial C_D}{\partial M} = 0.10$

ρ mass density of air, slugs per cubic foot

α angle of attack, degrees

α_o angle of attack at zero lift, degrees

$$C_{L_\alpha} = \left(\frac{\partial C_L}{\partial \alpha}\right)_M$$

$$C_{m_{C_L}} = \left(\frac{\partial C_m}{\partial C_L}\right)_M$$

$$C_{L_{n_\alpha}} = \left(\frac{\partial C_{L_n}}{\partial \alpha}\right)_M$$

$$C_{m_{n_\alpha}} = \left(\frac{\partial C_{m_n}}{\partial \alpha}\right)_M$$

Subscripts:

c denotes chordwise distance of local-chord leading edge to nacelle leading edge, positive rearward

p denotes chordwise location of peak minimum pressure

f fuselage

n nacelle

M at constant Mach number

cr critical

l denotes local condition

MODELS AND APPARATUS

Basic Wing and Fuselage Models

The investigation was conducted in the Langley high-speed 7- by 10-foot tunnel with a semispan model of a wing swept back 45° with respect to the quarter-chord line and a fuselage. The wing had an aspect ratio of 6 and taper ratio of 0.6. The airfoil sections were NACA 65A009 profiles parallel to the free air stream. The wing was constructed of a steel spar covered with a bismuth-tin alloy. Two spanwise rows of static-pressure orifices were located in the upper and lower surfaces of the wing in planes that were parallel to the plane of symmetry of the model and in such a spanwise position as to be near the junctures of wing and nacelle (fig. 1). Chordwise locations of the pressure orifices are presented in table I.

The fuselage was half a body of revolution of actual fineness ratio 10 (basic fineness ratio 12) and was constructed of mahogany. Ordinates of the fuselage are presented in table II. A drawing of the wing-fuselage showing the various test locations of the nacelle is presented in figure 1.

Nacelle Model

The nacelle was a body of revolution designed to simulate a housing for a single jet power unit. The size of the nacelle relative to the size of the model was established by considering the model to be a scale model of a bomber-type airplane. The nacelle was constructed of mahogany and had a fineness ratio of 5. The nacelle profile (table III) was a modified NACA 65 series airfoil section. The modification consisted of replacing the trailing-edge cusp with a straight line that was tangent to the model profile and passed through the trailing edge.

No attempt was made in this investigation to provide fairings for the junctures of the wing and the nacelle at any of the various vertical and chordwise locations.

Wing-Fuselage Test Installation

The semispan model was suspended from the mechanical-balance system of the tunnel by a support member that extended through the tunnel ceiling. Air flow into the flow field of the model from outside of the tunnel was minimized by maintaining a gap of about 1/16 inch between the model support and the tunnel ceiling. Photographs showing the model mounted in the tunnel are presented in figure 2.

Nacelle Test Installation

The isolated nacelle was investigated on a reflection-plane plate that was located 3 inches from the tunnel wall to bypass the wall boundary layer. Force data were obtained on a half model of the nacelle and static-pressure measurements were obtained on a whole body of revolution that was located away from the reflection-plane plate by a thin support strut. Photographs of the half nacelle and the whole nacelle mounted on the reflection-plane plate are presented in figures 3 and 4. Figure 5 is a drawing showing the nacelle models mounted on the reflection-plane plate.

Force measurements on the half nacelle were made by an electrical strain-gage balance system located outside the tunnel. The balance was enclosed in a sealed container to minimize air flow into the flow field of the model. Angle-of-attack changes were accomplished by a conventional geared drive system actuated by a small electric motor. The whole nacelle had pressure orifices located along the upper surface of the model. For this setup, angle-of-attack changes were accomplished by a manual rotation of the model and support strut.

TESTS

Force measurements of lift, drag, and pitching moments were obtained on the wing-fuselage model alone and with the nacelle located in four chordwise positions in both an underwing and a symmetrical vertical location over an angle-of-attack range that usually extended from -0.8° to 11.3°. Some data are also given for an overwing location of the nacelle. These data were obtained by extending the negative angle-of-attack range of the underwing nacelle and presenting these data as results obtained on an overwing nacelle. Force data were also obtained on the wing alone and with the nacelle in three chordwise positions in the underwing vertical location on the wing. The test Mach number range for this investigation extended from $M = 0.4$ to $M = 0.9$. The variation of the mean test Reynolds number over this range of Mach numbers is presented in figure 6.

Static-pressure measurements at spanwise stations on the wing corresponding to the inboard and outboard junctures of the wing and nacelle were obtained simultaneously with force measurements at angles of attack of 1.3°, 5.3°, and 9.3° and at Mach numbers of 0.4, 0.7, 0.8, and 0.9, for the wing-fuselage model alone and with the nacelle in four chordwise positions in both an underwing and a symmetrical vertical location.

Lift, drag, and pitching moments were also obtained on the nacelle alone over an angle-of-attack range from -0.7° to 11.3° and a Mach number range from 0.41 to 0.96. Static-pressure measurements over the nacelle were obtained at angles of attack of ±5.3° and 0° and at Mach numbers of 0.42, 0.73, 0.81, and 0.86.

CORRECTIONS

Jet-boundary corrections to the angle of attack and drag coefficient of the basic wing and wing-fuselage models were determined by the method of reference 3 and computed by the following equations:

$$\alpha = \alpha_M + 0.124C_L$$

$$C_D = C_{D_M} + 0.0022C_L^2$$

where the subscript M denotes measured values. The jet-boundary corrections to the pitching-moment coefficient were considered negligible and therefore were not applied.

The drag has been corrected for the horizontal bouyancy produced by the longitudinal static-pressure gradient in the tunnel. The drag of the wing-fuselage configurations presented herein includes the drag due to base pressure acting on the fuselage.

Corrections have been added to the dynamic pressure and the Mach number to account for the blockage effect of the model. The corrections were determined by the method of reference 4.

PRESENTATION OF RESULTS

An outline of the figures presenting the results of this investigation is given below:

Figure

DISCUSSION

FORCE DATA

The results obtained for the basic rodels, that is, the wing-fuselage combination and the wing alone, are presented for better comparison on the figures summarizing the results obtained with the nacelle in place. For the most part, discussion of the results for the basic model will be confined to those points necessary to illustrate nacelle effects.

It is to be recognized that reflection effects, particularly in connection with drag, can have an appreciable influence on the absolute values of coefficients. Comparison of unpublished results of a change in drag due to a nacelle in an intermediate spanwise location such as that utilized in this investigation have shown, however, good agreement between results obtained on a semispan model and a three-dimensional model.

Wing-Fuselage with Nacelle

Drag.- It is usually found that when a nacelle is added to the wing of a model the principal change in aerodynamic characteristics of the model is an increase in drag that is frequently larger than the drag contributions of the individual members of the system. The nacelle is also usually found to reduce the Mach number at which drag rise of the model occurs. These effects due to interference seem to exist for the test model (fig. 15). Although the effect of interference on the increment in drag due to the nacelle will be more fully discussed in a following section, it can be seen from these data that the drag due to the nacelle is considerably higher at 0.3 lift coefficient than at zero. Nacelle chordwise position is also seen to have an appreciable effect on the drag due to the nacelle.

As expected, the nacelle reduces the Mach number for drag rise. It is significant to note that with the exception of the forward-located overwing nacelle the reduction in drag-break Mach number appears to be essentially the same for all positions of the nacelle at both lift coefficients presented. To better illustrate the effect of lift coefficient on drag-break Mach number, figure 16 is presented which shows M_B, defined as that Mach number where $\frac{\partial C_D}{\partial M} = 0.1$, as a function of lift coefficient. The values of M_B and, as will be shown later, values of nacelle-interference drag coefficients are presented over a lift-coefficient range of 0 to 0.4 in an effort to show the effect of the various nacelle positions for the range of lift coefficients usually encountered in high-speed flight. It is apparent that with the

previously stated exception, the maximum change in M_B is about 0.05. It might be expected, however, that interference effects which result in appreciable changes in the drag due to the nacelle at various lift coefficients and chordwise locations might result in considerably larger changes in M_B than indicated by these data. By inspection, the drag rise of the isolated nacelle is found to occur at about 0.88 Mach number, which is seen (fig. 15) to be very nearly the same as the Mach number for drag rise of the model with nacelle. It appears then that the attainment of critical-flow conditions over the nacelle has, in this investigation, established a limit to the drag-rise Mach number of the model, and that, because of these characteristics of the nacelle changes in nacelle chordwise location, have relatively little effect on M_B.

It is seen, however, (figs. 15 and 16) that, when the nacelle is located in such a chordwise position $\left(\frac{x_c}{c} = -0.4\right)$ in the overwing location as to impinge on the high local velocity field generated at the higher lift coefficients over the upper surface of the wing, a considerably larger reduction in M_B occurs and also large increases in drag coefficient.

These results illustrate the penalties in performance that can be expected when a low-fineness-ratio, low-critical-speed nacelle is utilized at high subsonic speeds.

Changes in both the chordwise location and vertical position of the nacelle produce changes in the drag coefficients of the model. To better illustrate these effects, the drag increments (herein called interference drag coefficients) obtained by a subtraction of the drag coefficients of the basic model and the isolated nacelle from the model with nacelle are presented in figure 18 as a function of nacelle chordwise position for zero lift coefficient and 0.3 lift coefficient of the model. This interference drag coefficient is equivalent to that obtained on a complete model with two nacelles. These results show that a general reduction in interference drag coefficient accompanies a rearward movement of the nacelle in both an underwing and a symmetrical vertical location. Up to the drag-break Mach number which occurs between Mach numbers of 0.8 and 0.9 the effect of Mach number is small. Lift coefficient exerts a marked influence on C_{D_I}. In general, the interference drag is considerably higher at a lift coefficient of 0.3 than at 0. It can be seen (fig. 17) that this trend is representative of the changes in C_{D_I} that occur over the lift-coefficient range investigated.

In order to establish a quantitative basis of comparison for the interference effects of the nacelle positions investigated, the interference drag coefficients (fig. 18) are referred to the drag of the isolated

nacelle (fig. 9) and the results are presented as a function of nacelle position for the underwing and symmetrical nacelle positions at a lift coefficient of 0.3 (fig. 19). These results show that the reduction in C_{D_I} at subcritical Mach numbers, due to rearward movement of the nacelle, is of the order of two to three times the drag of the isolated nacelle.

Angle of zero lift.- The effects of nacelle chordwise position on the angle of zero lift are presented in figure 20(a), from which it is seen that forward nacelle positions result in a positive change in the angle of zero lift for the underwing nacelle while rearward positions result in a negative change. In the overwing location an opposite effect exists; that is, a forward nacelle position gives a negative change in α_o while a rearward nacelle position gives a positive change. The maximum change in α_o due to changes in nacelle chordwise position is fairly constant up to Mach numbers of about 0.88 and is of the order of 1°. A rapid negative change in the angle of zero lift occurs at Mach numbers higher than about 0.88 which it will be remembered is the Mach number for drag rise. The change seems to be the least severe for the rearward nacelle locations.

It is seen that the angles of zero lift for the symmetrical nacelle are not exactly zero. The small departures from zero shown in these data are representative of the accuracy involved in the determination of α_o from data obtained on the semispan mounting used for this investigation.

Lift-curve slope.- The nacelle generally reduces the lift-curve slope of the basic model (fig. 20(b)). The maximum reduction in C_{L_α} for any vertical nacelle location is about 10 percent and, although the effects of changes in nacelle chordwise position are somewhat inconsistent, occurs for the rearward nacelle positions. For the most part, forward nacelle positions produce smaller reductions in C_{L_α}. Abrupt changes in magnitude of the lift-curve slope develop at the higher Mach numbers for most chordwise locations of the underwing and the symmetrical nacelle. These variations appear to be erratic in regard to the Mach number for the onset of the changes for each nacelle location as well as in the nature of the variation after the break has been reached. The lift-curve slopes of the model with the overwing nacelle, however, show no such rapid changes in C_{L_α} to the highest Mach numbers investigated.

Pitching moment.- Examination of the pitching-moment coefficient of the wing-fuselage model with the nacelle in various locations (figs. 10 to 12) shows that the nacelle has considerable influence on the pitching-moment characteristics. At the higher lift coefficients, the forward nacelle locations in both the underwing and symmetrical vertical positions

generally exert a stabilizing influence on the basic model throughout the Mach number range. Rearward nacelle locations show some effect of vertical position in that the underwing positions of the nacelle influences the stability of the basic model only at low Mach numbers, where the effect is destabilizing, and a symmetrical position of a rearward located nacelle appears to change the stability of the basic model only at the higher Mach numbers. The rearward nacelle, however, also produces a destabilizing effect on the basic model in this vertical position.

It should be noted that pitching-moment characteristics of the model with overwing positions of the nacelle were obtained at the higher lift coefficients only at the lower Mach numbers. Although an overwing position of the nacelle generally exerts a stabilizing influence on the model at these lift coefficients, changes in nacelle chordwise location in the two locations investigated in the overwing position have (fig. 12) little effect on the stability of the model.

The slope of the pitching-moment coefficient as a function of lift coefficient which is an indication of the aerodynamic-center location relative to the quarter-chord point of the mean aerodynamic chord is presented in figure 20(c) as a function of Mach number. Slopes were measured generally at a lift coefficient of 0.1. The results show that a rather abrupt stabilizing movement of the aerodynamic-center exists for the underwing and symmetrical nacelles at the higher Mach numbers. In these vertical locations, forward chordwise nacelle positions exert a destabilizing influence and rearward chordwise positions produce a stabilizing effect on the model. Comparison of the slopes of the pitching-moment curves for the underwing and the overwing nacelle shows very similar trends although the variations in $C_{m_{C_L}}$ appear to be somewhat less consistent for the various chordwise locations of the overwing nacelle at the higher Mach numbers.

Thus, it appears that in assessing the over-all aerodynamic merits of nacelles located on models, it is of particular interest to examine the slopes of the pitching-moment curves. As has been seen, a rearward location of the underwing nacelle, which gave promising interference drag characteristics, also gave appreciable changes in the stability of the model. Characteristics such as these appear to warrant consideration before accepting such a nacelle location on the basis of drag studies alone.

Wing with Nacelle

Drag.- It is of interest to compare the results obtained for the wing-fuselage combination with those of the wing alone to determine the

extent to which the fuselage influences the interference characteristics of the nacelles. The total drag coefficients (figs. 15 and 21) show that additions of the fuselage aggravates the rise of drag at force break and results in slightly lower drag-break Mach numbers (defined herein as $\frac{\partial C_D}{\partial M} = 0.1$) than were obtained for the wing alone. Drag-break Mach numbers are, in fact, slightly higher in some instances than the highest test Mach number (M = 0.9) and hence could not be quantitatively determined.

For better comparison of the effect of the fuselage on the nacelle interference drag coefficient, figure 22 is presented. This figure shows C_{D_I} for comparable chordwise locations of the underwing nacelle on the wing-fuselage and on the wing alone as a function of Mach number for representative lift coefficients of 0 and 0.3. A more complete indication of the effect of lift coefficient and nacelle chordwise location on the change in C_{D_I} due to the fuselage can be obtained by comparison of the results shown in figures 23, 24, and 25 for the wing alone with those of figures 17, 18, and 19 for the wing fuselage.

It is seen (fig. 22) that throughout a large part of the Mach number range investigated the fuselage has little effect on the nacelle interference drag coefficient. The largest apparent effect of the fuselage is seen to exist at the lowest test Mach number where the least accuracy of data was obtained and at the highest test Mach numbers. The effect of the fuselage in the high Mach number range, however, appears to be somewhat smaller than might be anticipated in view of the fuselage-induced increases in the rate of rise of the total drag coefficient and, as will be shown later, increases in the rate of change of the lift- and pitching-moment-curve slopes with Mach numbers.

Angle of zero lift.- The fuselage has little effect on the angle-of-zero-lift variations for the forward chordwise position of the nacelle (figs. 20(a) and 26) but seems to produce a negative change in α_o of about 0.5° at the lower Mach numbers with the rearward nacelle. The fuselage also increases the rapidity of the change in α_o at the break although the onset of the break was delayed to higher Mach numbers with the fuselage in place.

Lift-curve slope.- A comparison of the lift-curve slopes of the wing with nacelle (fig. 26) with those of wing-fuselage with nacelle (fig. 20(b)) shows that on the wing the nacelle increases the lift-curve slope whereas, as previously indicated, for the wing-fuselage combination the nacelle reduces the lift-curve slope. It is felt that the apparent effect of the fuselage on the nacelle increments of this parameter may be unduly affected by the small amount of leakage present during the investigation around the root chord of the semispan model.

The rapid changes in C_{L_α} discussed previously for the wing-fuselage combination appear also to be due to the fuselage since the lift curves of the wing with the nacelle in several chordwise locations show smooth variations to the highest test Mach numbers.

Pitching moment.- The effects of the nacelle at various chordwise locations on the pitching-moment characteristics of the wing alone are similar to those previously discussed for the wing-fuselage model. It is to be noted that, for the wing alone, removal of the strong stabilizing influence of the fuselage, combined with the destabilizing effect of the rearward-located nacelle, results in an appreciable destabilizing break in the pitching-moment curves at the higher Mach numbers and lift coefficients.

It is also seen (figs. 20(c) and 26) that the fuselage is responsible for the abrupt stabilizing break in the variation of $C_{m_{C_L}}$ after force break. The erratic variations in $C_{m_{C_L}}$ for the rearward nacelle position on the wing-fuselage combination (fig. 20(c)) are not present on the wing alone. In fact, the variation in aerodynamic-center location for this nacelle position on the wing alone is less than 1.5 percent of the mean aerodynamic chord throughout the Mach number range investigated.

PRESSURE DATA

As might be anticipated, vertical displacement of the nacelle from the underwing to the symmetrical locations (figs. 29 and 30) in any chordwise position generally results in an increase in pressure coefficients of the upper-surface nacelle junctures and a reduction in the lower-surface juncture pressures. The results show that regions of critical pressure develop in the inboard juncture at the wing leading edge with the nacelle in the forward position. Rearward movement of the nacelle results in a rearward movement and diminution of the peak pressures and in the development of somewhat lower peak pressures in the outboard nacelle juncture. To illustrate the influence of the nacelle chordwise position on the location of the peak minimum pressure, figure 31 is presented for a representative angle of attack of 5.3°.

Consideration of the pressure coefficients on the wing of the basic wing-fuselage combination (fig. 27) and the isolated nacelle (fig. 28) shows that attainment of sonic flow in the nacelle junctures (figs. 29 and 30) at Mach numbers between 0.7 and 0.8 is due largely to the high pressure coefficients generated over the nacelle. This condition, however, does not lead to well-established compression shock in the junctures until a Mach number of 0.9 which is approximately drag-rise Mach number ($M_B = 0.88$).

Below force-break Mach numbers, a large variation in the nacelle interference drag coefficient has been shown to exist with change in nacelle chordwise position. To analyze this effect it will be helpful to examine the increment in section pressure-drag coefficient in the nacelle junctures (fig. 32). It should be emphasized that the component of drag is due to surface pressures and does not include the effects of viscosity except as viscosity affects the surface pressure distribution. The results show that forward nacelle positions give negative increments in section pressure-drag coefficient in the inboard juncture and that the increment increases positively with rearward nacelle movement. These results are, of course, not surprising because of the formation and movement of the peak pressures with nacelle positions, but it does demonstrate quantitatively the relative magnitudes of the changes in the pressure coefficients involved. Accordingly, the growth and rearward movement of the peak pressures in the outboard junctures beginning at $\frac{x_c}{c} = -0.4$ also result in a positive increase of incremental section pressure drag coefficient. Thus, it is obvious that the general reductions in interference drag coefficients that have been shown to accompany rearward movement of the nacelle are not due directly to changes in shape of the static-pressure distribution in the nacelle junctures. It is also obvious then that there are other effects which compensate for the changes in incremental section pressure drag in the nacelle junctures. These effects may include pressure changes over sections of the wing other than the junctures and changes in the viscous contribution to the nacelle interference drag coefficient. If the effects of viscosity prove to be significant, Reynolds number may also have a significant bearing on the drag characteristics indicated by this investigation.

CONCLUSIONS

The results of an investigation of the effect of a nacelle at various chordwise and vertical positions on the aerodynamic characteristics of a 45° sweptback wing combined with a fuselage over a Mach number range from 0.4 to 0.9 and a Reynolds number range from about 1.5×10^6 to 2.5×10^6 indicate the following conclusions:

1. The nacelle reduced the drag-rise Mach number of the model. The reduction appeared to be due to flow conditions over the nacelle which were in general little affected by changes in interference due to changes in nacelle position.

2. An appreciable reduction in nacelle interference drag accompanied rearward chordwise movement of the nacelle in both an underwing and a symmetrical vertical location below force break. An overwing location of the nacelle showed increased nacelle interference drag as well as appreciable reductions in drag-rise Mach number.

3. In contrast to the nacelle interference drag coefficient the static-pressure distributions in the nacelle junctures showed that the incremental section pressure-drag coefficient increased with rearward chordwise movement of the nacelle and that a rearward movement of the peak minimum pressure in the nacelle junctures accompanied rearward movement of the nacelle. It was obvious then that there are other effects which compensate for the changes in incremental section pressure drag coefficients in the nacelle junctures.

4. The nacelle reduced the lift-curve slope of the wing-fuselage model with the largest reductions occurring for the rearward chordwise position of the nacelle. The nacelle produced an increase, however, in the lift-curve slope of the wing alone.

5. In addition to giving evidence of appreciable effects on the stability of the model at the higher lift coefficients, the various nacelle positions showed that forward chordwise locations in either an underwing or a symmetrical vertical position produced a destabilizing change in the aerodynamic-center location of the model at a low lift coefficient and a stabilizing change was obtained with rearward nacelle locations. Stabilizing changes were, however, evident for both forward and rearward nacelle locations in an overwing position.

6. Although the addition of the fuselage resulted in reductions in the drag-break Mach numbers of the model with nacelle, it appeared to have only negligible effect on the interference drag coefficients in this speed range. Below force break the fuselage also had little effect on nacelle interference drag coefficients. The fuselage was, however, responsible for abrupt changes in the aerodynamic-center locations, lift-curve slopes, and angles of zero lift at force break.

Langley Aeronautical Laboratory
National Advisory Committee for Aeronautics
Langley Field, Va.

REFERENCES

1. Hieser, Gerald, and Whitcomb, Charles F.: Investigation of the Effects of a Nacelle on the Aerodynamic Characteristics of a Swept Wing and the Effects of Sweep on a Wing Alone. NACA TN 1709, 1948.

2. Boltz, Frederick W., and Beam, Benjamin H.: The Effects of Compressibility on the Pressures on a Body of Revolution and on the Aerodynamic Characteristics of a Wing-Nacelle Combination Consisting of the Body of Revolution Mounted on A Swept-Back Wing. NACA RM A50E09, 1950.

3. Gillis, Clarence L., Polhamus, Edward C., and Gray, Joseph L., Jr.: Charts for Determining Jet-Boundary Corrections for Complete Models in 7- by 10-Foot Closed Rectangular Wind Tunnels. NACA ARR L5G31, 1945.

4. Herriot, John G.: Blockage Corrections for Three-Dimensional-Flow Closed-Throat Wind Tunnels, with Consideration of the Effect of Compressibility. NACA Rep. 995, 1950. (Formerly NACA RM A7B28.)

TABLE I.- WING PRESSURE ORIFICE LOCATIONS

[Percent local chord]

Inboard juncture		Outboard juncture	
Upper surface	Lower surface	Upper surface	Lower surface
0	0	0	0
10	5	10	5
20	10	20	10
31	15	31	15
43	20	43	20
50	25	50	25
59	31	58	31
69	43	69	43
80	50	80	50
90	55	90	55
	59		58
	65		65
	69		69
	75		75
	80		80
	90		90

NACA

TABLE II.- FUSELAGE ORDINATES

[Basic fineness ratio 12; actual fineness ratio 10 achieved by cutting off rear one-sixth of body; $\bar{c}/4$ located at $l_f/2$]

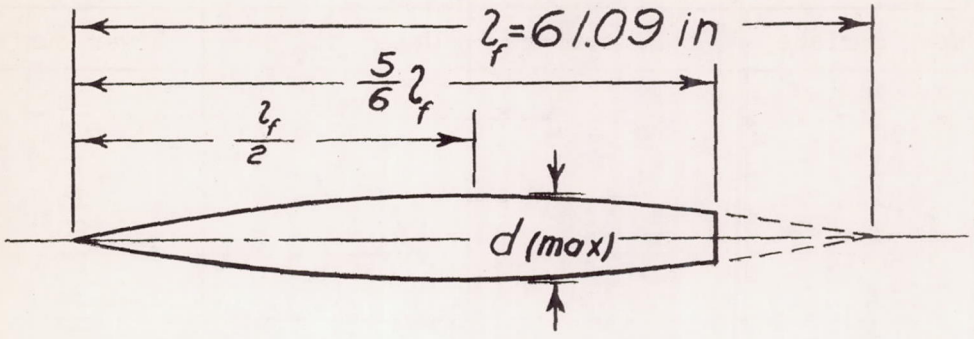

Ordinates, percent length			
Station	Radius	Station	Radius
0	0	45.0	4.143
.5	.231	50.0	4.167
.75	.298	55.0	4.130
1.25	.428	60.0	4.024
2.5	.722	65.0	3.842
5.0	1.205	70.0	3.562
7.5	1.613	75.0	3.128
10.0	1.971	80.0	2.526
15.0	2.593	83.33	2.083
20.0	3.090	85.0	1.852
25.0	3.465	90.0	1.125
30.0	3.741	95.0	.439
35.0	3.933	100.0	0
40.0	4.063		
L.E. radius = 0.05			

NACA

TABLE III.- NACELLE ORDINATES

[Fineness ratio 5]

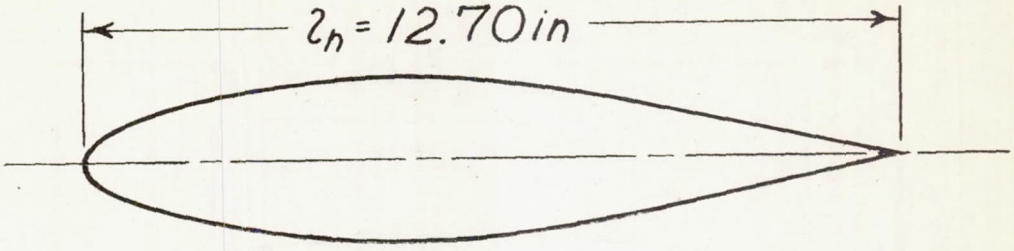

Ordinates, percent length			
Station	Radius	Station	Radius
0	0	40.0	9.997
.5	1.539	45.0	9.917
.75	1.849	50.0	9.597
1.25	2.312	55.0	9.022
2.5	3.126	60.0	8.240
5.0	4.344	65.0	7.275
7.5	5.288	70.0	6.237
10.0	6.080	75.0	5.197
15.0	7.338	80.0	4.157
20.0	8.293	85.0	3.119
25.0	9.012	90.0	2.078
30.0	9.529	95.0	1.039
35.0	9.855	100.0	0
L.E. radius = 1.00			

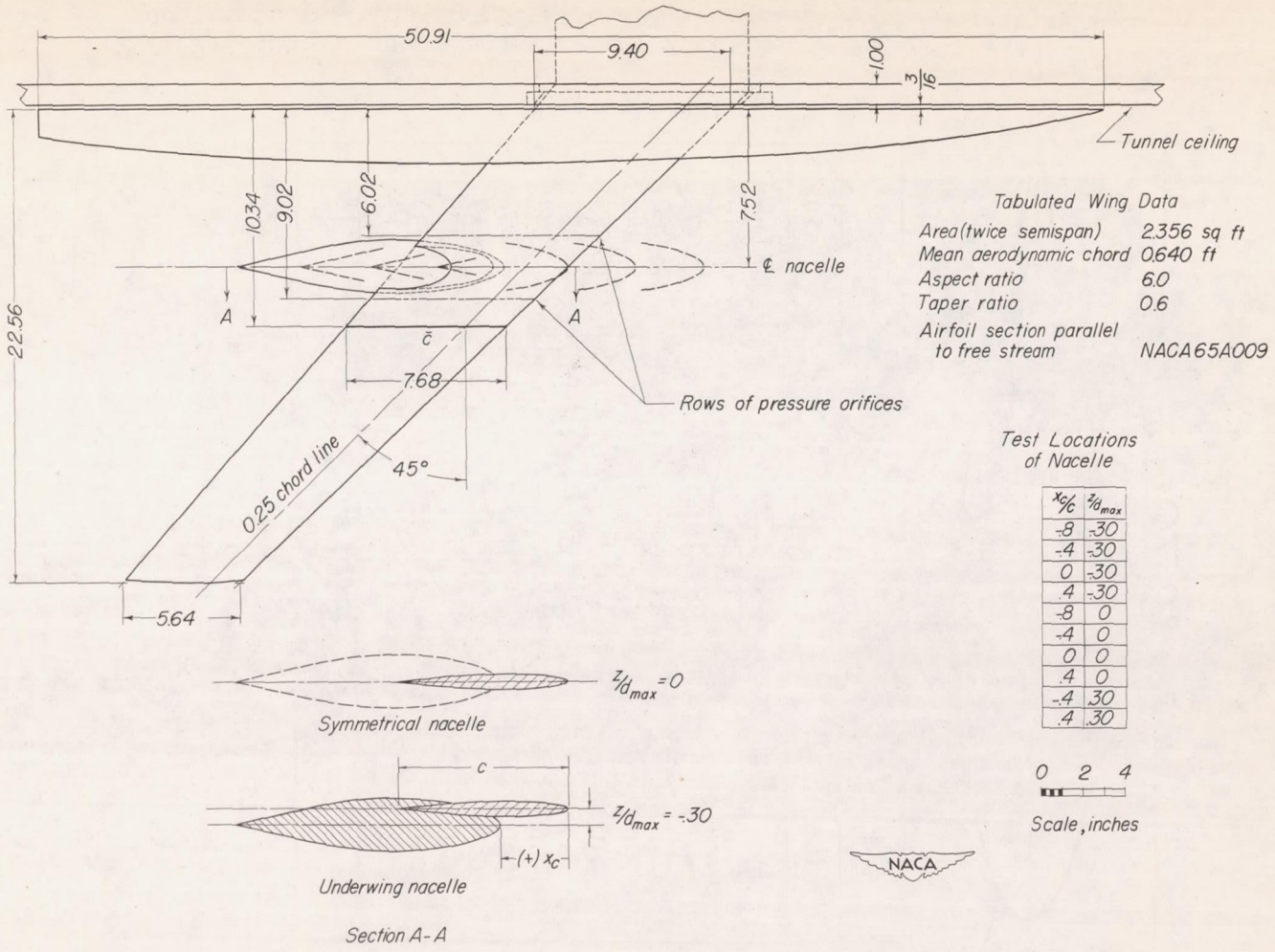

Figure 1.- The semispan model of 45° sweptback wing, fuselage of fineness ratio 10, and nacelle of fineness ratio 5 mounted on the ceiling of the Langley high-speed 7- by 10-foot tunnel.

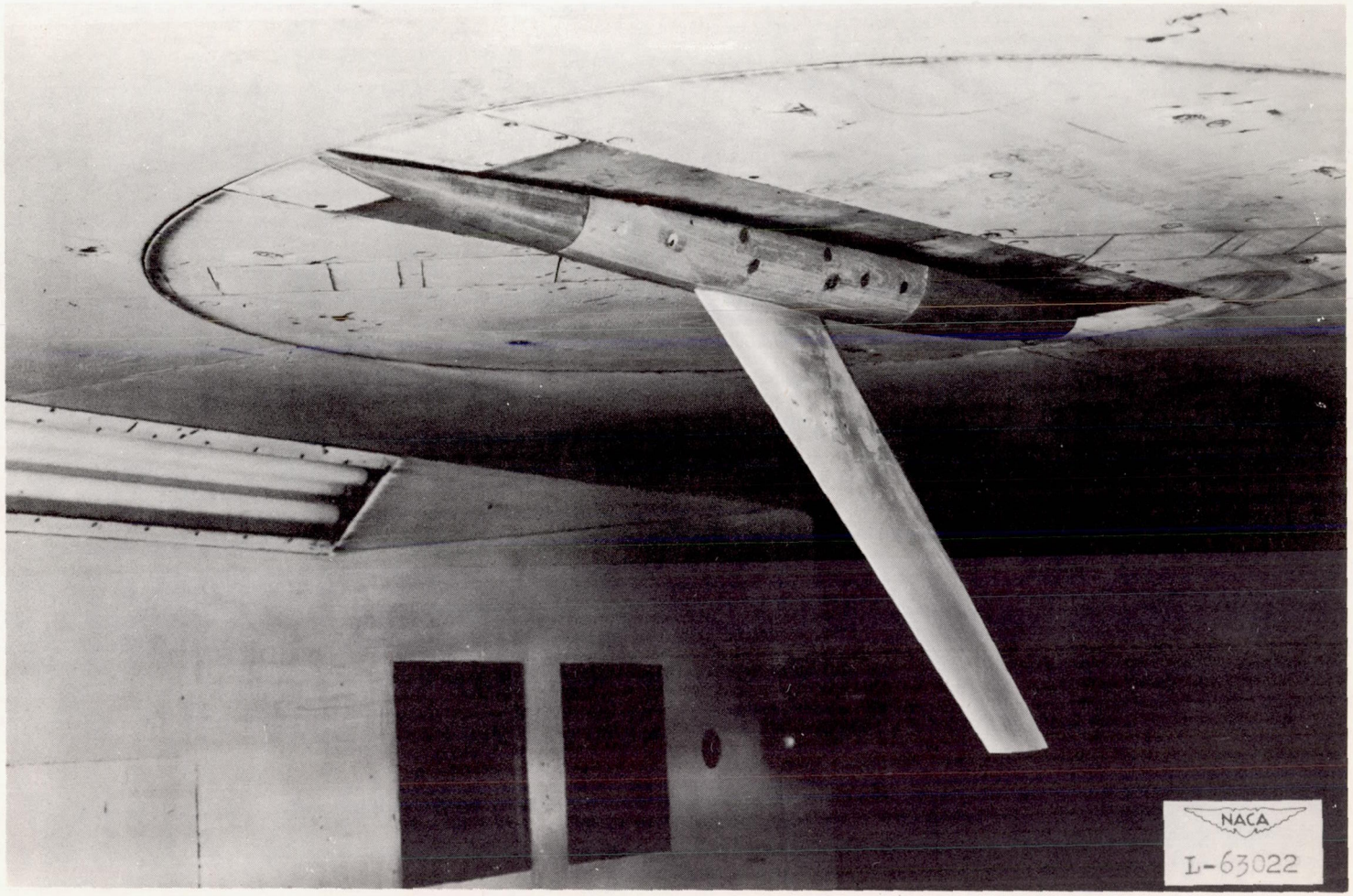

(a) Basic model.

Figure 2.- The 45° sweptback wing and fuselage of fineness ratio 10 mounted on the ceiling of the Langley high-speed 7- by 10-foot tunnel.

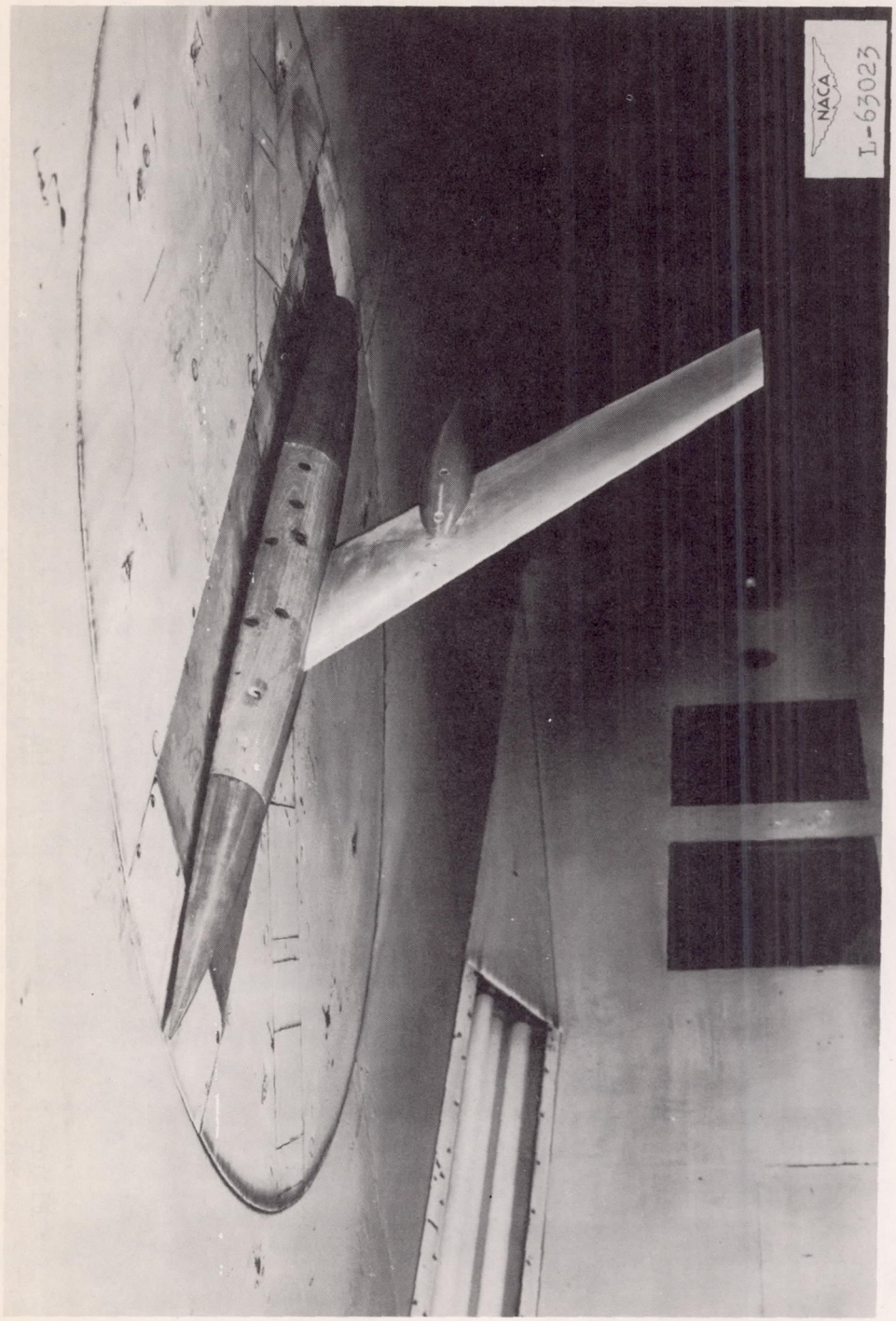

(b) Wing-fuselage with nacelle.

Figure 2.- Concluded.

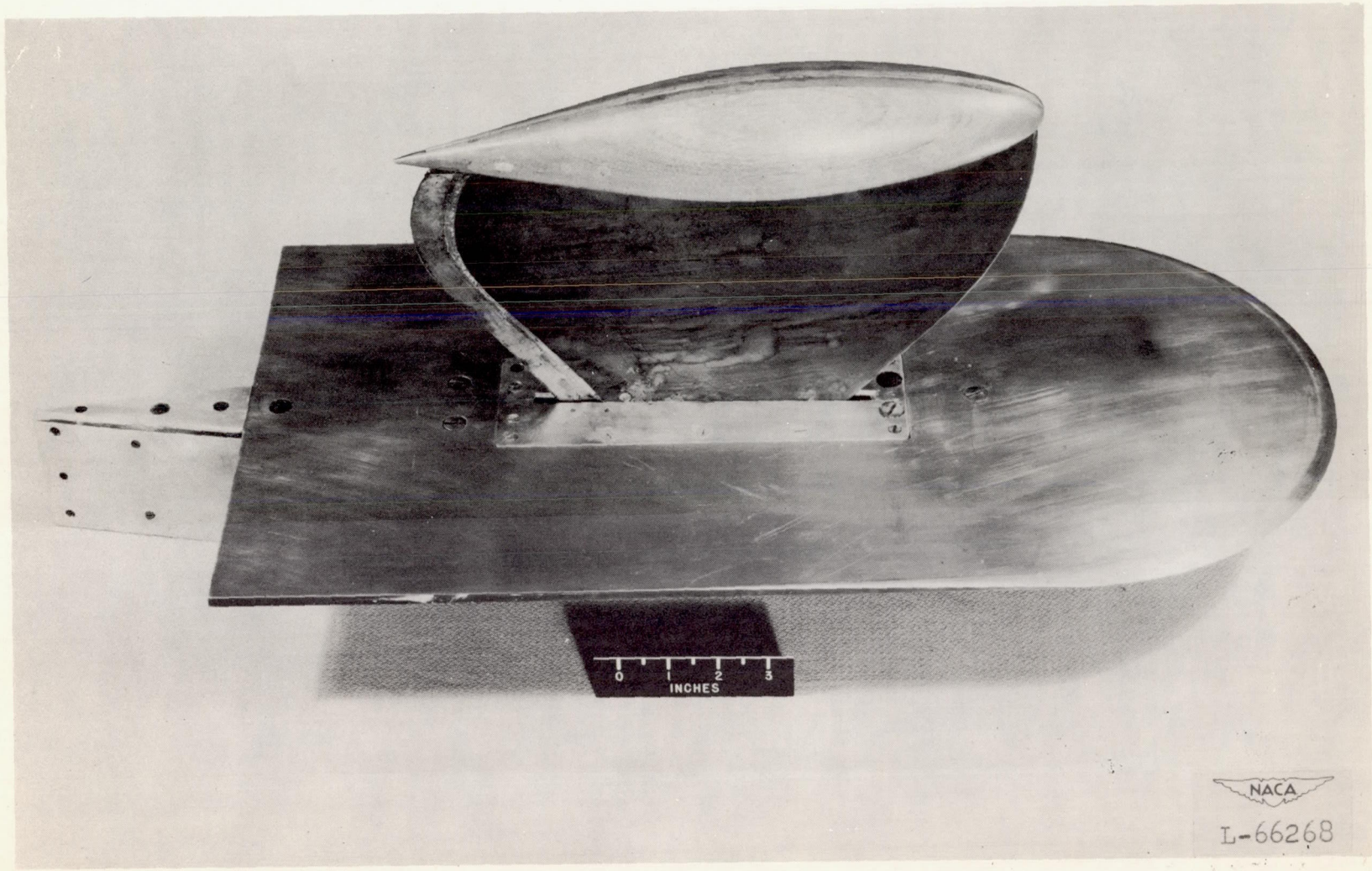

Figure 3.- The nacelle of fineness ratio 5 strut-mounted on reflection plane setup as tested in the Langley high-speed 7- by 10-foot tunnel.

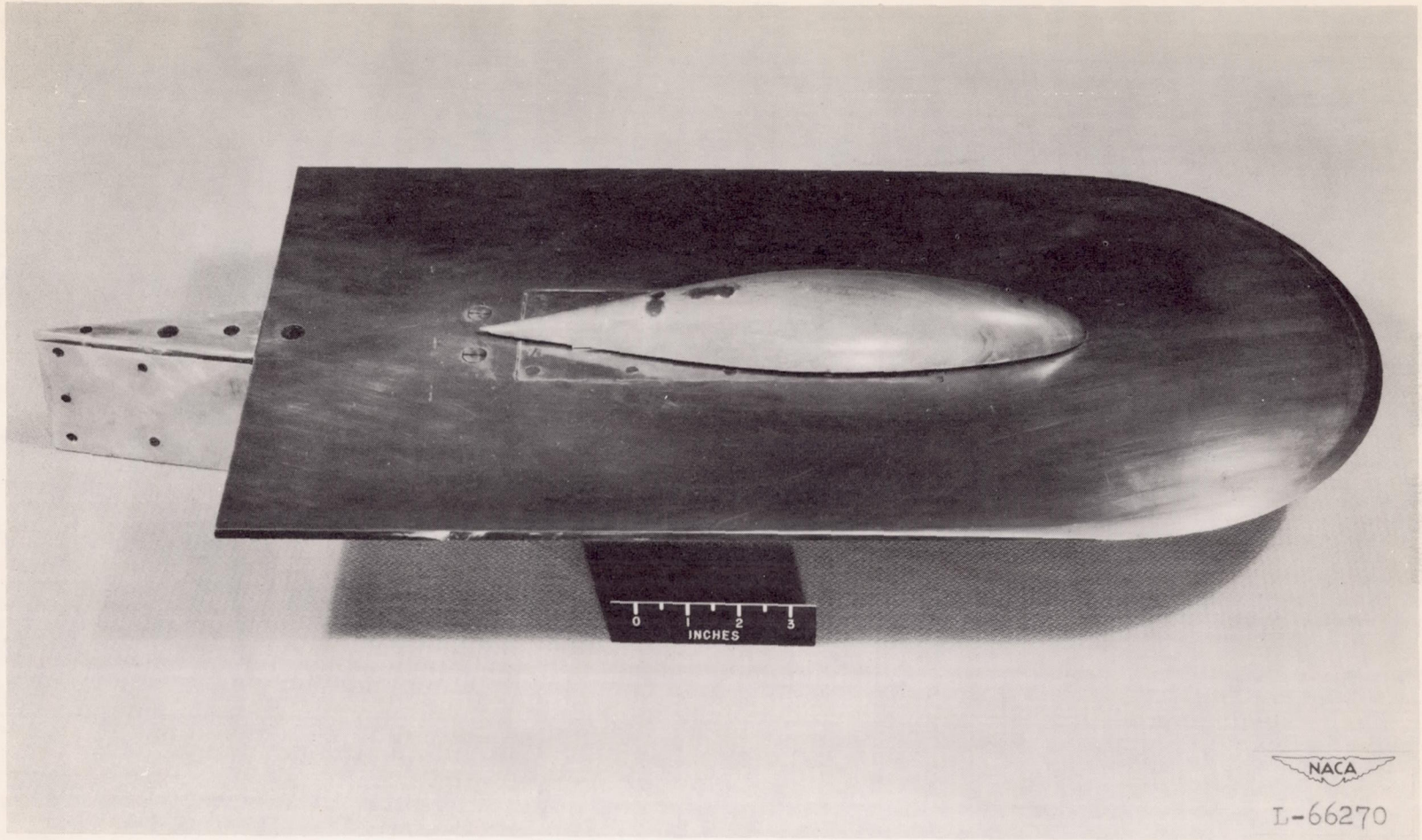

Figure 4.- The half-model nacelle of fineness ratio 5 mounted on reflection plane setup as tested in the Langley high-speed 7- by 10-foot tunnel.

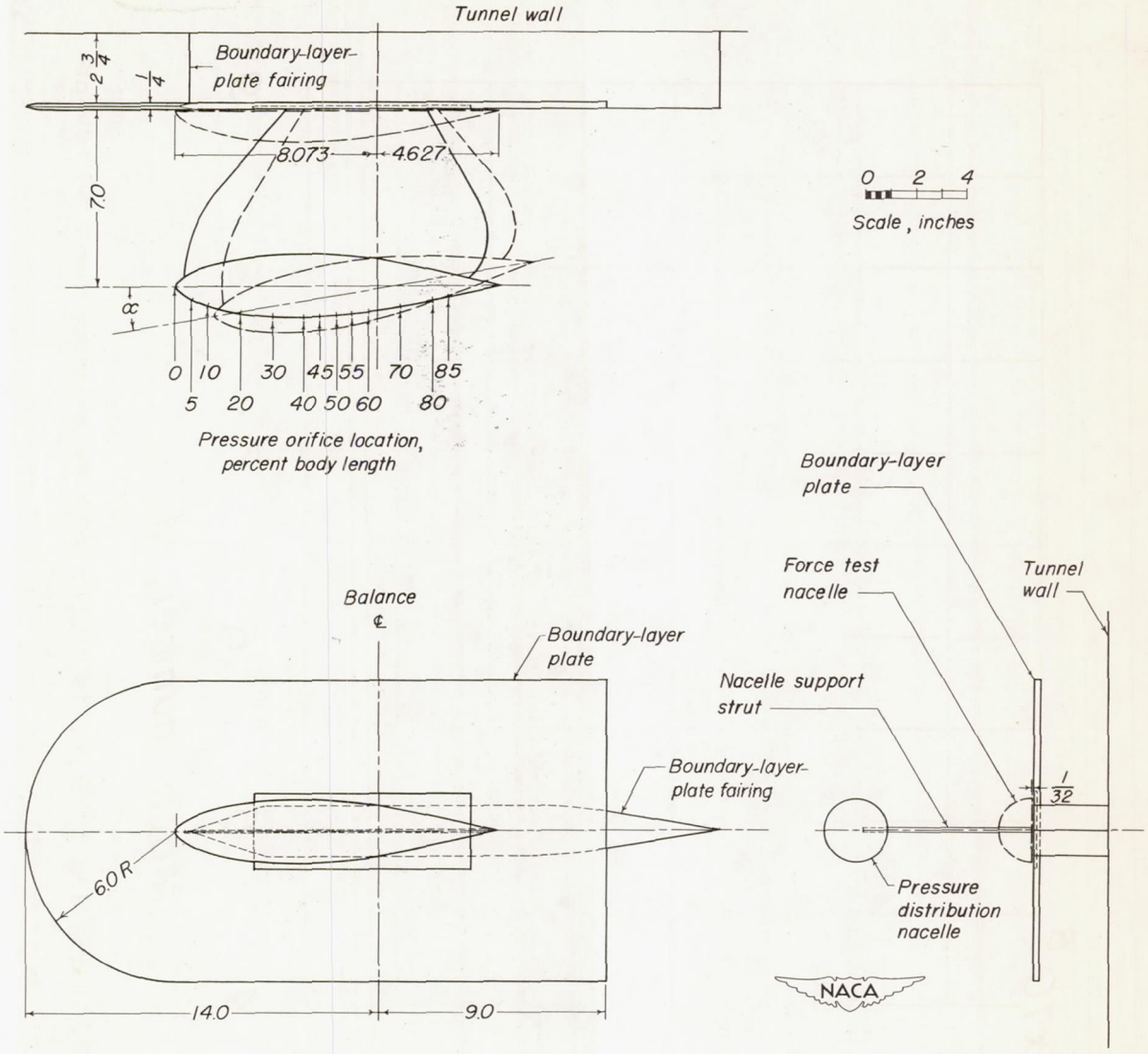

Figure 5.-Sidewall reflection plane setup showing half-model nacelle and strut-mounted nacelle of fineness ratio 5.

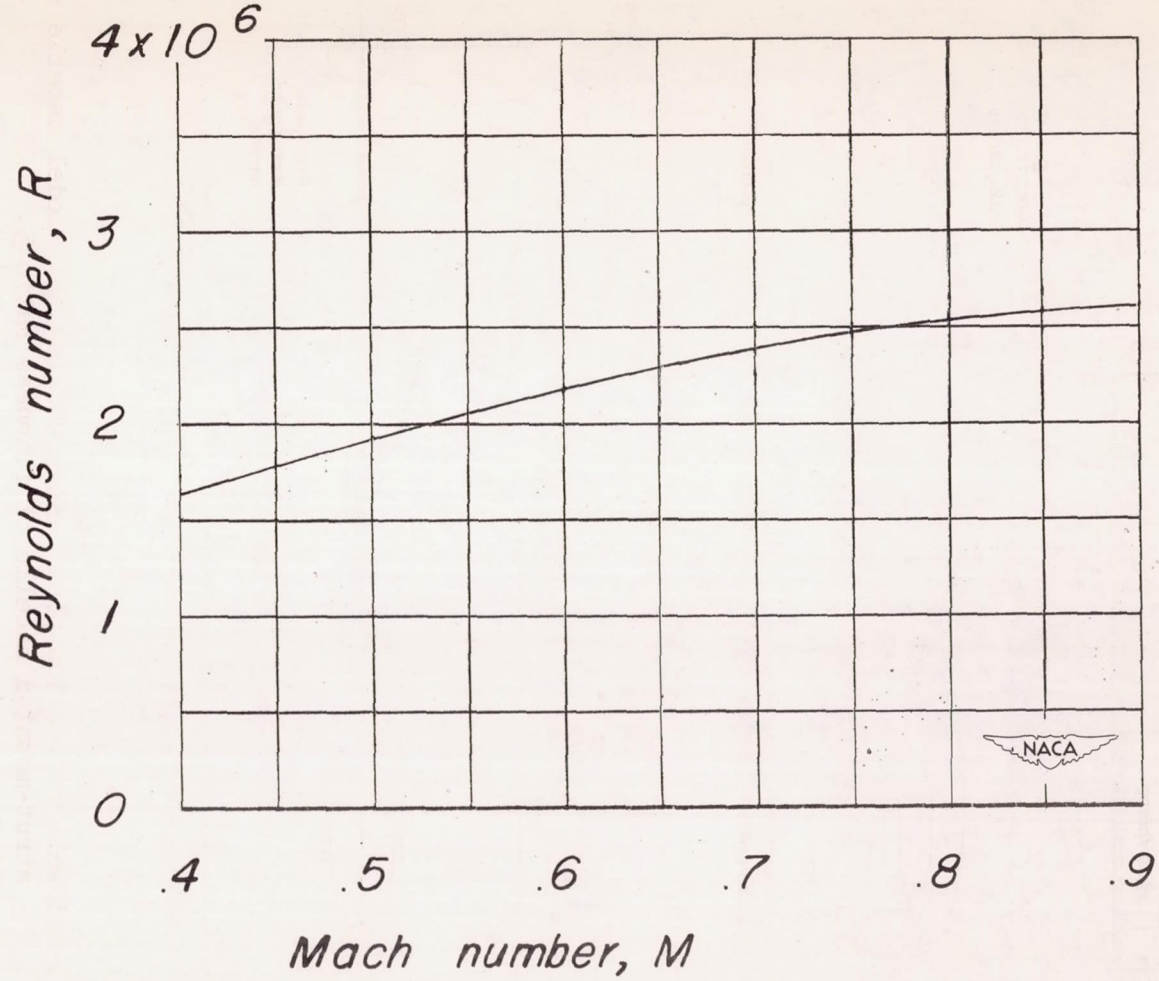

Figure 6.- Variation of Reynolds number with Mach number for a 45° swept-back wing.

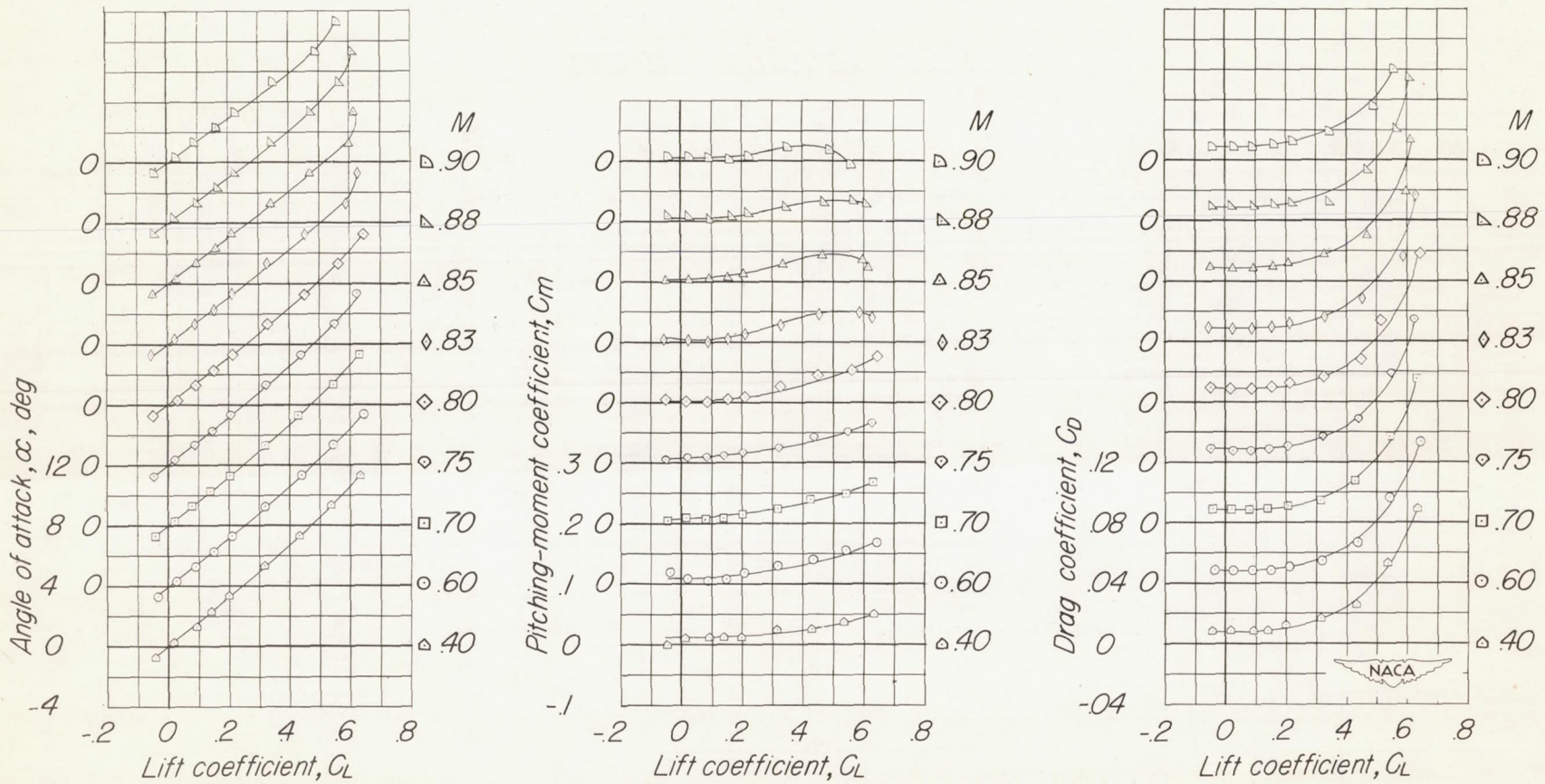

Figure 7.- Aerodynamic characteristics of a 45° sweptback wing and fuselage of fineness ratio 10.

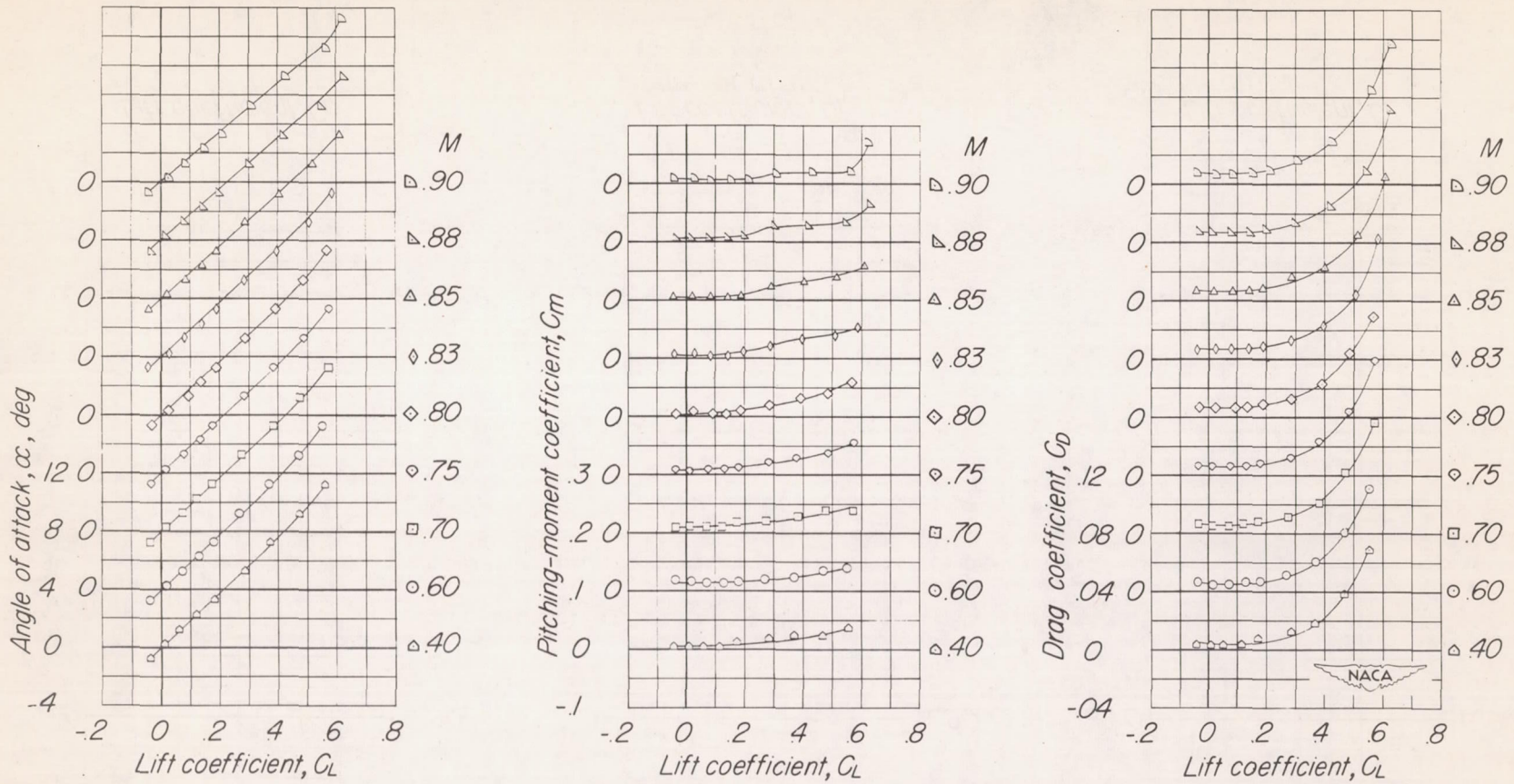

Figure 8.- Aerodynamic characteristics of a 45° sweptback wing.

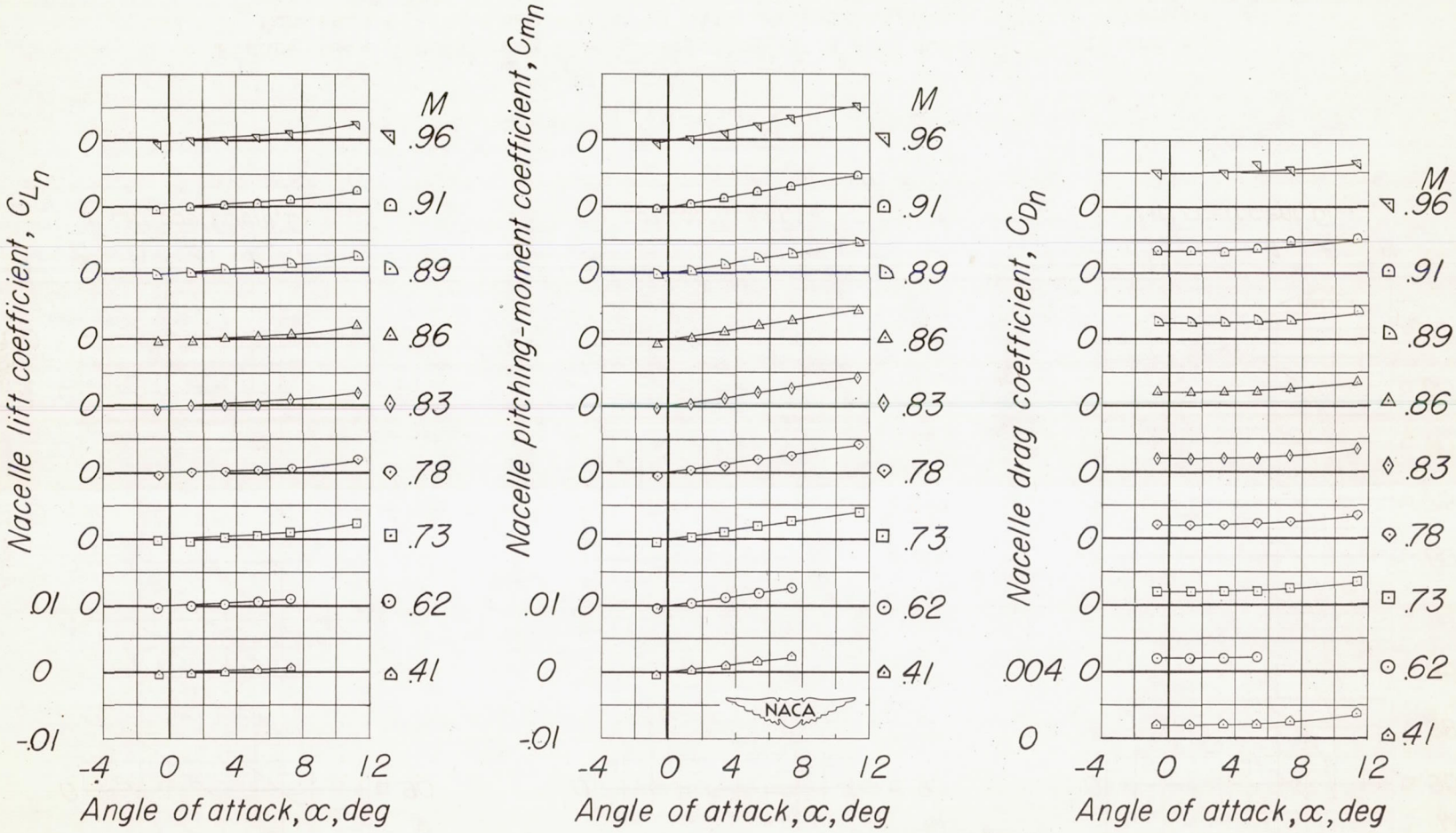

Figure 9.- Aerodynamic characteristics of a nacelle of fineness ratio 5.

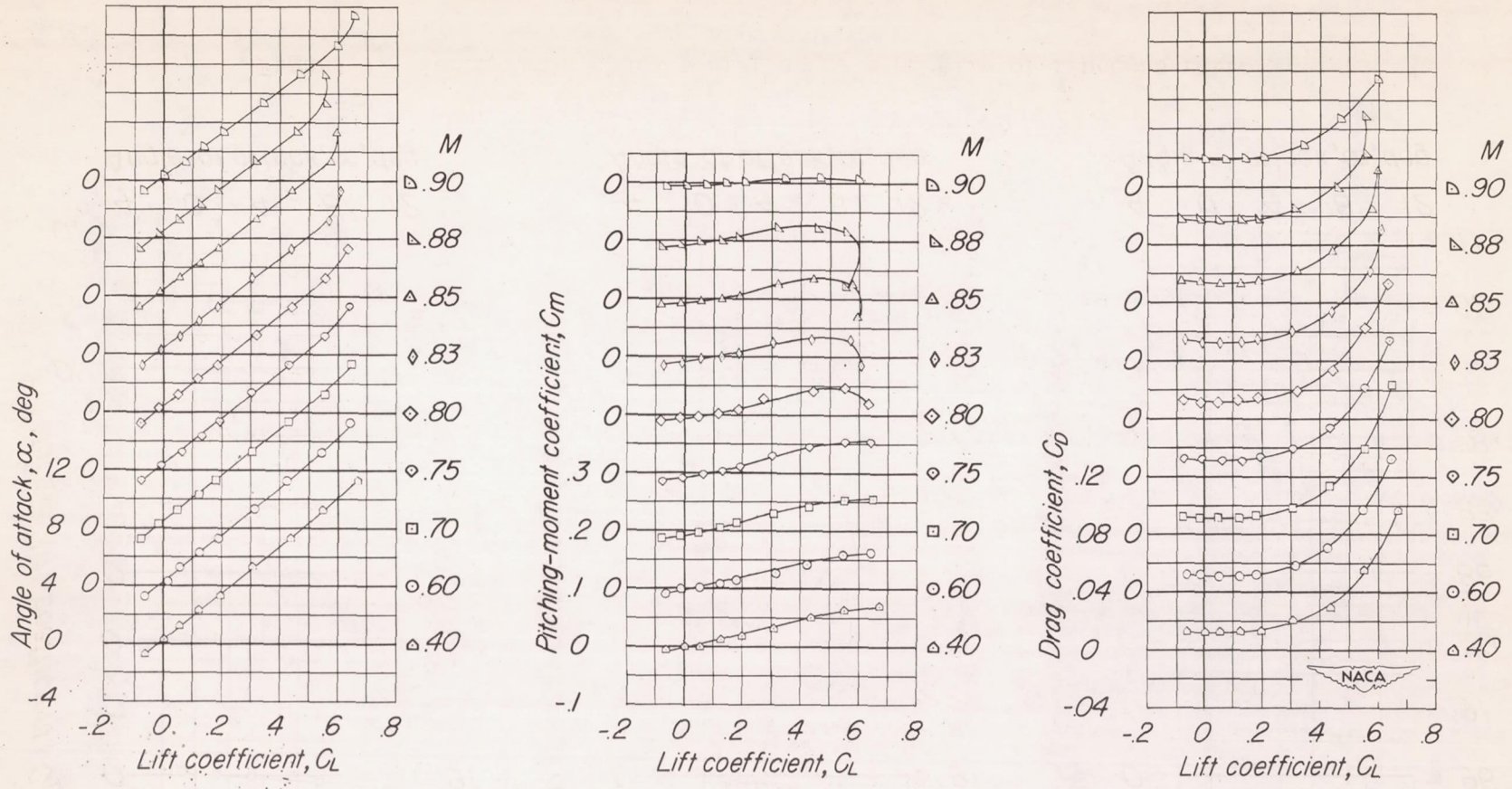

(a) $\frac{x_c}{c} = -0.8$.

Figure 10.- Aerodynamic characteristics of a 45° sweptback wing and a fuselage of fineness ratio 10 with an underwing nacelle of fineness ratio 5.

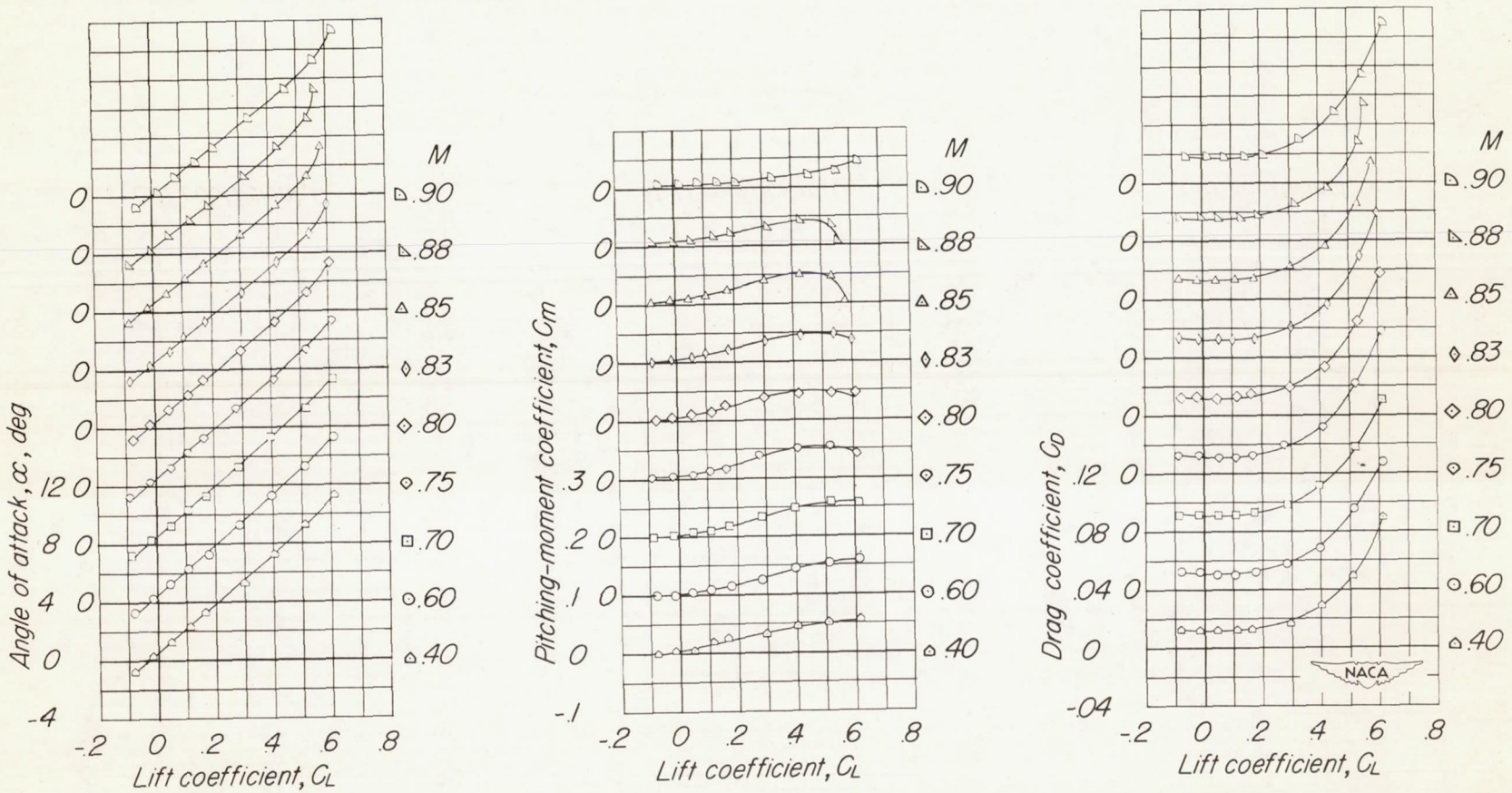

(b) $\frac{x_c}{c} = -0.4$.

Figure 10.- Continued.

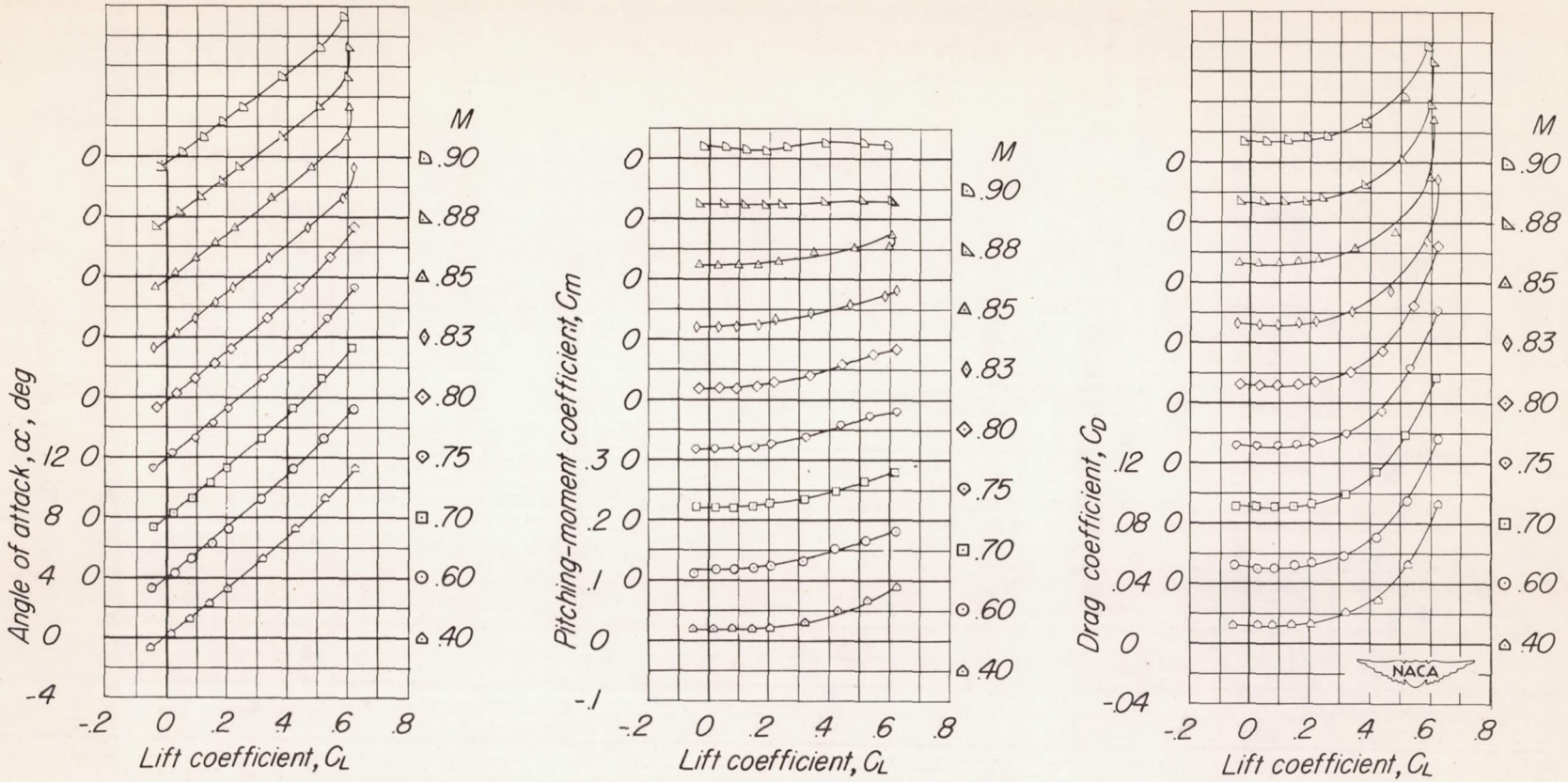

(c) $\frac{x_c}{c} = 0.$

Figure 10.- Continued.

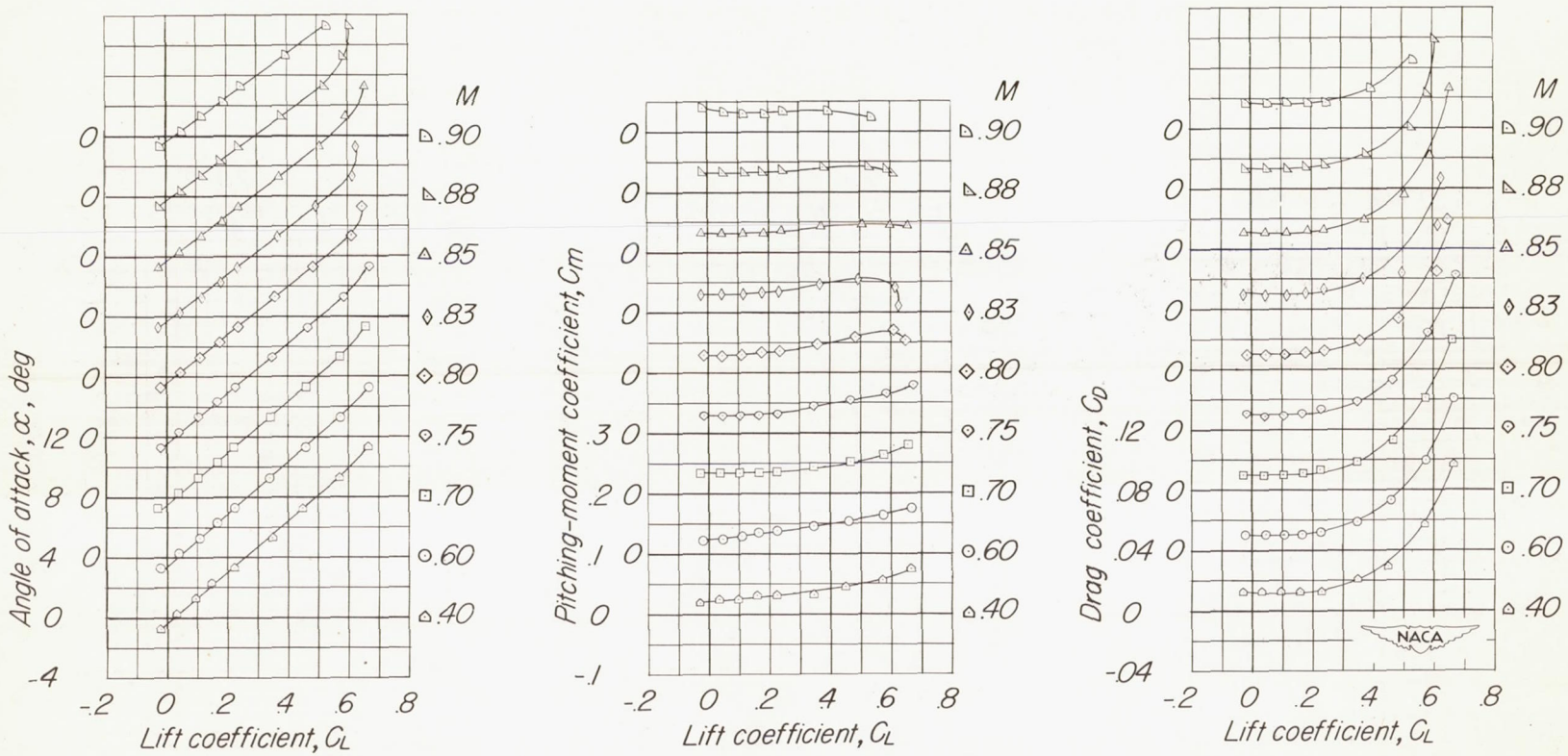

(d) $\frac{x_c}{c} = 0.4$.

Figure 10.- Concluded.

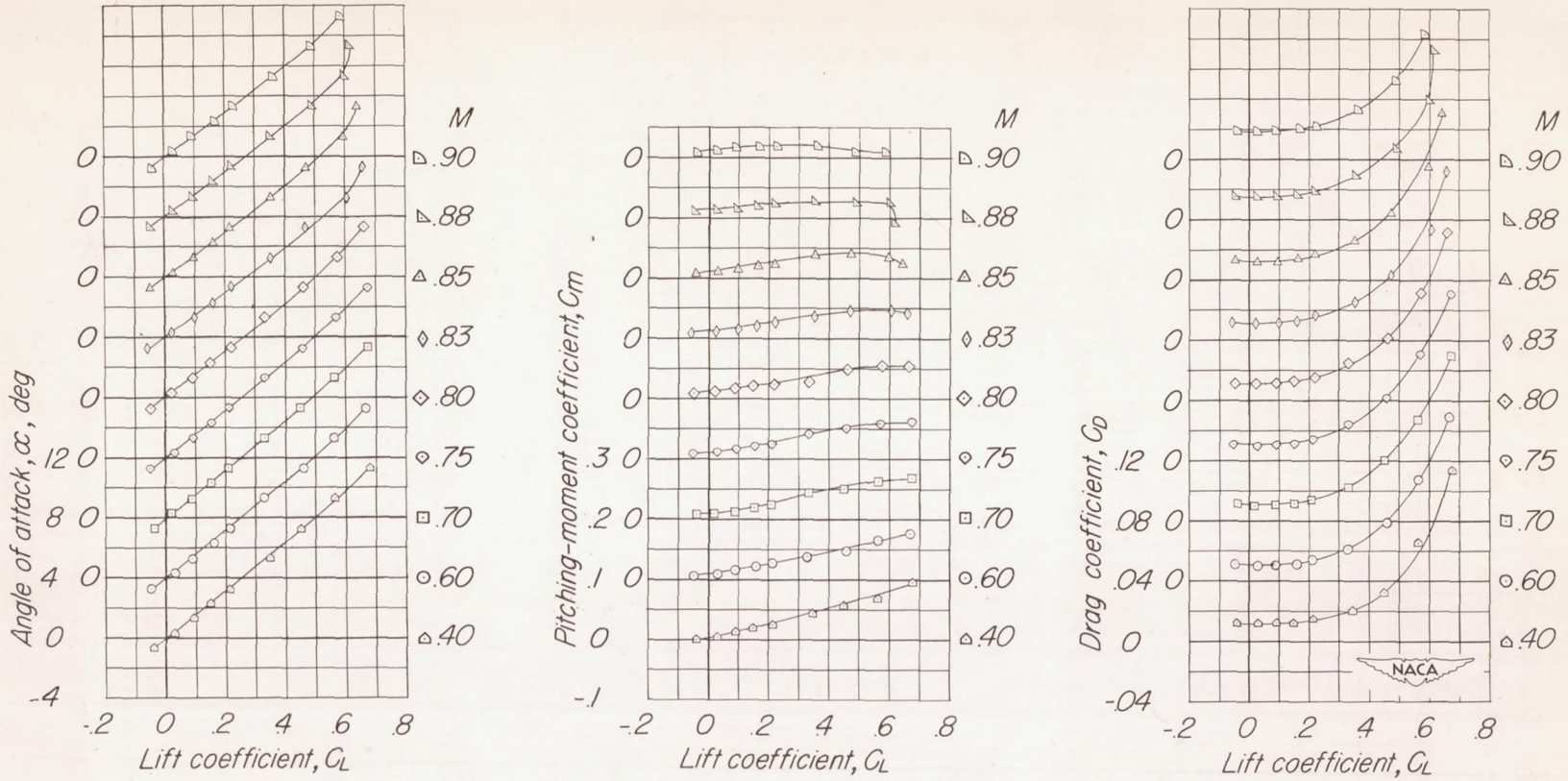

(a) $\frac{x_c}{c} = -0.8$.

Figure 11.- Aerodynamic characteristics of a 45° sweptback wing and a fuselage of fineness ratio 10 with a symmetrical nacelle of fineness ratio 5.

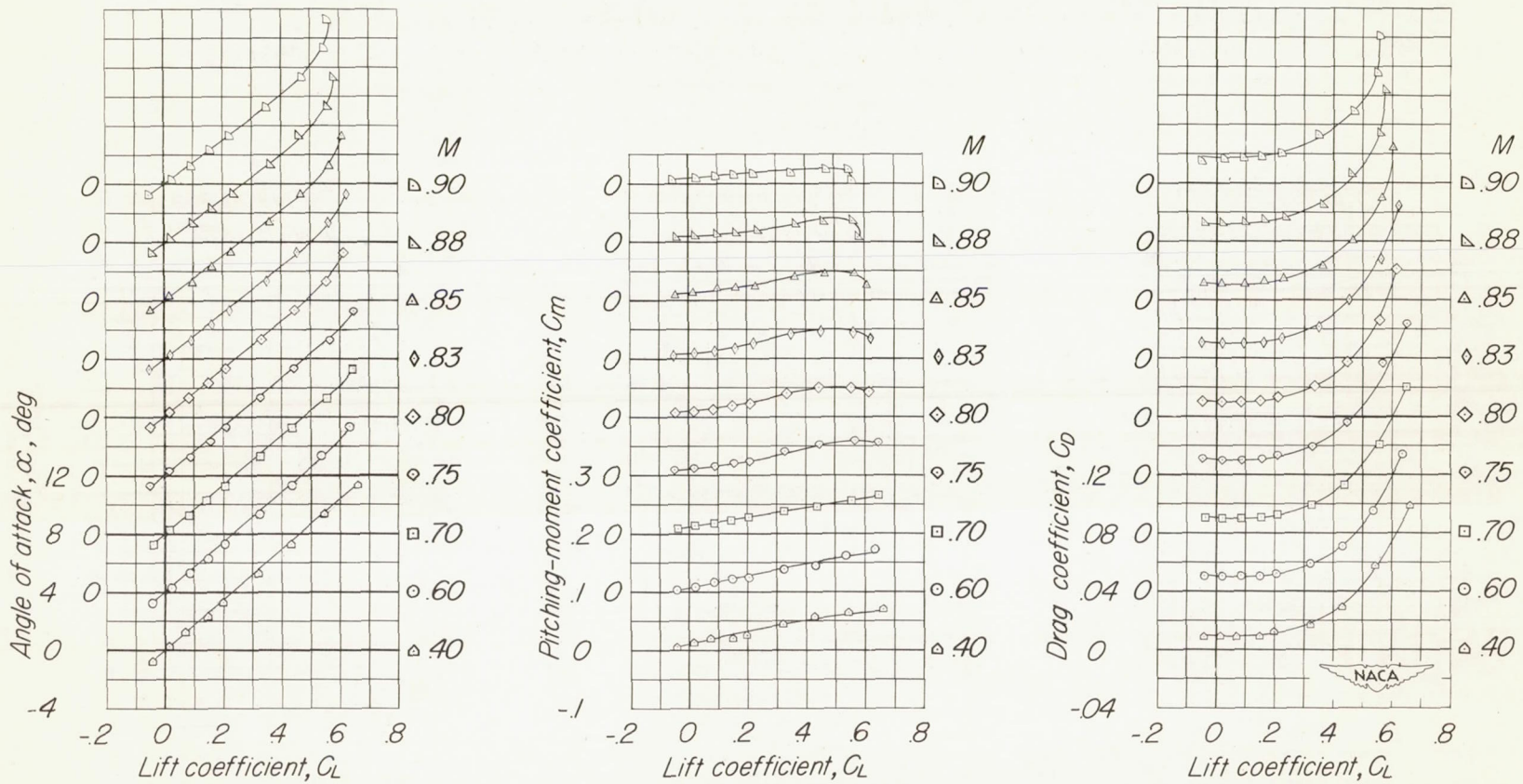

(b) $\frac{x_c}{c} = -0.4$.

Figure 11.- Continued.

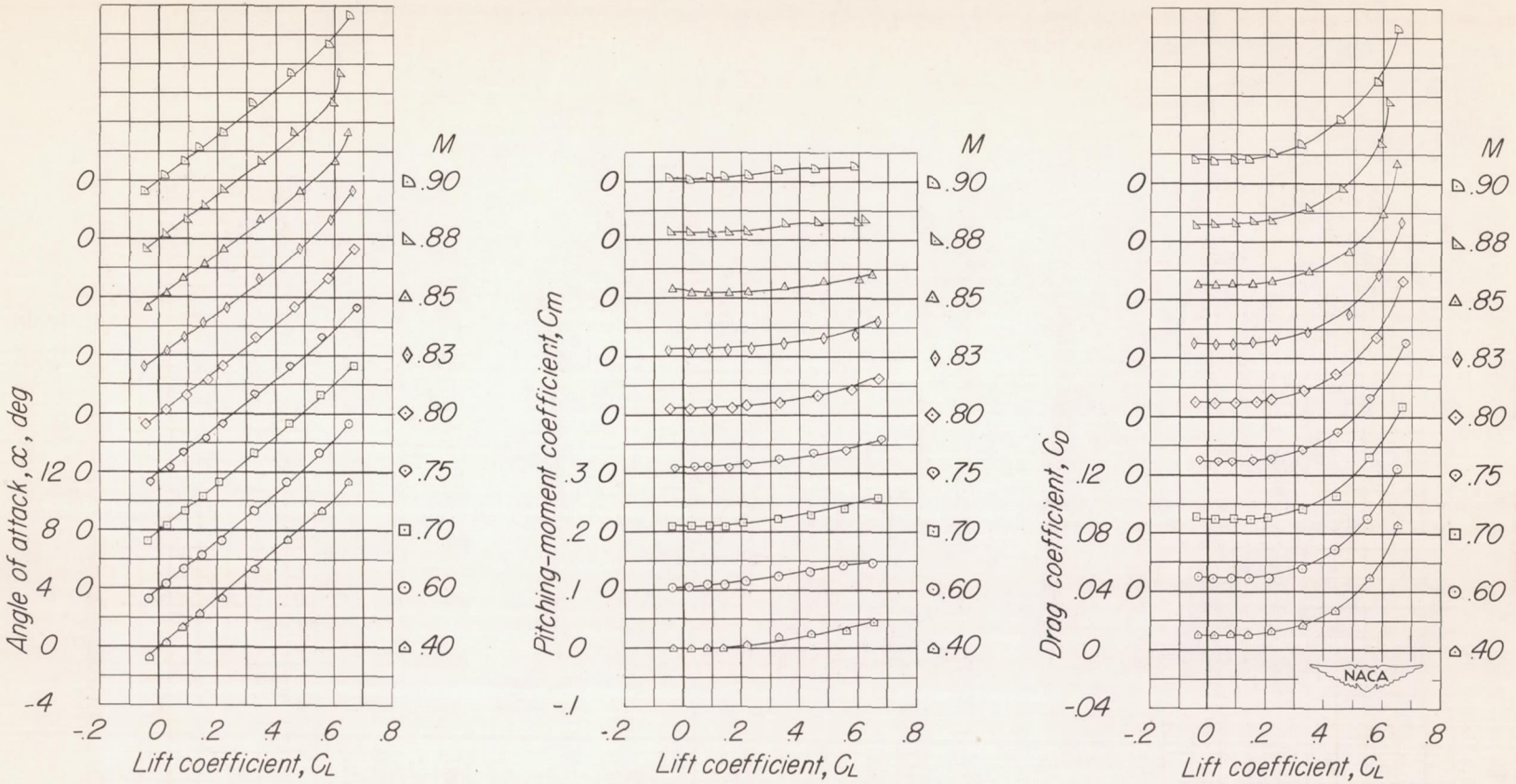

(c) $\frac{x_c}{c} = 0$.

Figure 11.- Continued.

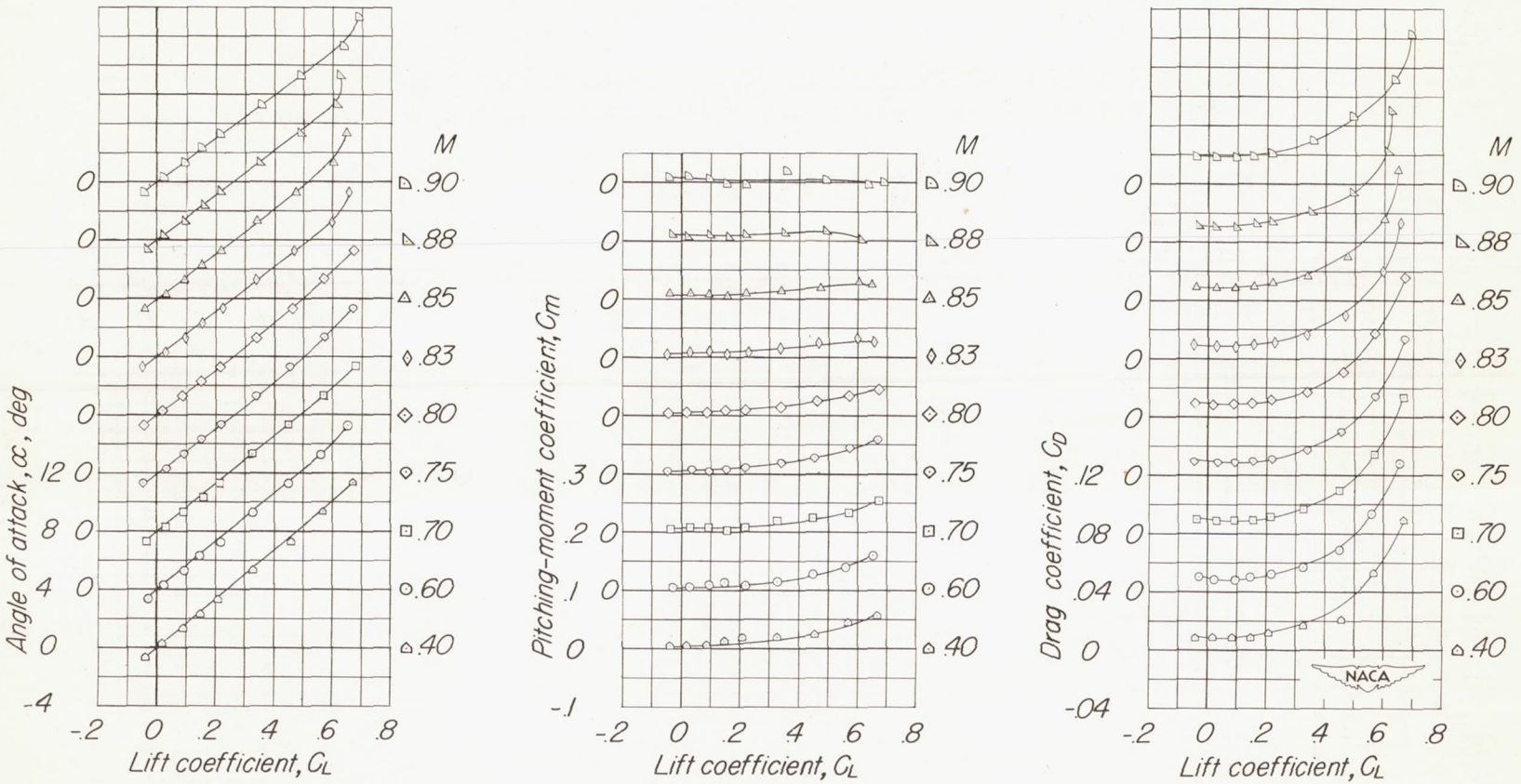

(d) $\frac{x_c}{c} = 0.4$.

Figure 11.- Concluded.

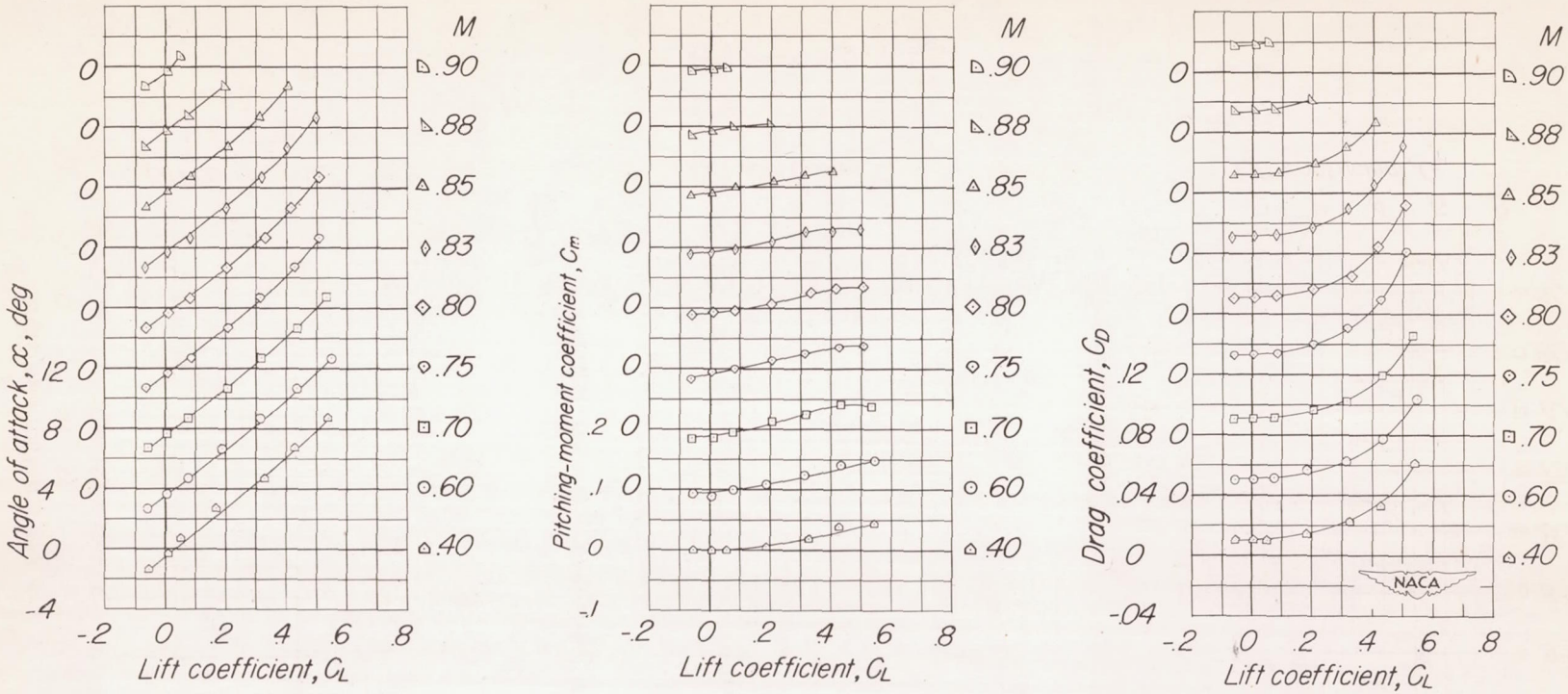

(a) $\frac{x_c}{c} = -0.4$.

Figure 12.- Aerodynamic characteristics of a 45° sweptback wing and a fuselage of fineness ratio 10 with an overwing nacelle of fineness ratio 5.

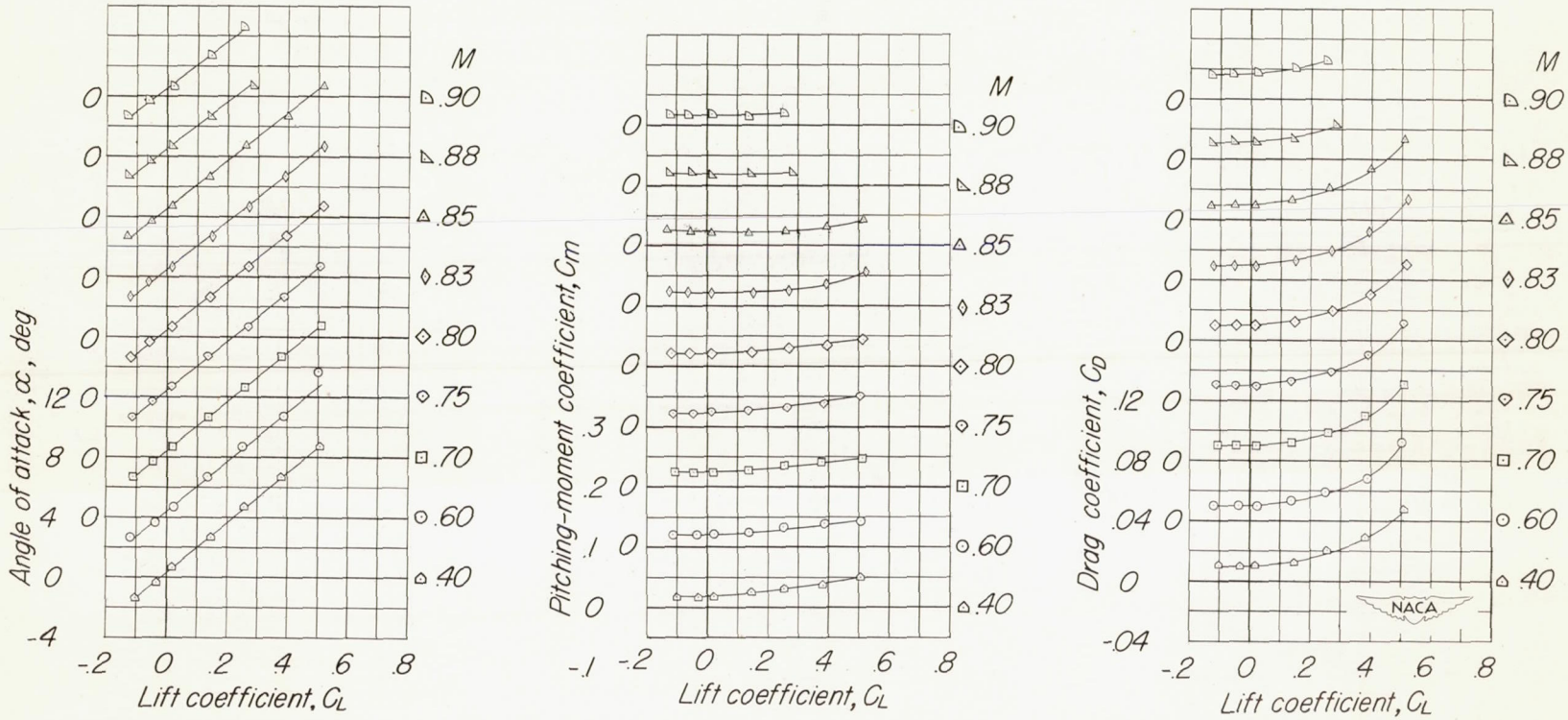

(b) $\frac{x_c}{c} = 0.4$.

Figure 12.- Concluded.

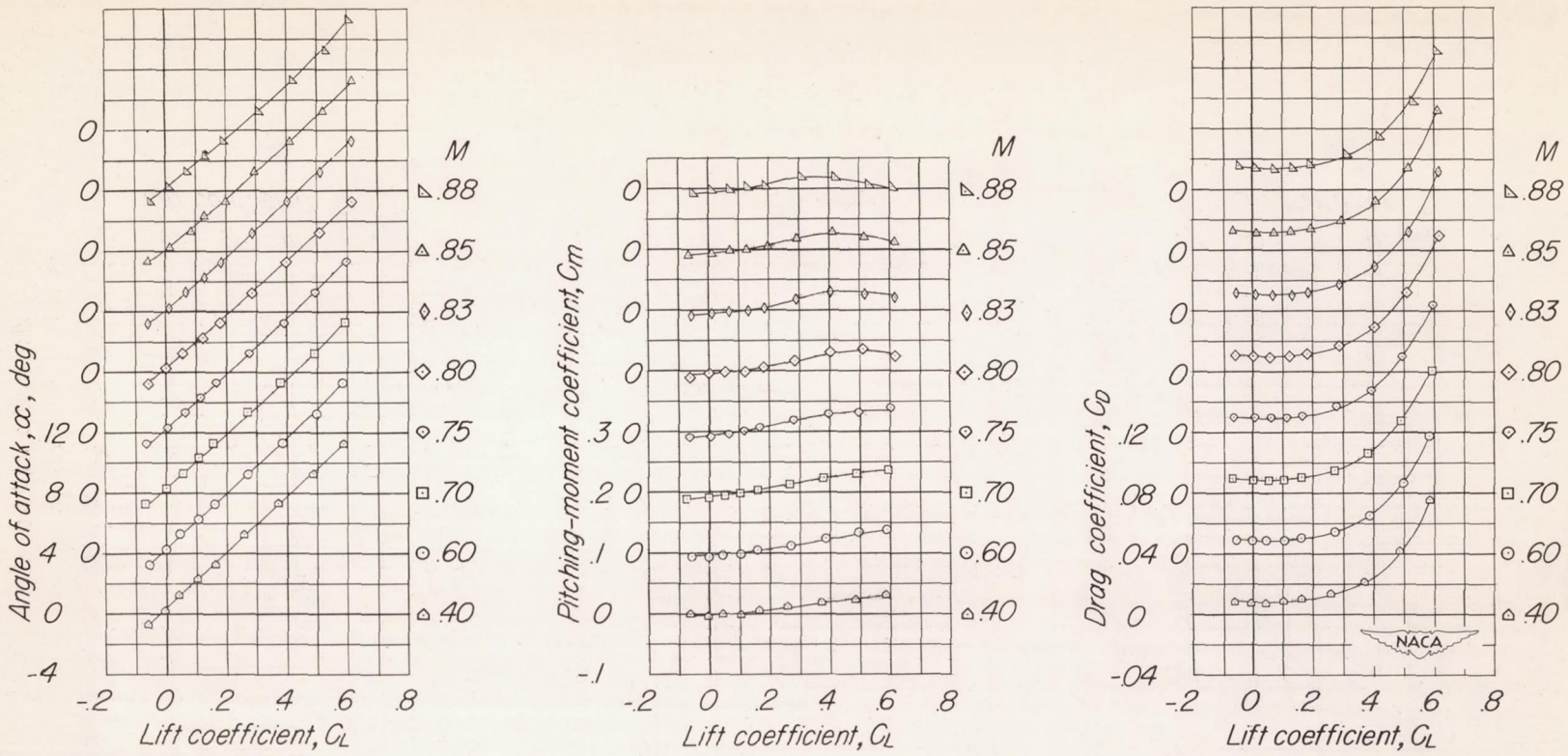

(a) $\frac{x_c}{c} = -0.8$.

Figure 13.- Aerodynamic characteristics of a 45° sweptback wing with an underwing nacelle of fineness ratio 5.

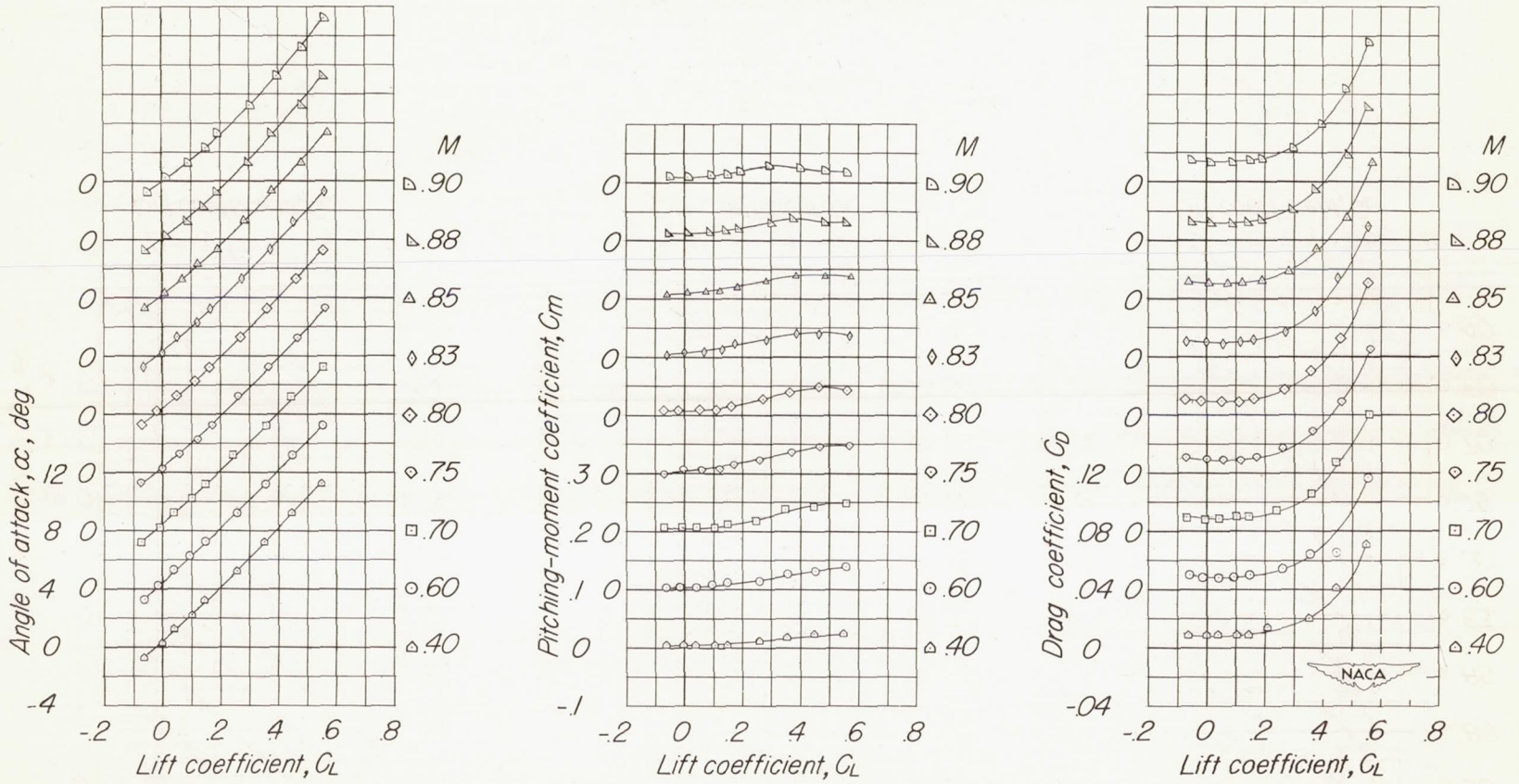

(b) $\frac{x_c}{c} = -0.4$.

Figure 13.- Continued.

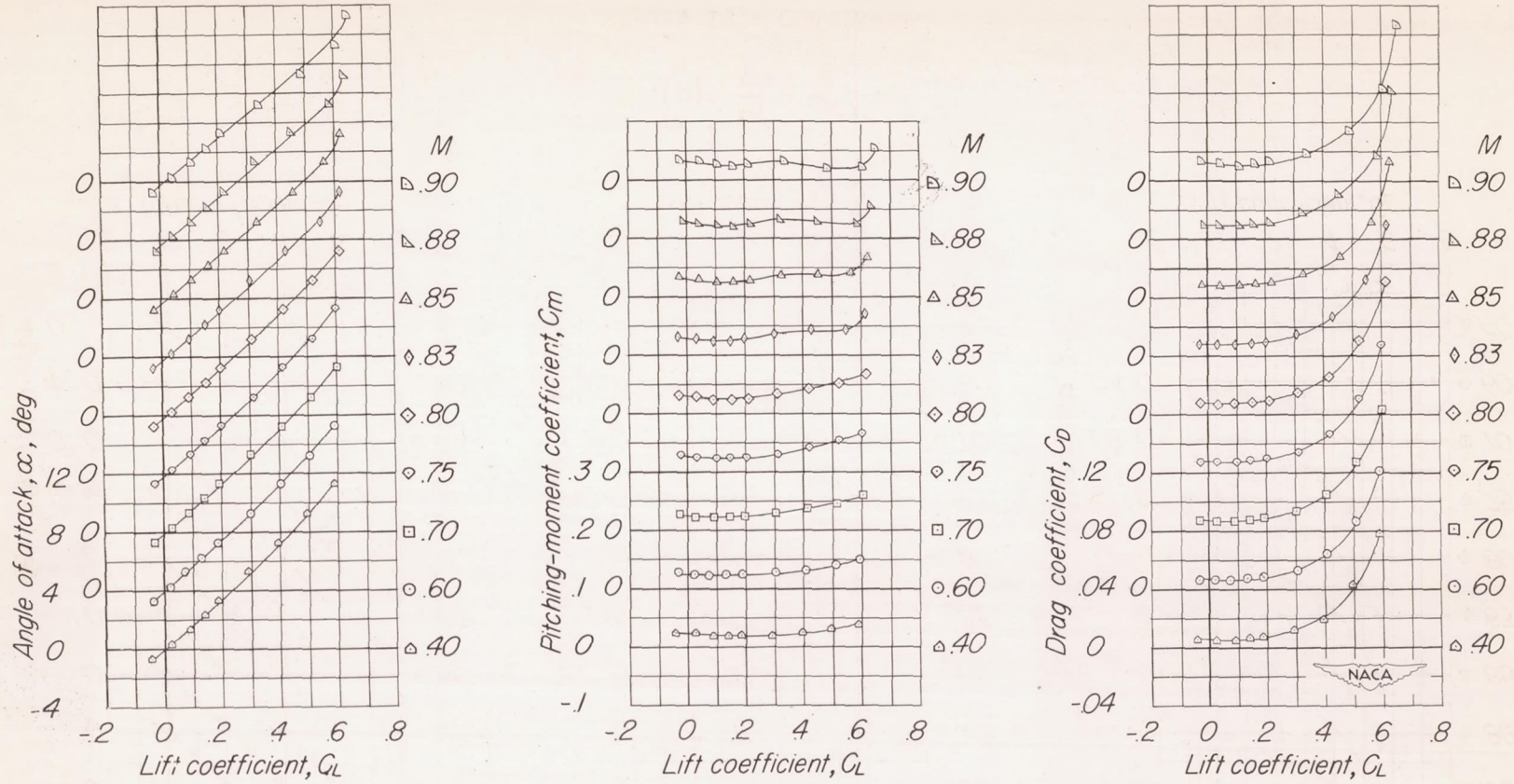

(c) $\frac{x_c}{c} = 0.4$.

Figure 13.- Concluded.

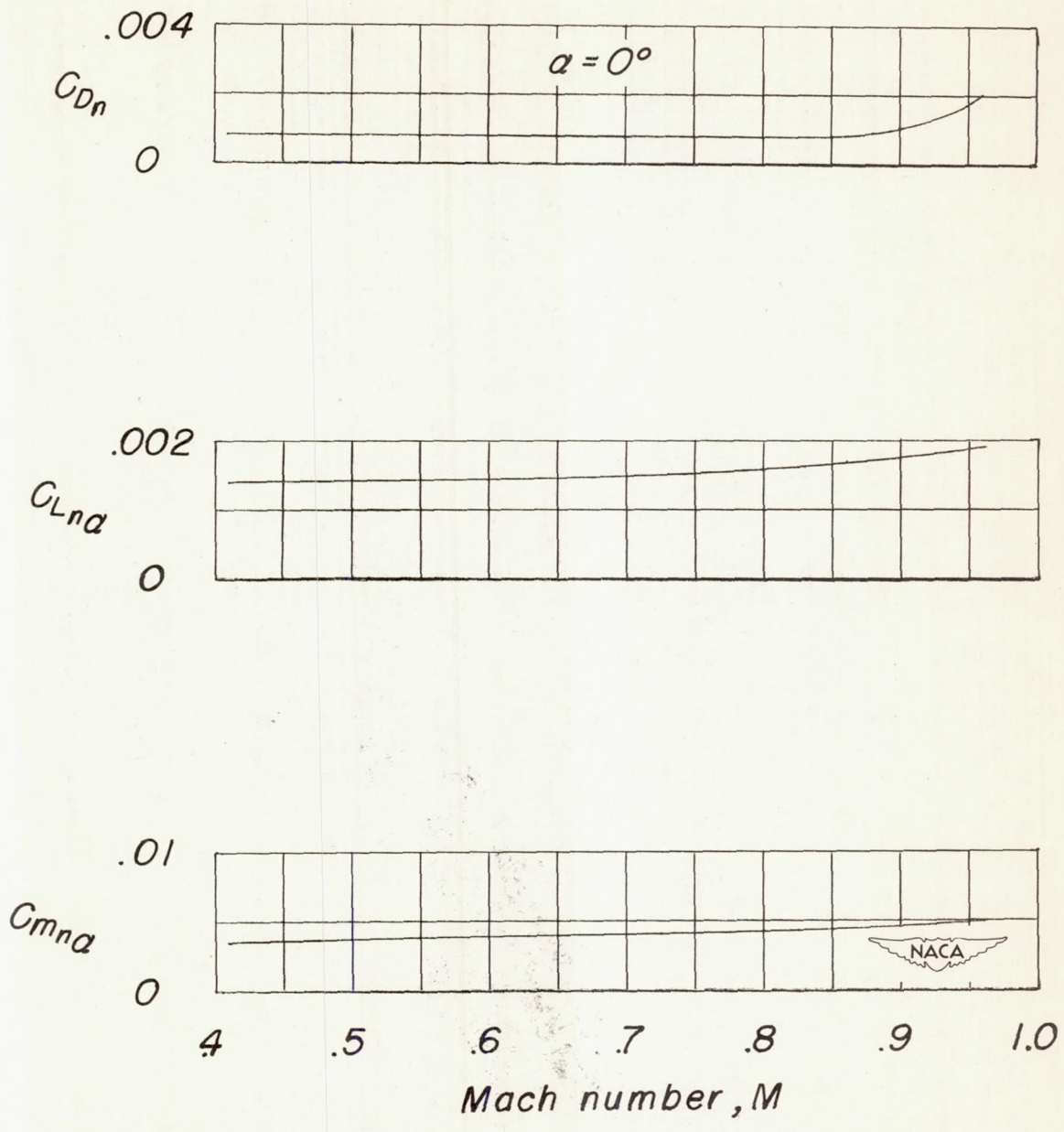

Figure 14.- Summary of aerodynamic characteristics of a nacelle of fineness ratio 5.

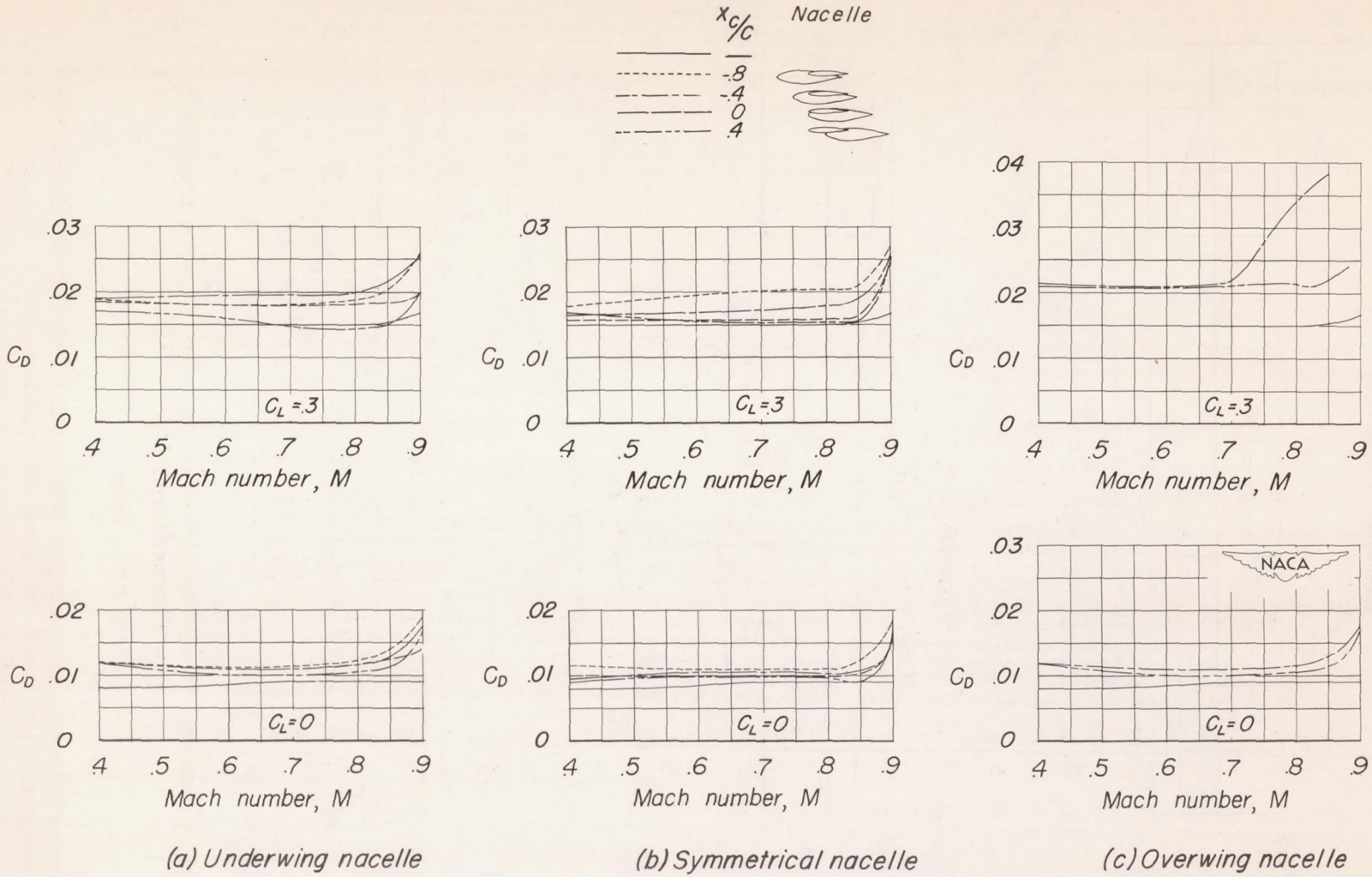

Figure 15.- Variation of drag coefficient with Mach number of a 45° swept-back wing and a fuselage of fineness ratio 10 with a nacelle of fineness ratio 5 at various chordwise and vertical positions.

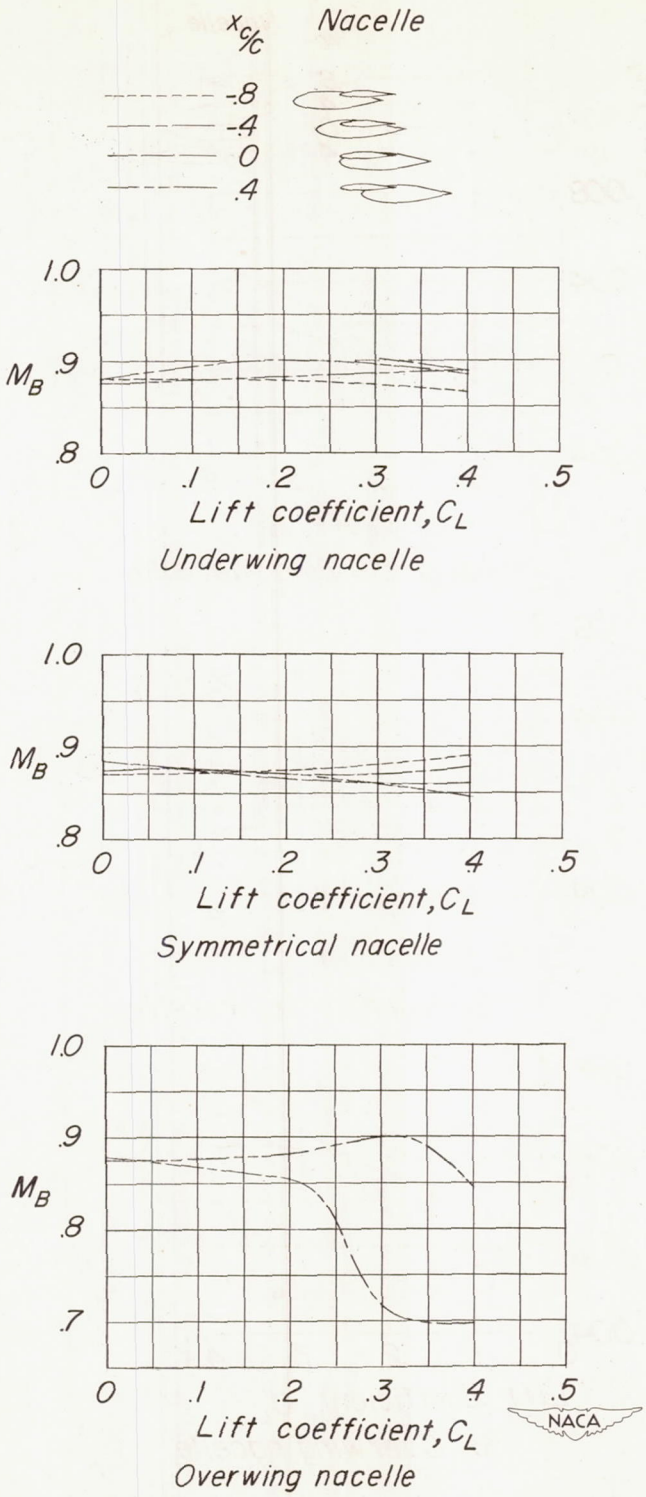

Figure 16.- Effect of lift coefficient on the drag break Mach number of a 45° sweptback wing and fuselage of fineness ratio 10 with a nacelle of fineness ratio 5 at various chordwise and vertical positions.

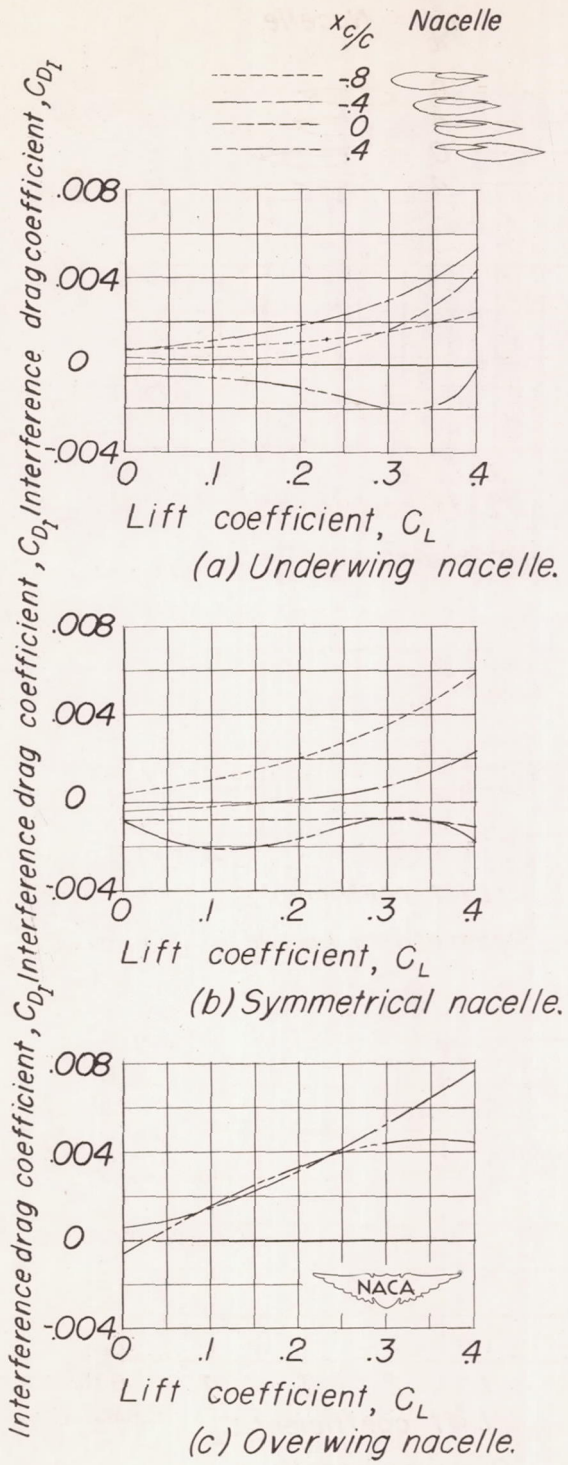

Figure 17.- Variation of interference drag coefficient with lift coefficient of a 45° sweptback wing and a fuselage of fineness ratio 10 with a nacelle of fineness ratio 5 at various chordwise and vertical positions. M = 0.70.

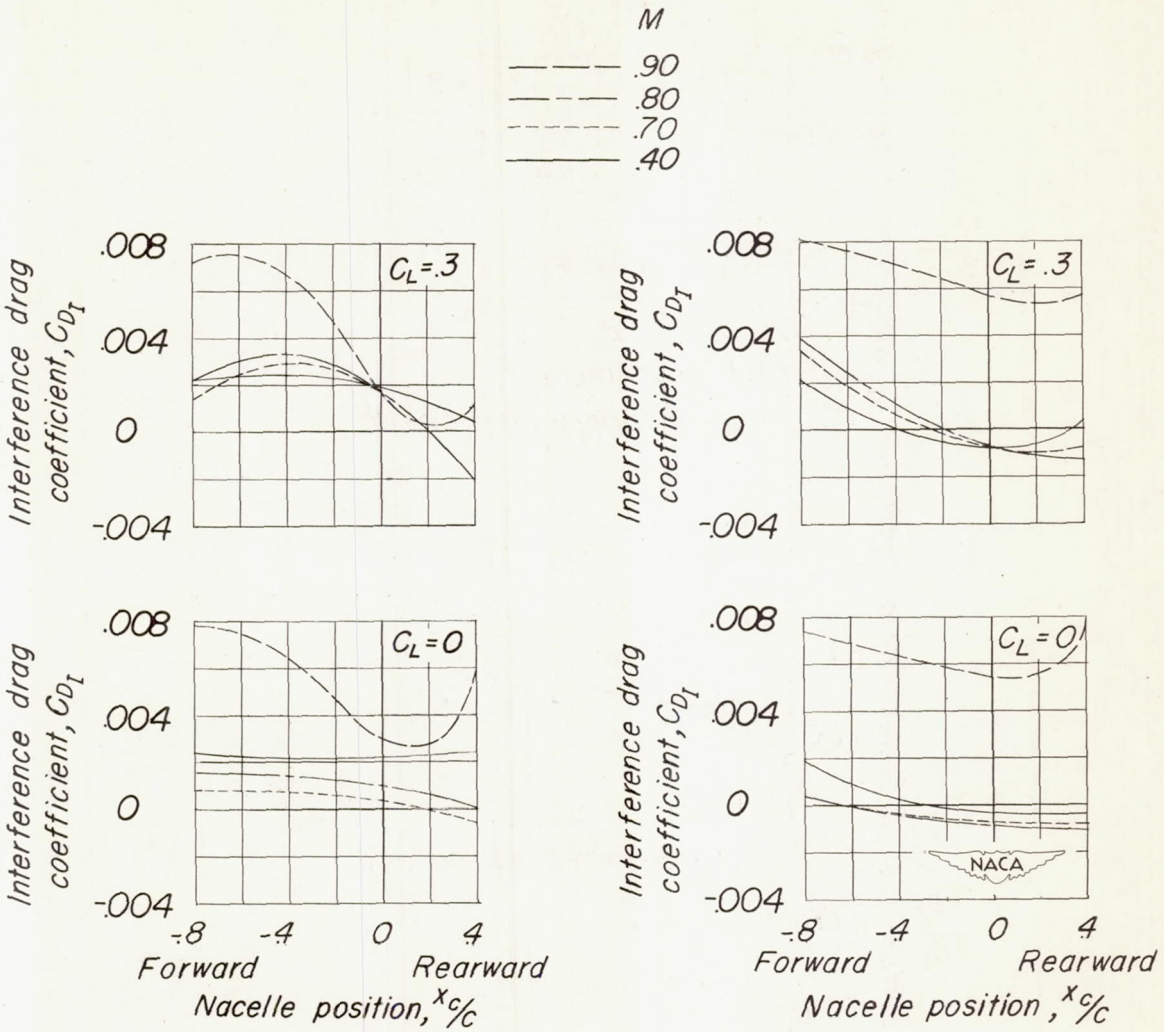

(a) Underwing nacelle

(b) Symmetrical nacelle

Figure 18.- Effect of nacelle position on the interference drag coefficient at various Mach numbers of a 45° sweptback wing and a fuselage of fineness ratio 10 with a nacelle of fineness ratio 5.

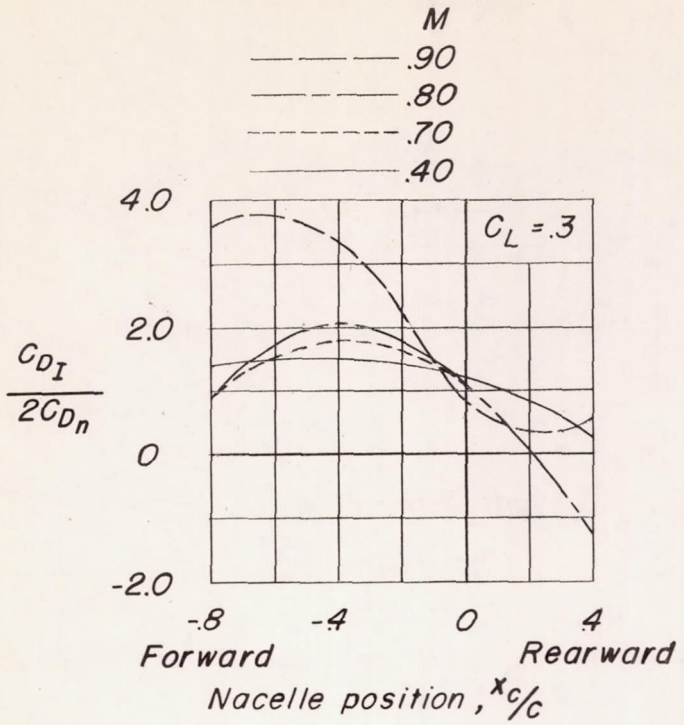

(a) Underwing nacelle

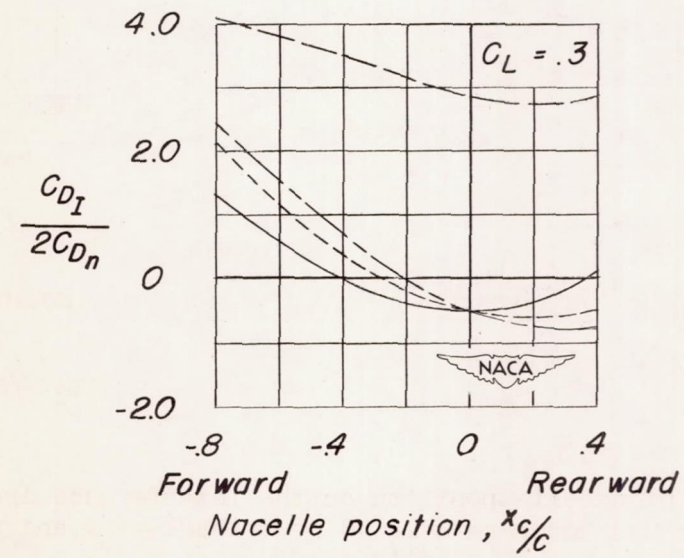

(b) Symmetrical nacelle

Figure 19.- Effect of nacelle position on the ratio of interference drag coefficient to nacelle drag coefficient at various Mach numbers for a 45° sweptback wing and a fuselage of fineness ratio 10 with a nacelle of fineness ratio 5.

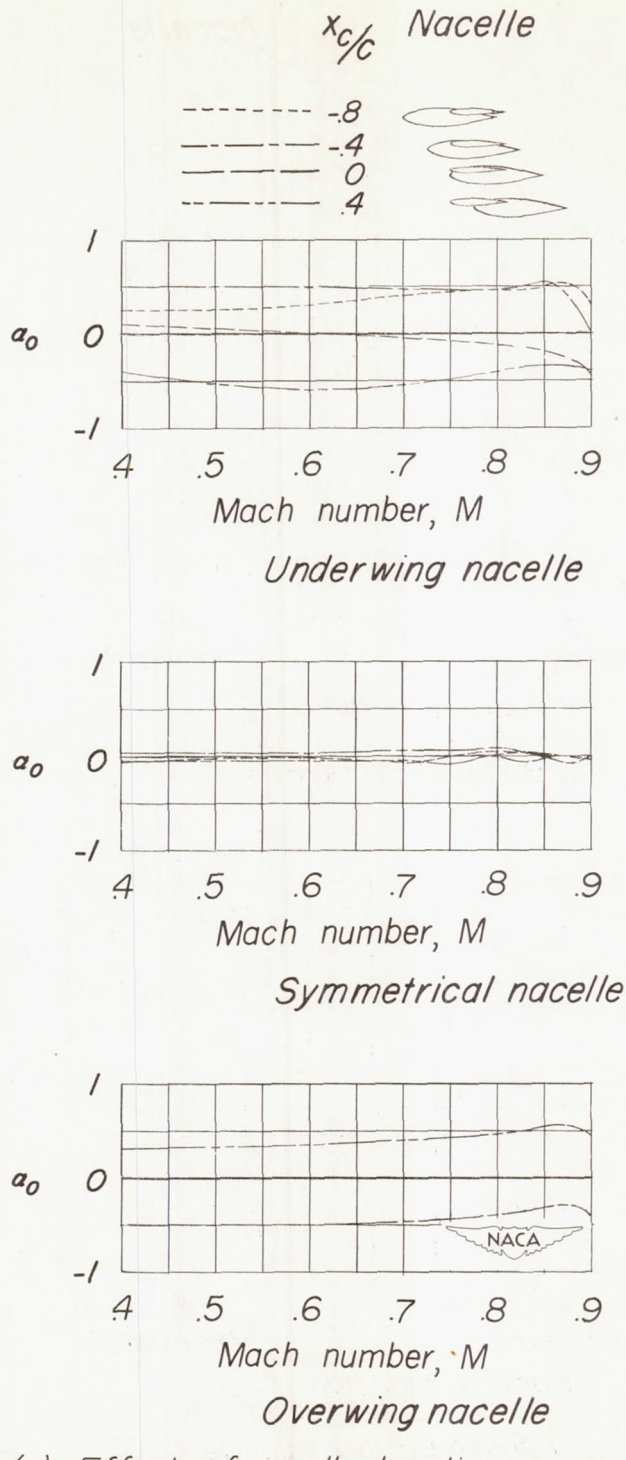

(a) Effect of nacelle location on α_o

Figure 20.- Summary of aerodynamic parameters of a 45° sweptback wing and a fuselage of fineness ratio 10 with a nacelle of fineness ratio 5 at various chordwise and vertical positions.

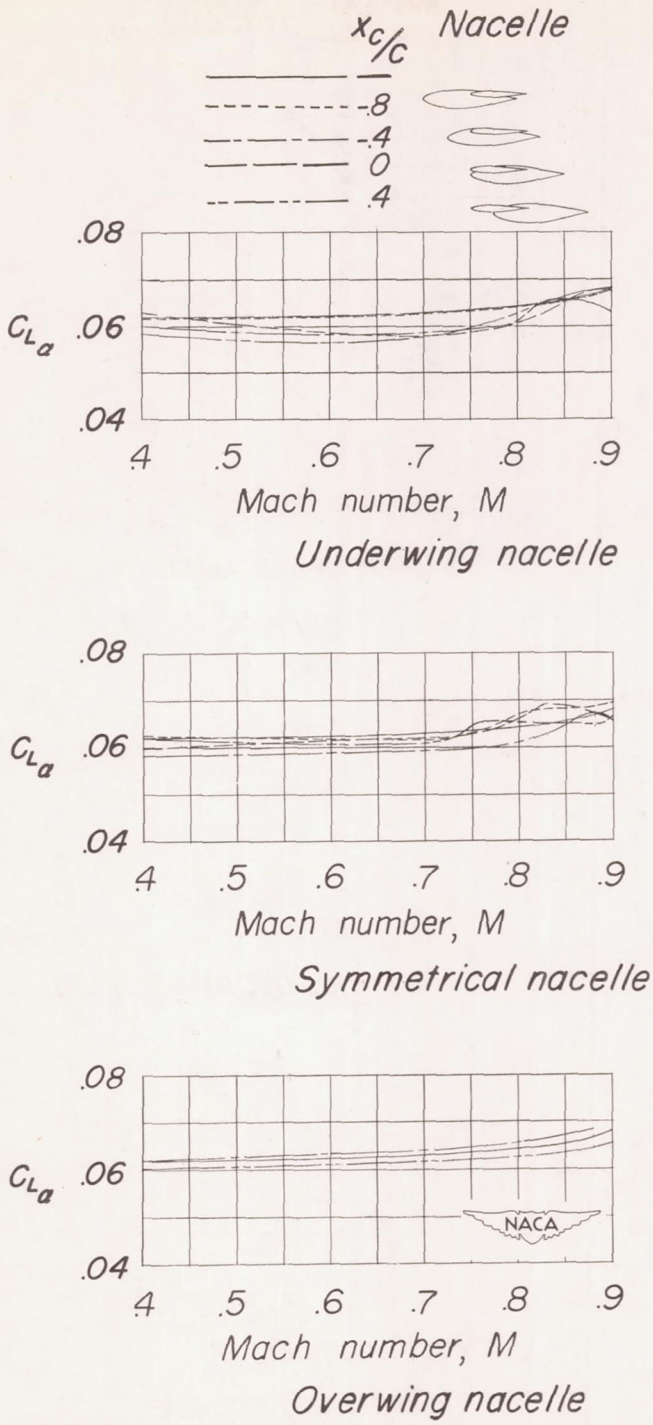

(b) Effect of nacelle location on C_{L_α}

Figure 20.- Continued.

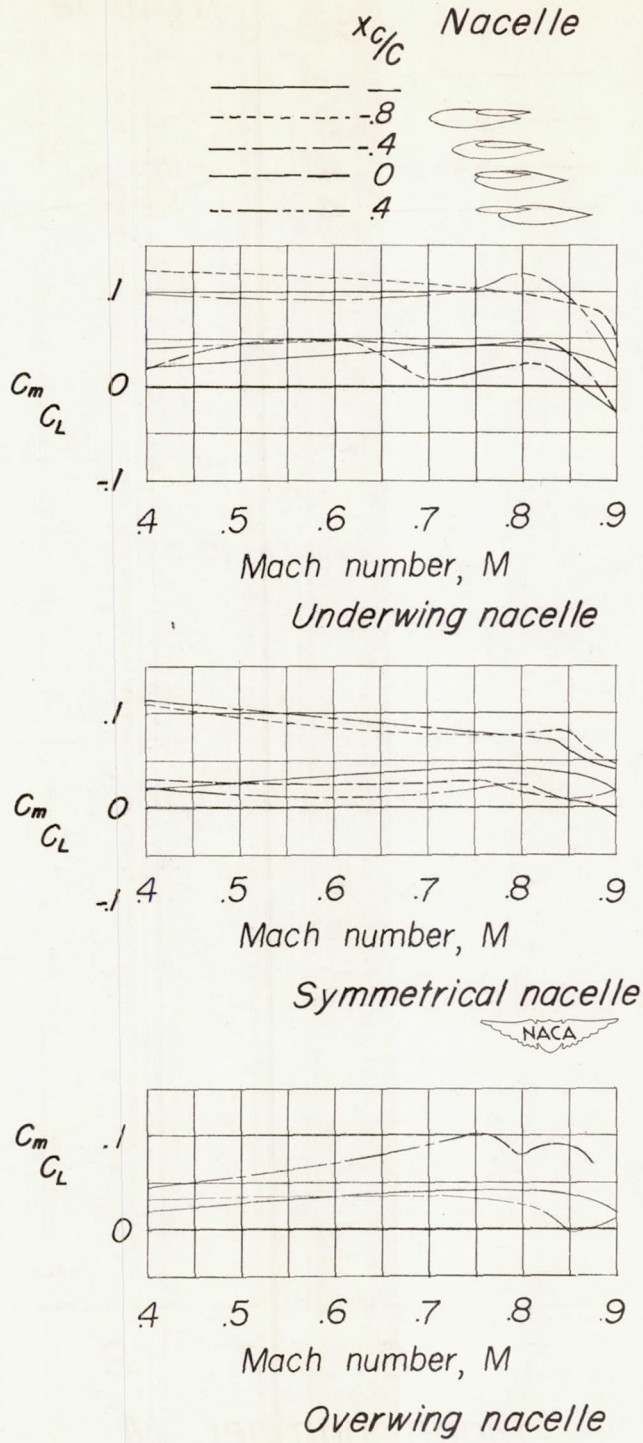

(c) Effect of nacelle location on $C_m C_L$

Figure 20.- Concluded.

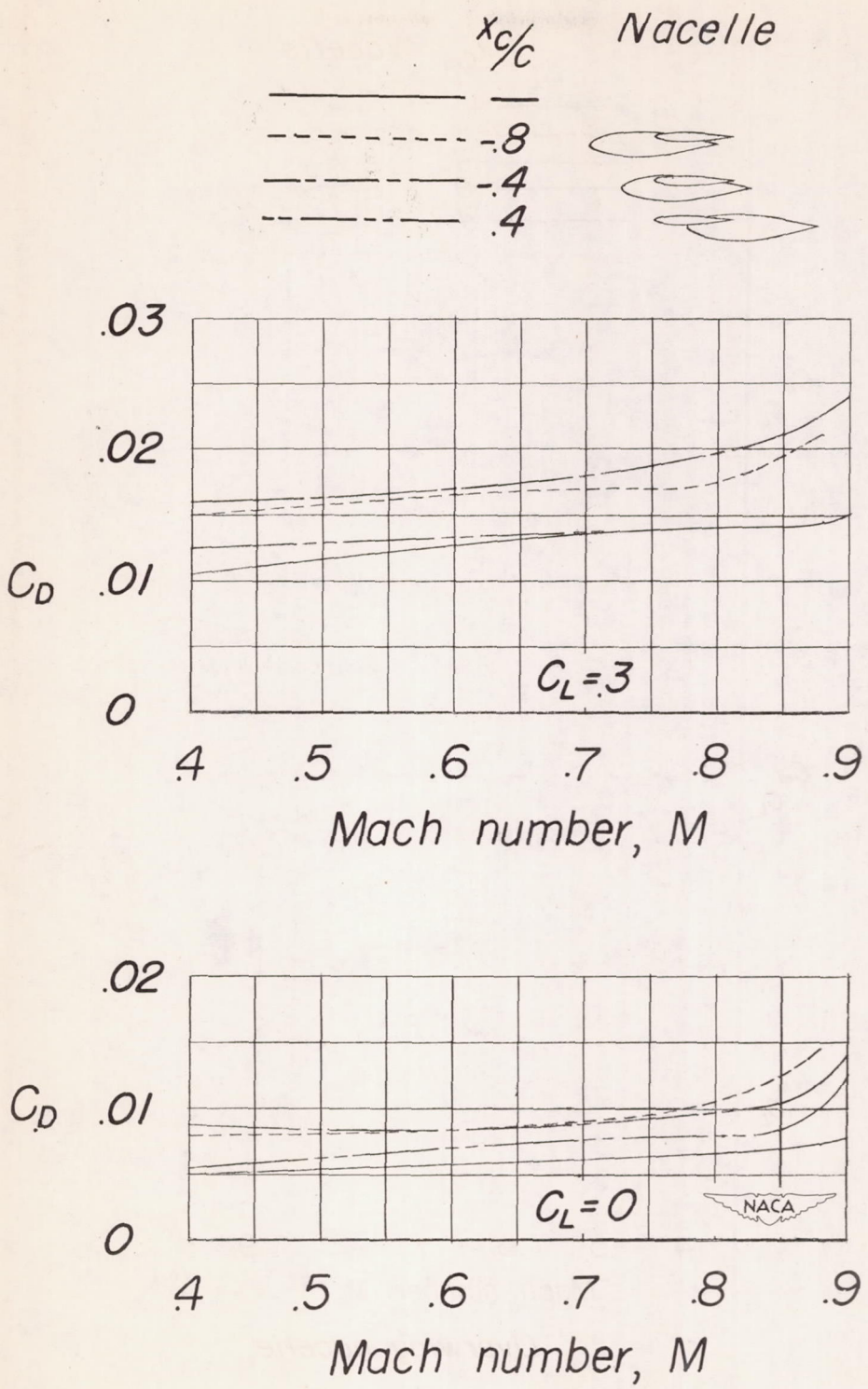

Figure 21.- Variation of drag coefficient with Mach number of a 45° swept-back wing with an underwing nacelle of fineness ratio 5 at various chordwise positions.

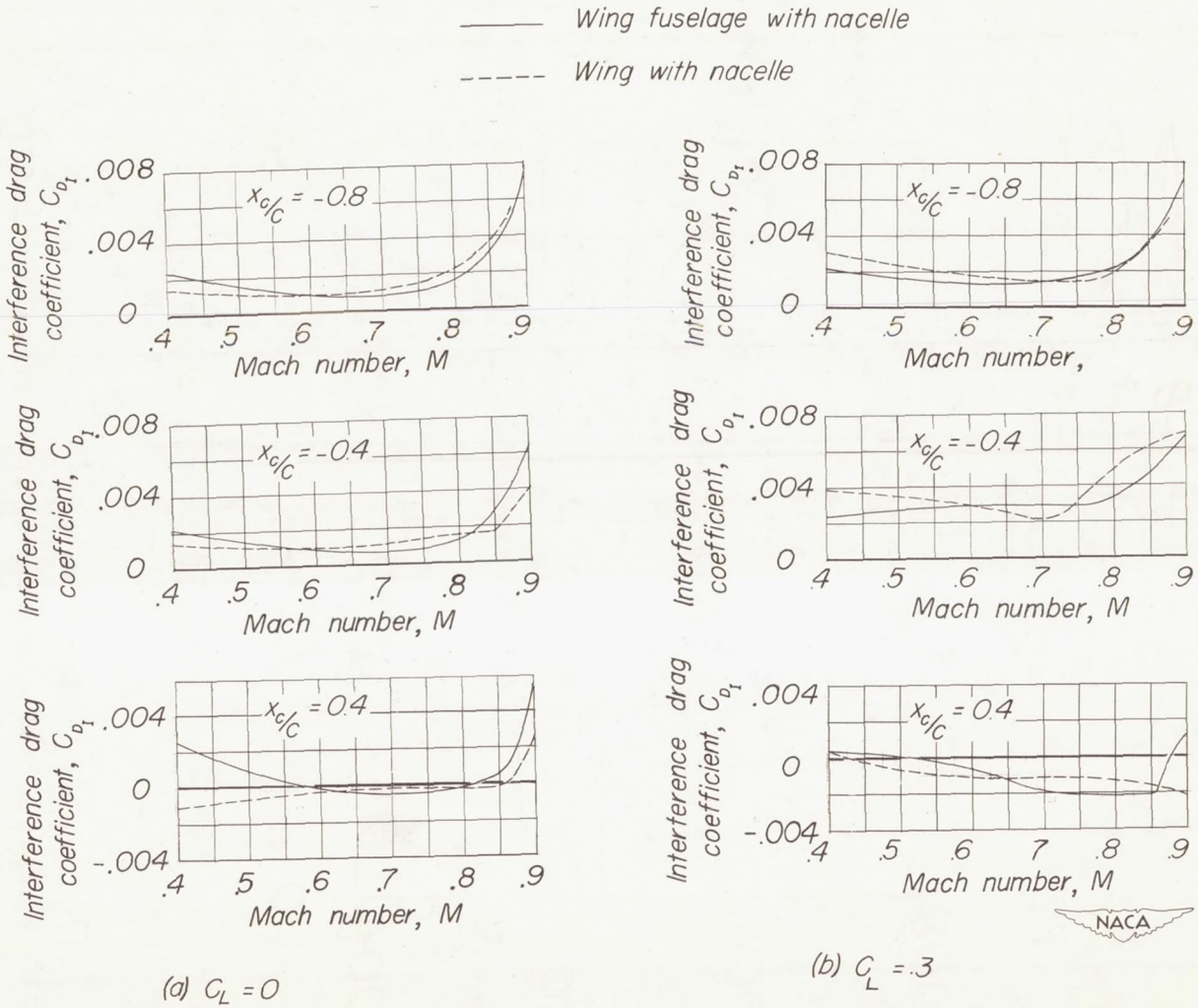

Figure 22.- Variation of interference drag coefficient with Mach number of a 45° sweptback wing with an underwing nacelle of fineness ratio 5 at various chordwise positions.

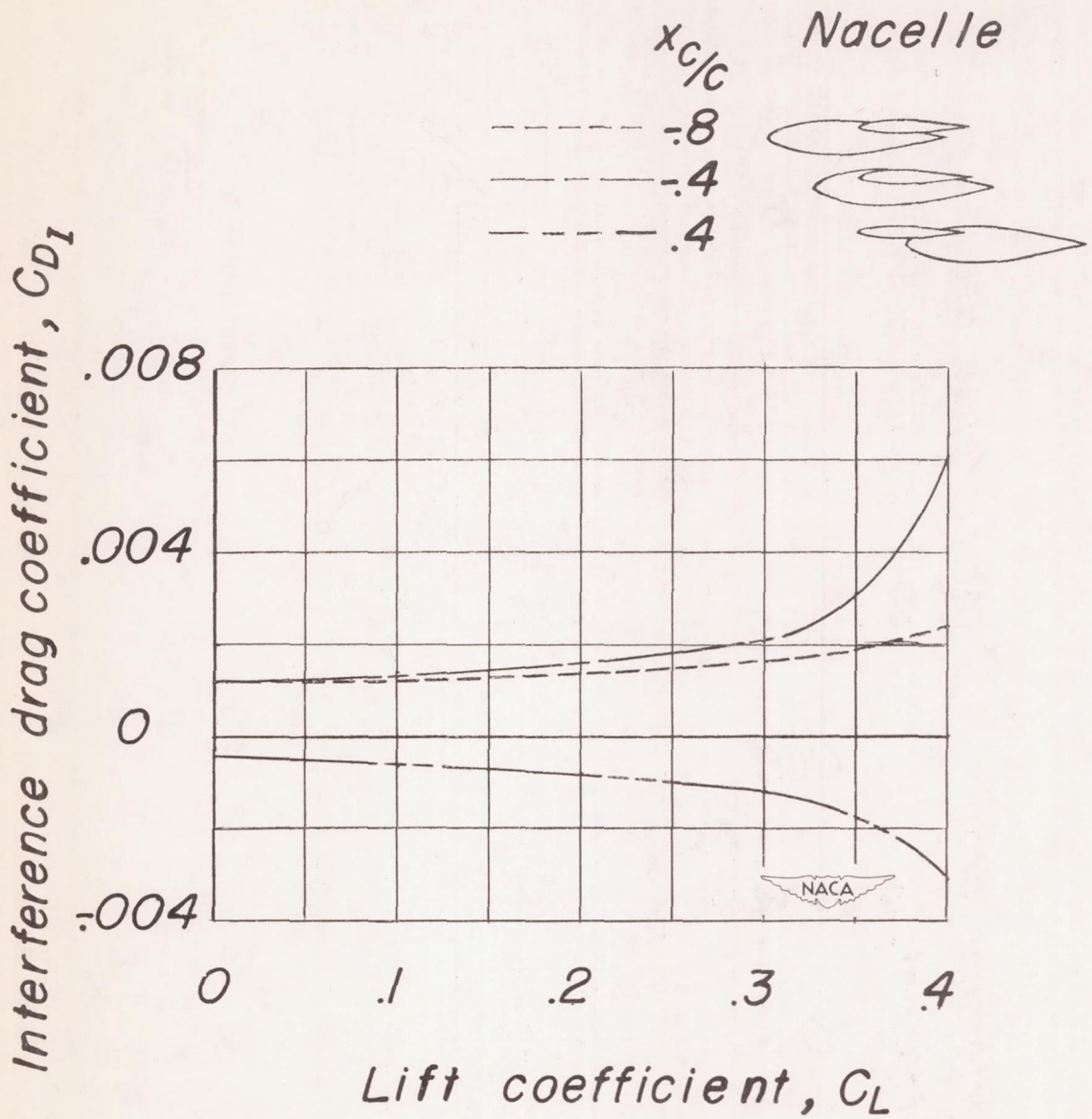

Figure 23.- Variation of interference drag coefficient with lift coefficient of a 45° sweptback wing with an underwing nacelle of fineness ratio 5 at various chordwise positions. M = 0.70.

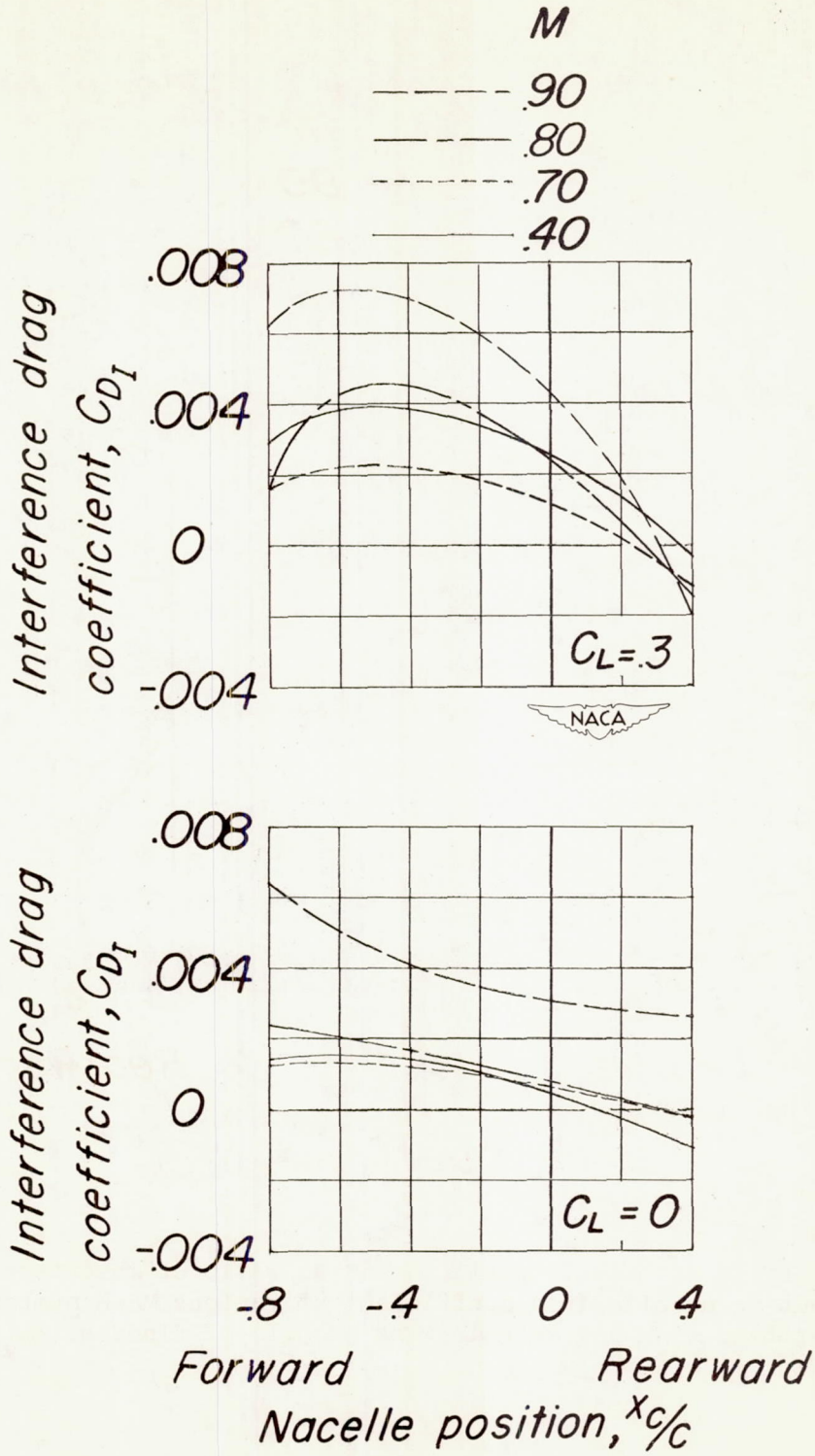

Figure 24.- Effect of nacelle position on the interference drag coefficient at various Mach numbers of a 45° sweptback wing with an underwing nacelle of fineness ratio 5.

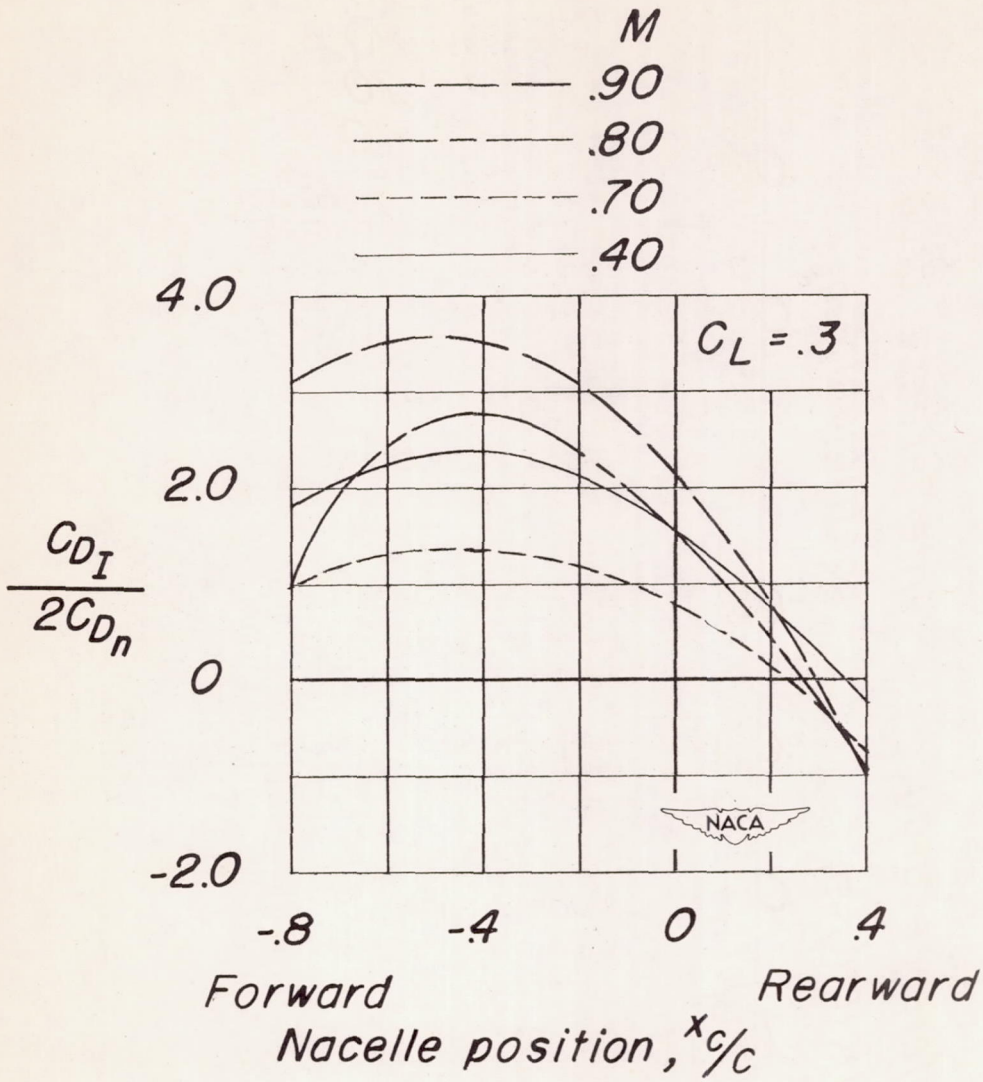

Figure 25.- Effect of nacelle position on the ratio of interference drag coefficient to nacelle drag coefficient at various Mach numbers for a 45° sweptback wing and an underwing nacelle of fineness ratio 5.

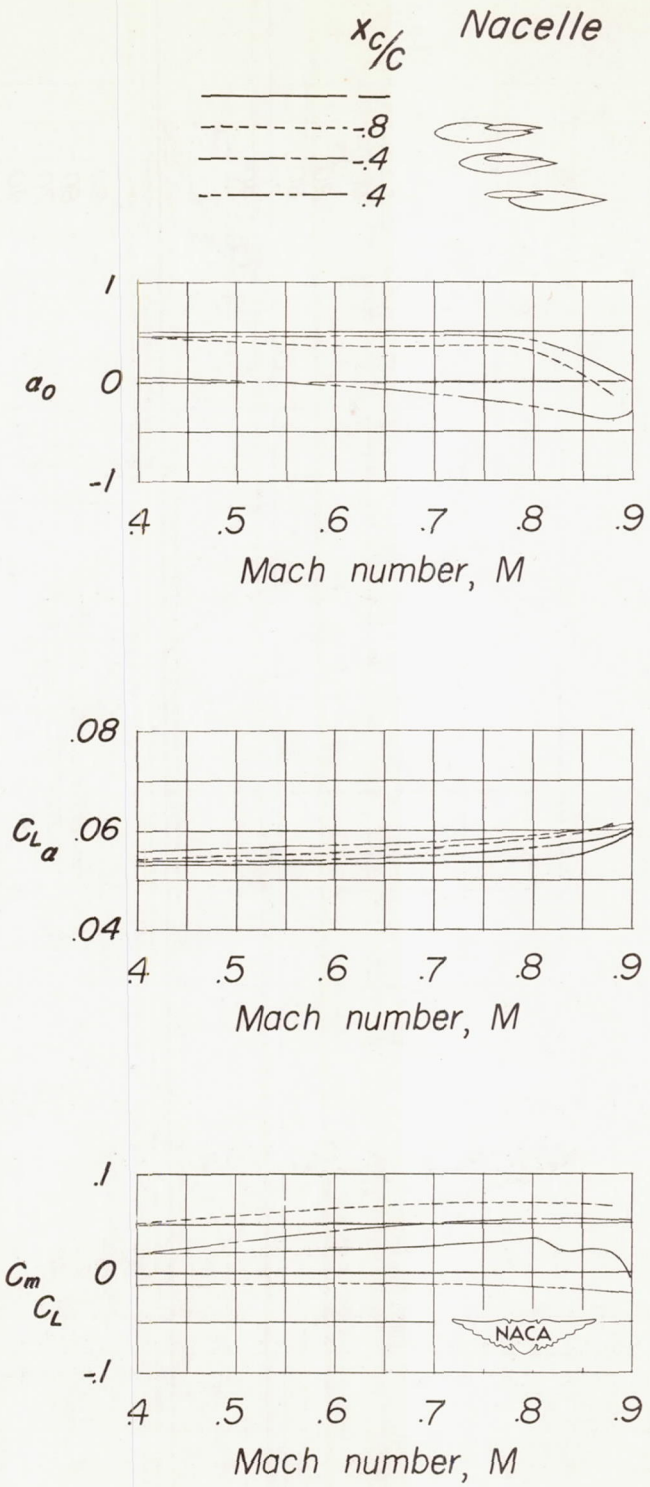

Figure 26.- Summary of aerodynamic parameters of a 45° sweptback wing with an underwing nacelle of fineness ratio 5 at various chordwise positions.

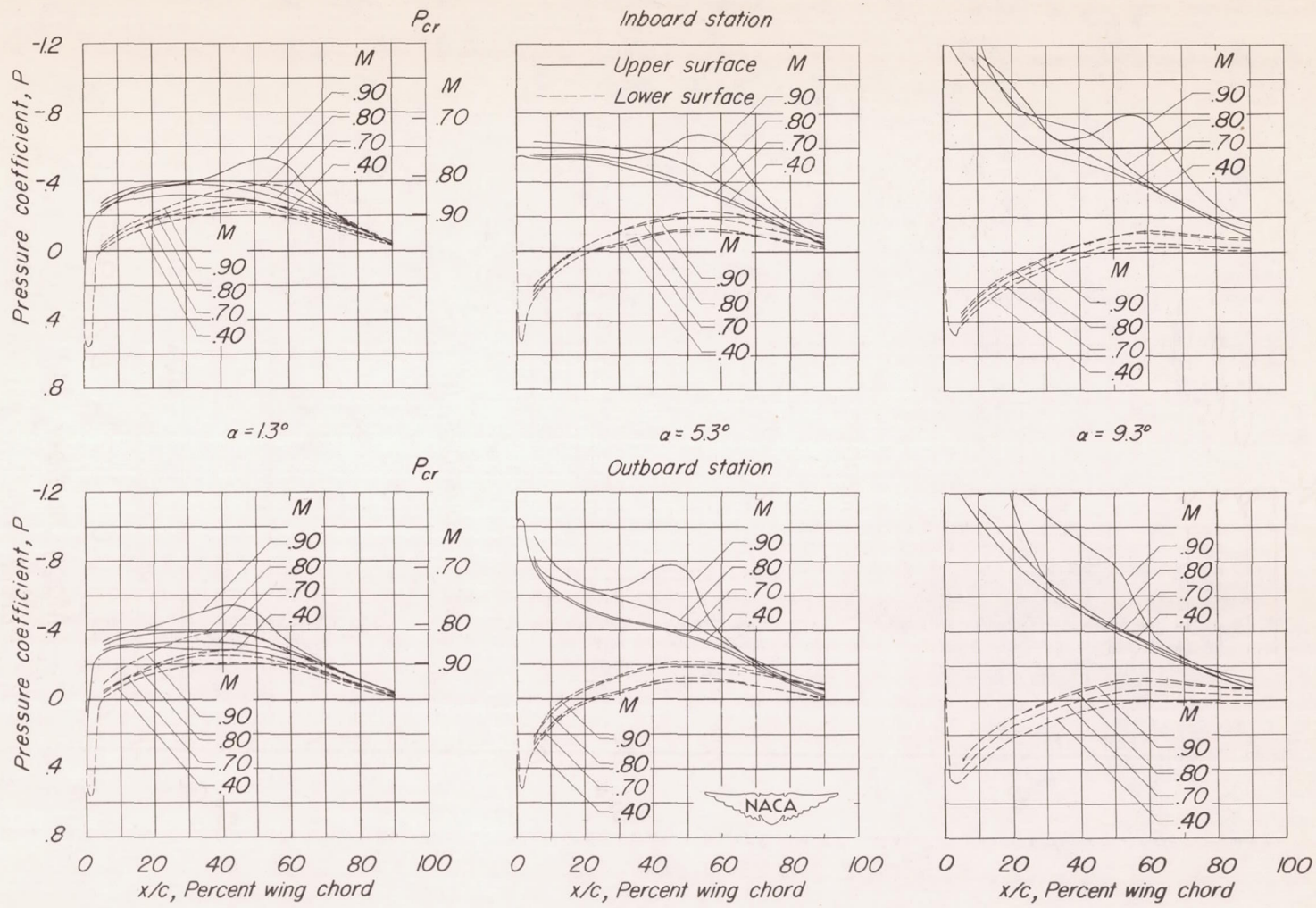

Figure 27.- Chordwise pressure distributions at two spanwise juncture stations of a 45° sweptback wing and fuselage of fineness ratio 10 for several angles of attack and Mach numbers.

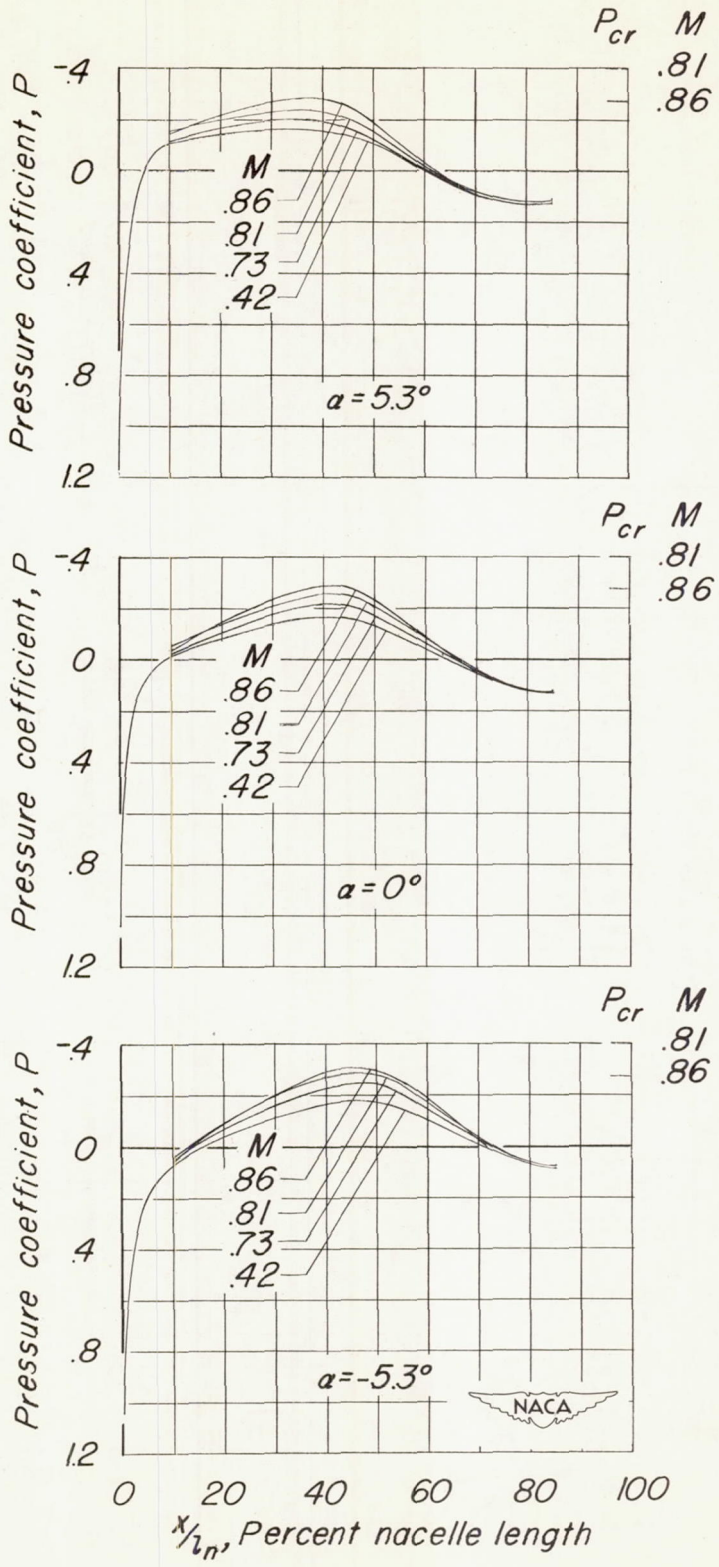

Figure 28.- Pressure distributions over a nacelle of fineness ratio 5 at several angles of attack and Mach numbers.

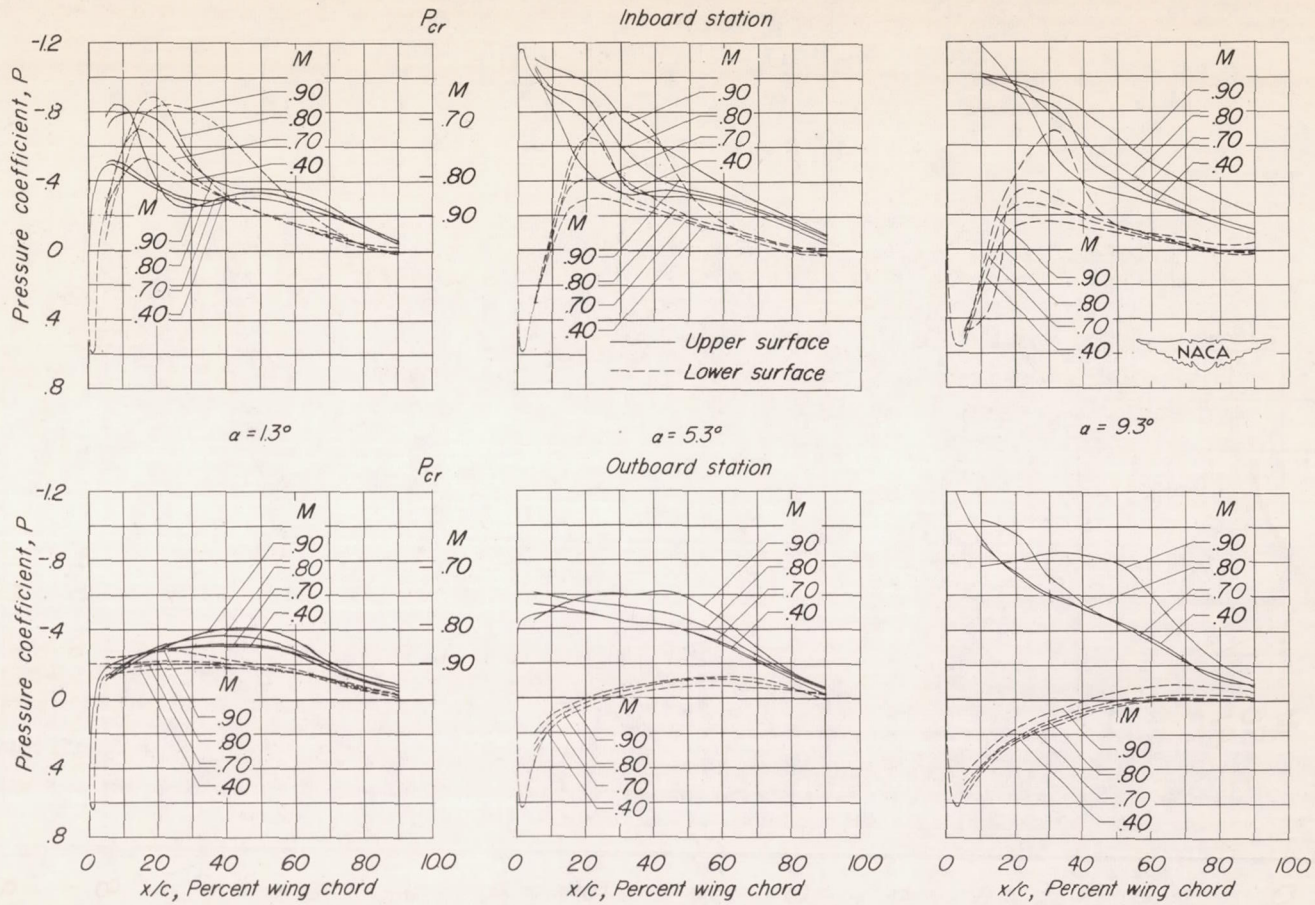

(a) $\frac{x_c}{c} = -0.8$.

Figure 29.- Chordwise pressure distribution at two spanwise juncture stations of a 45° sweptback wing and a fuselage of fineness ratio 10 with an underwing nacelle of fineness ratio 5 at several chordwise positions.

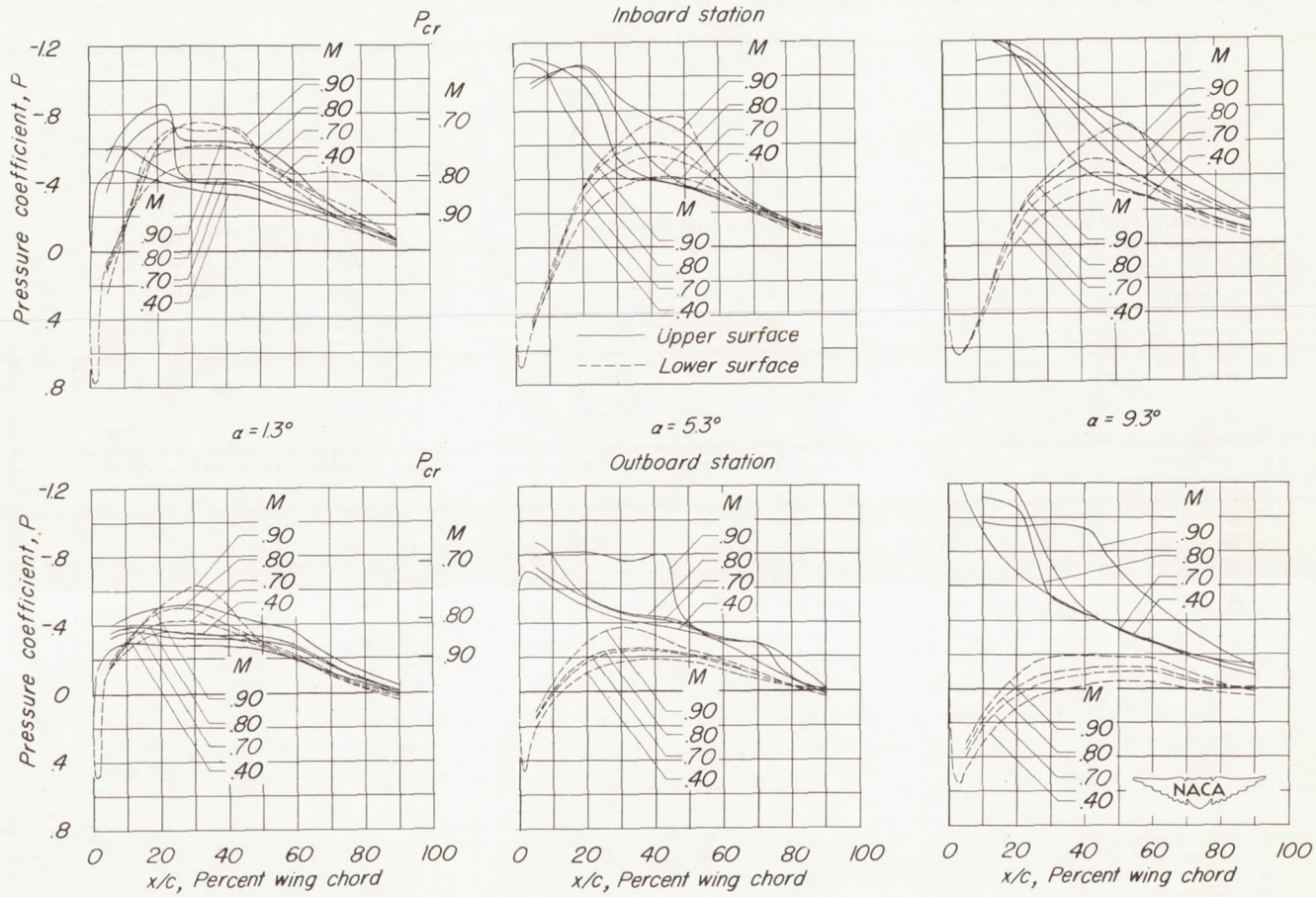

(b) $\frac{x_c}{c} = -0.4$.

Figure 29.- Continued.

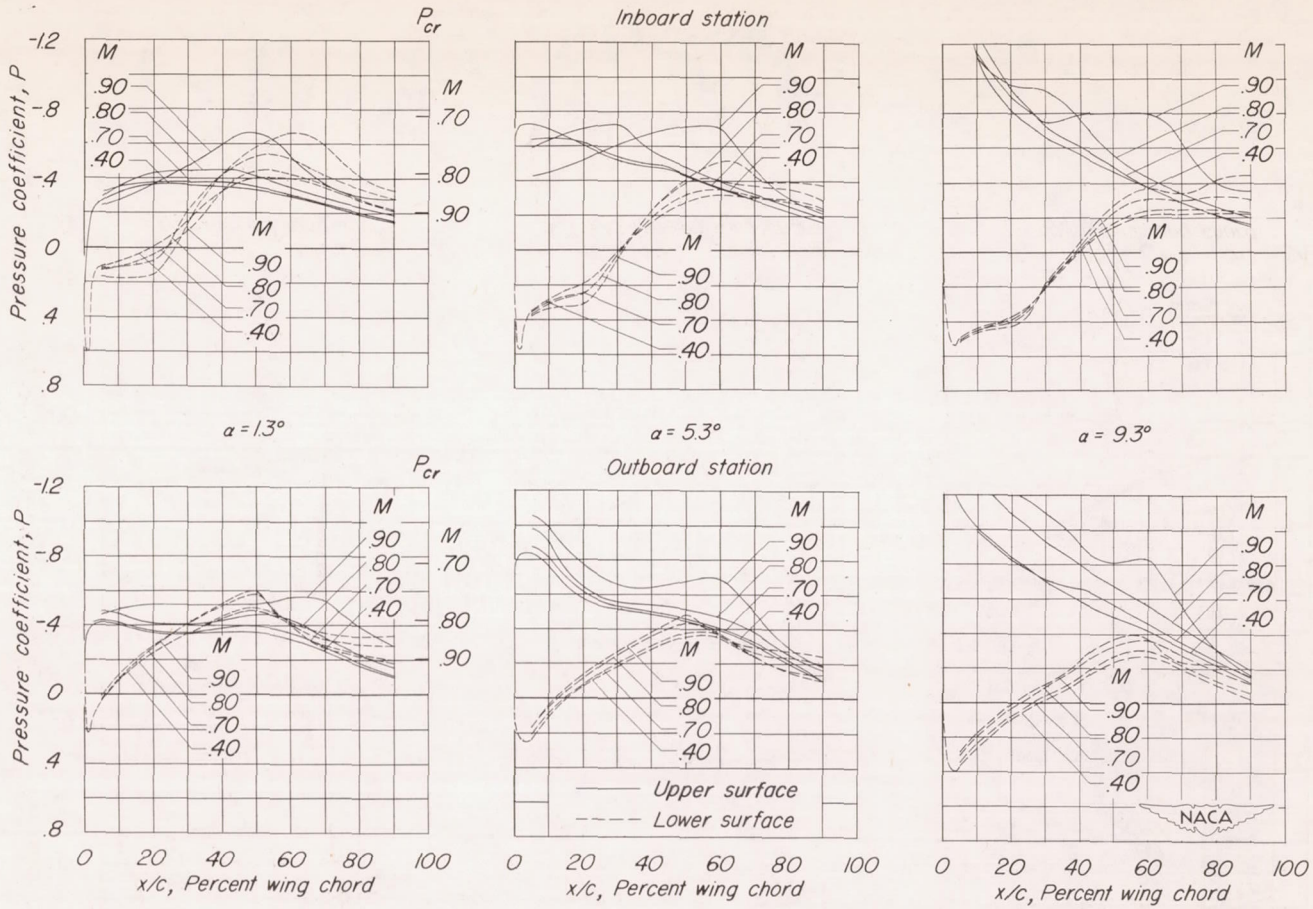

(c) $\frac{x_c}{c} = 0.$

Figure 29.- Continued.

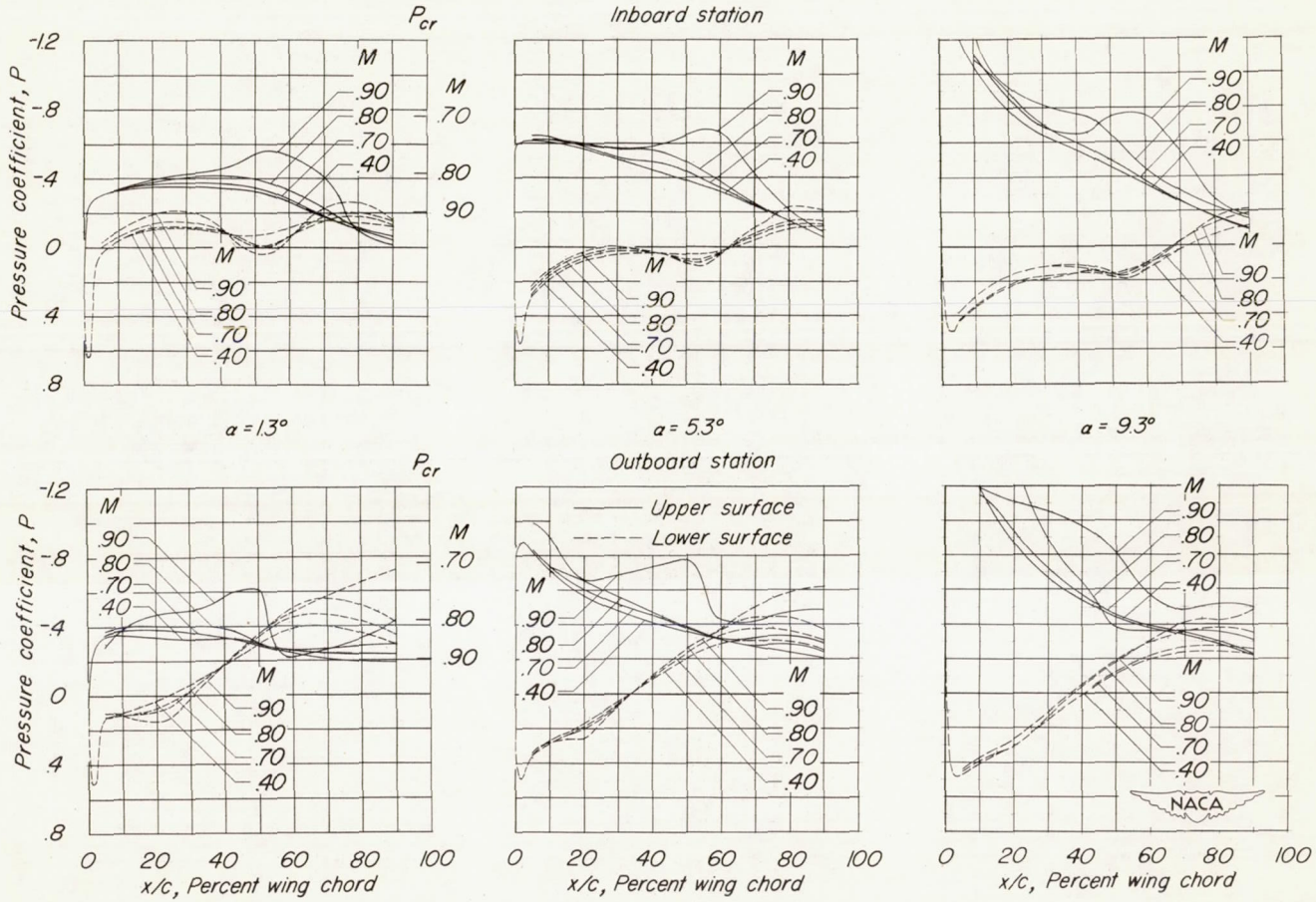

(d) $\frac{x_c}{c} = 0.4$.

Figure 29.- Concluded.

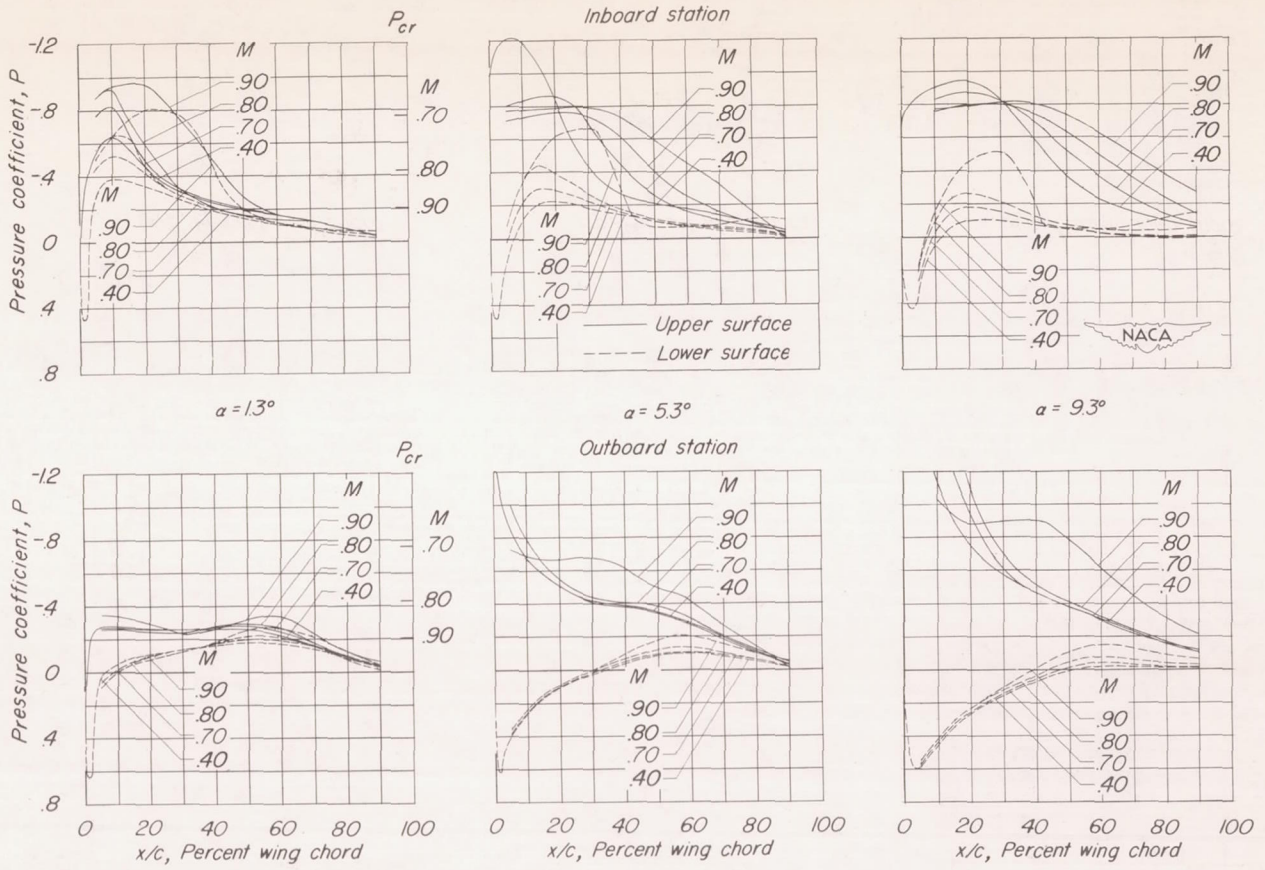

(a) $\frac{x_c}{c} = -0.8$.

Figure 30.- Chordwise pressure distribution at two spanwise juncture stations of a 45° sweptback wing and a fuselage of fineness ratio 10 with a symmetrical nacelle of fineness ratio 5 at several chordwise positions.

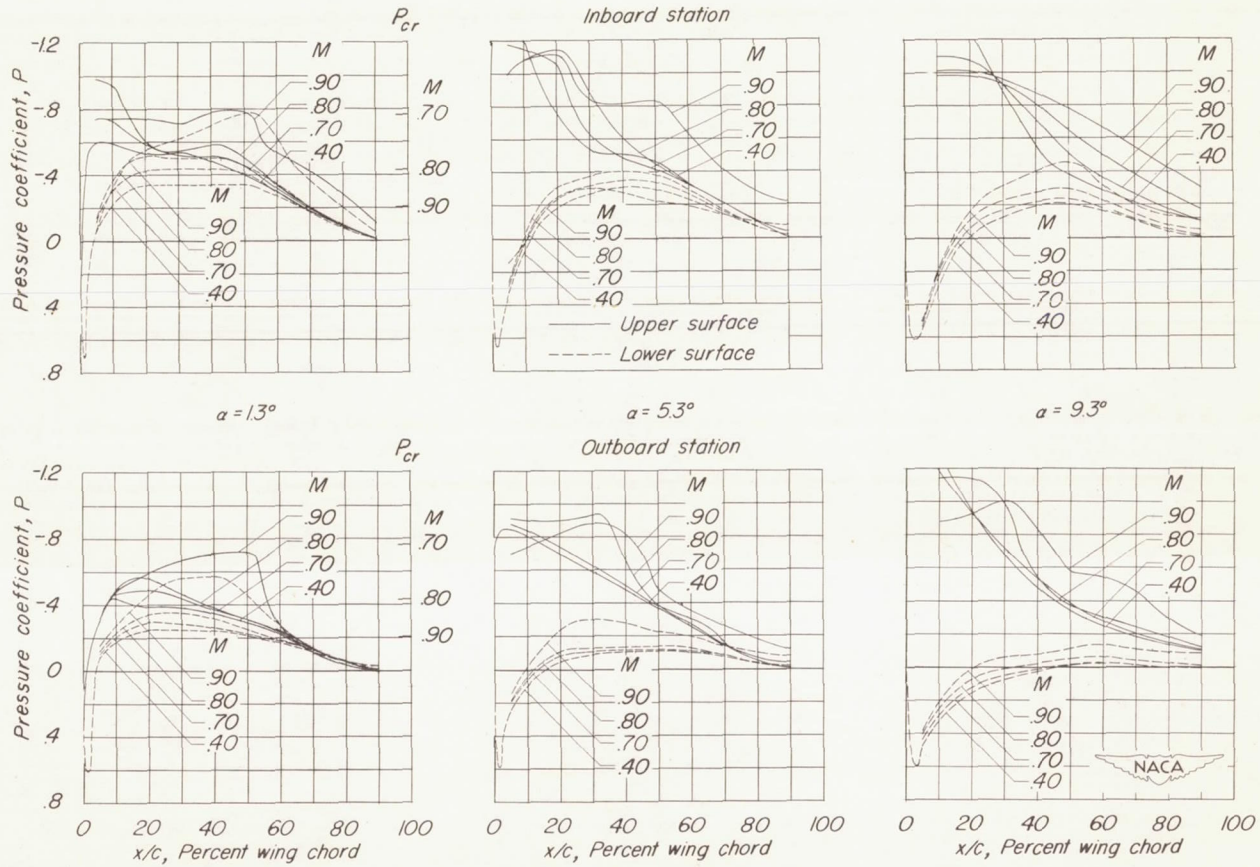

(b) $\frac{x_c}{c} = -0.4$.

Figure 30.- Continued.

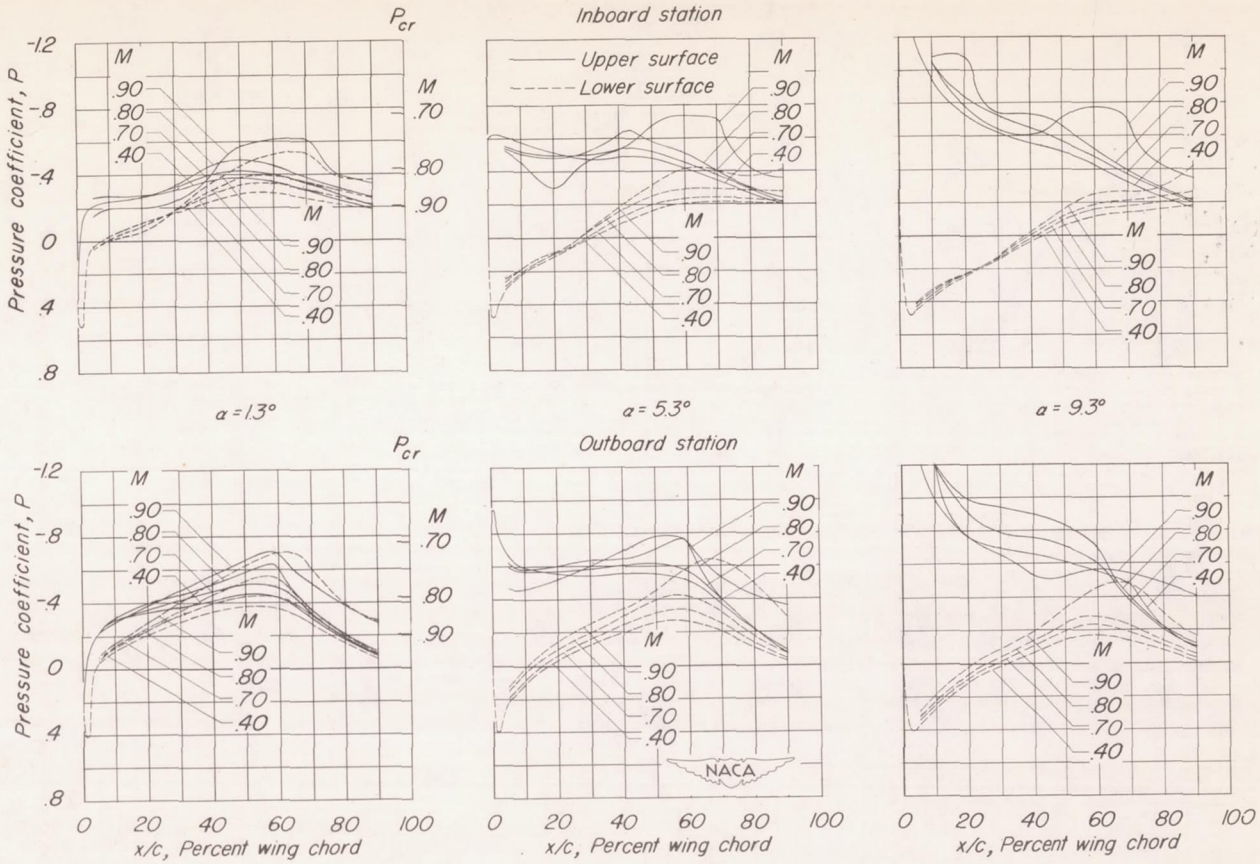

(c) $\frac{x_c}{c} = 0.$

Figure 30.- Continued.

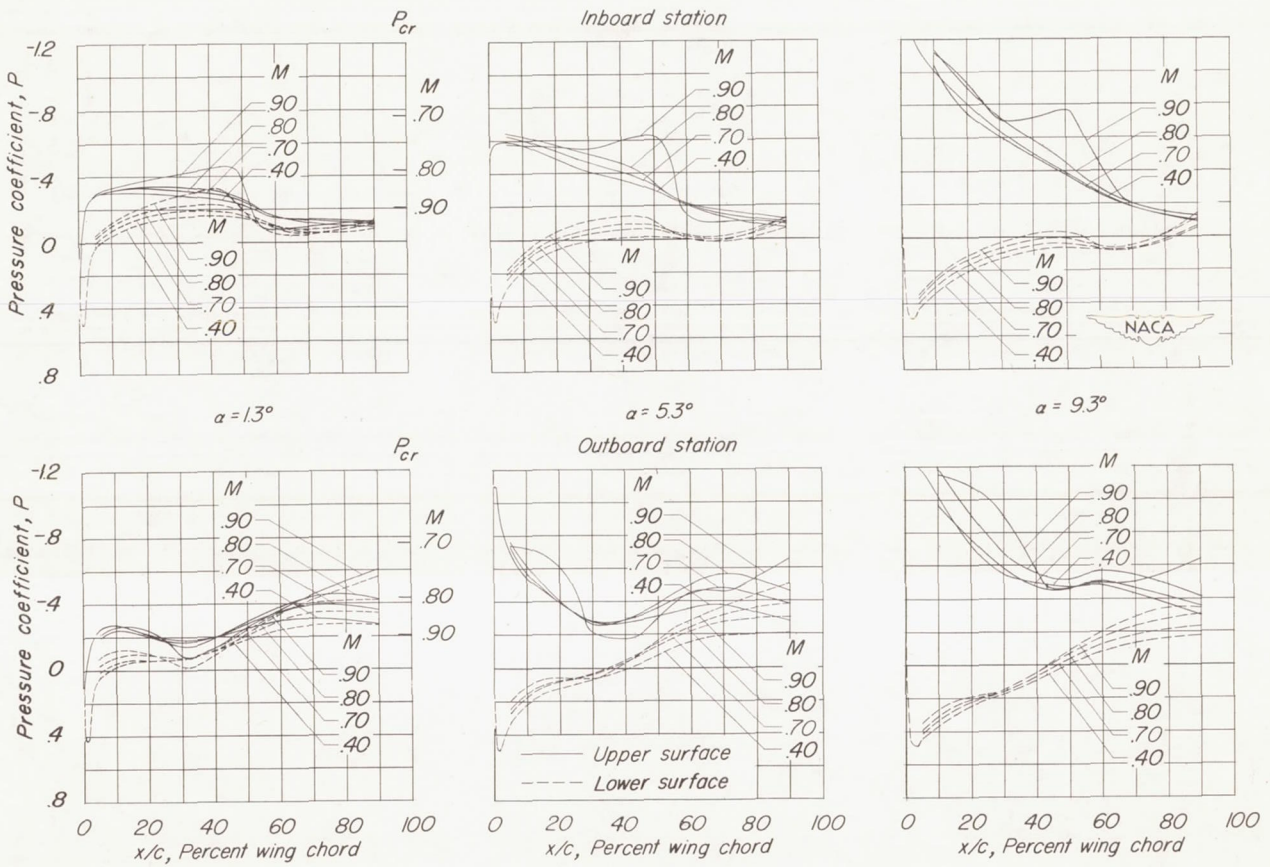

(d) $\frac{x_c}{c} = 0.4$.

Figure 30.- Concluded.

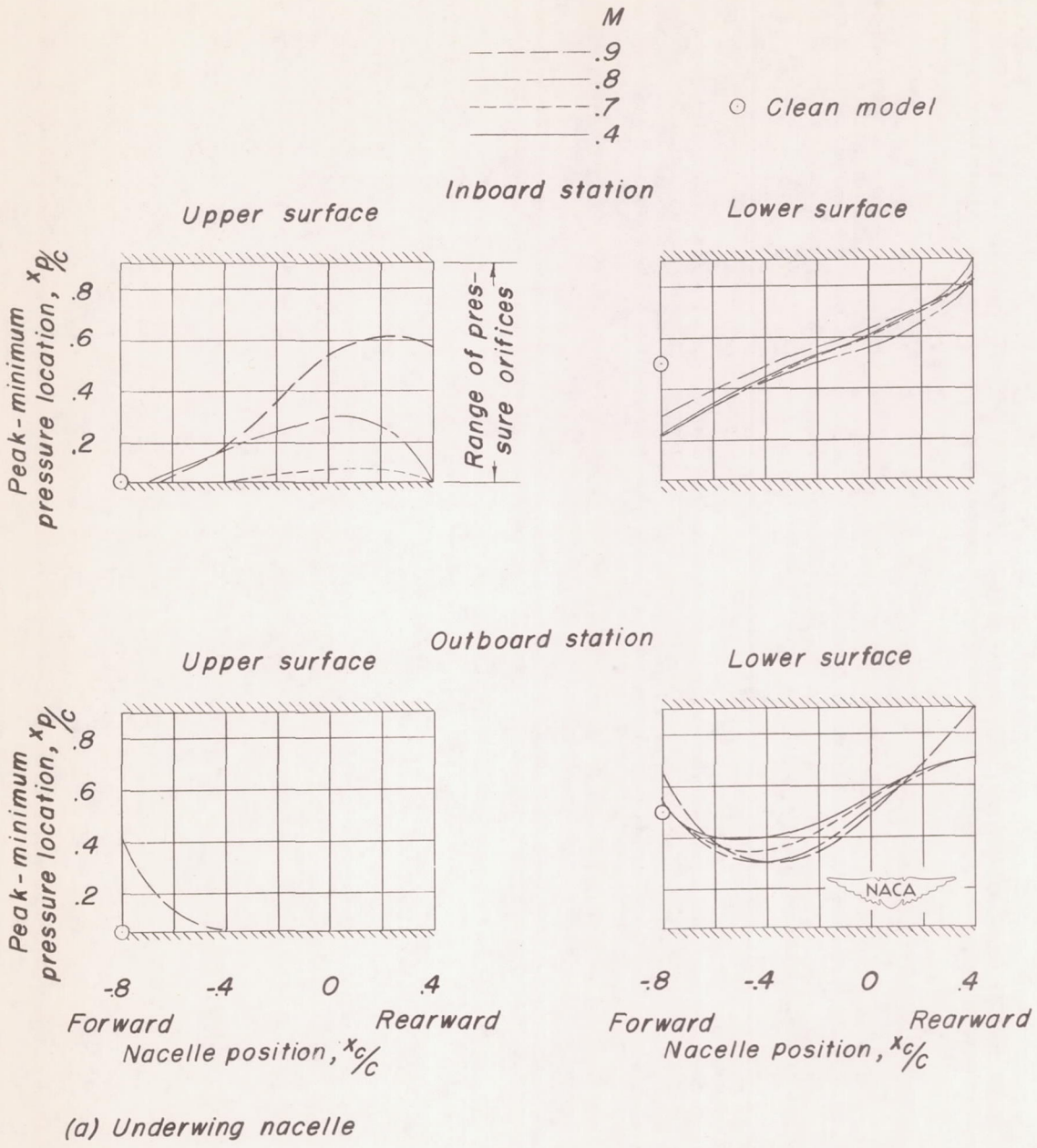

(a) Underwing nacelle

Figure 31.- Effect of nacelle position on the peak-minimum-pressure location at two spanwise juncture stations on a 45° sweptback wing and a fuselage of fineness ratio 10 with a nacelle of fineness ratio 5. $\alpha = 5.3^\circ$.

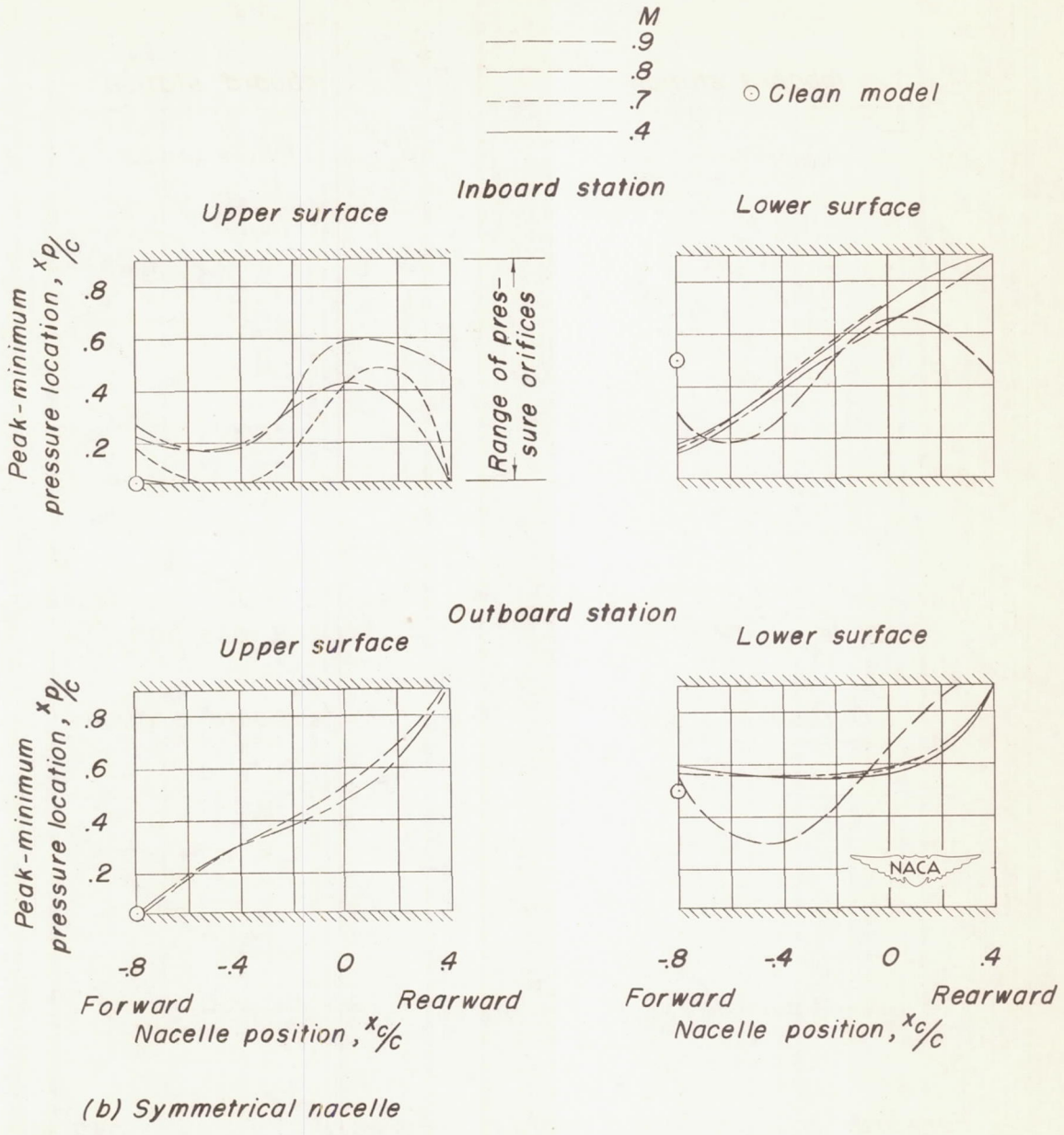

(b) Symmetrical nacelle

Figure 31.- Concluded.

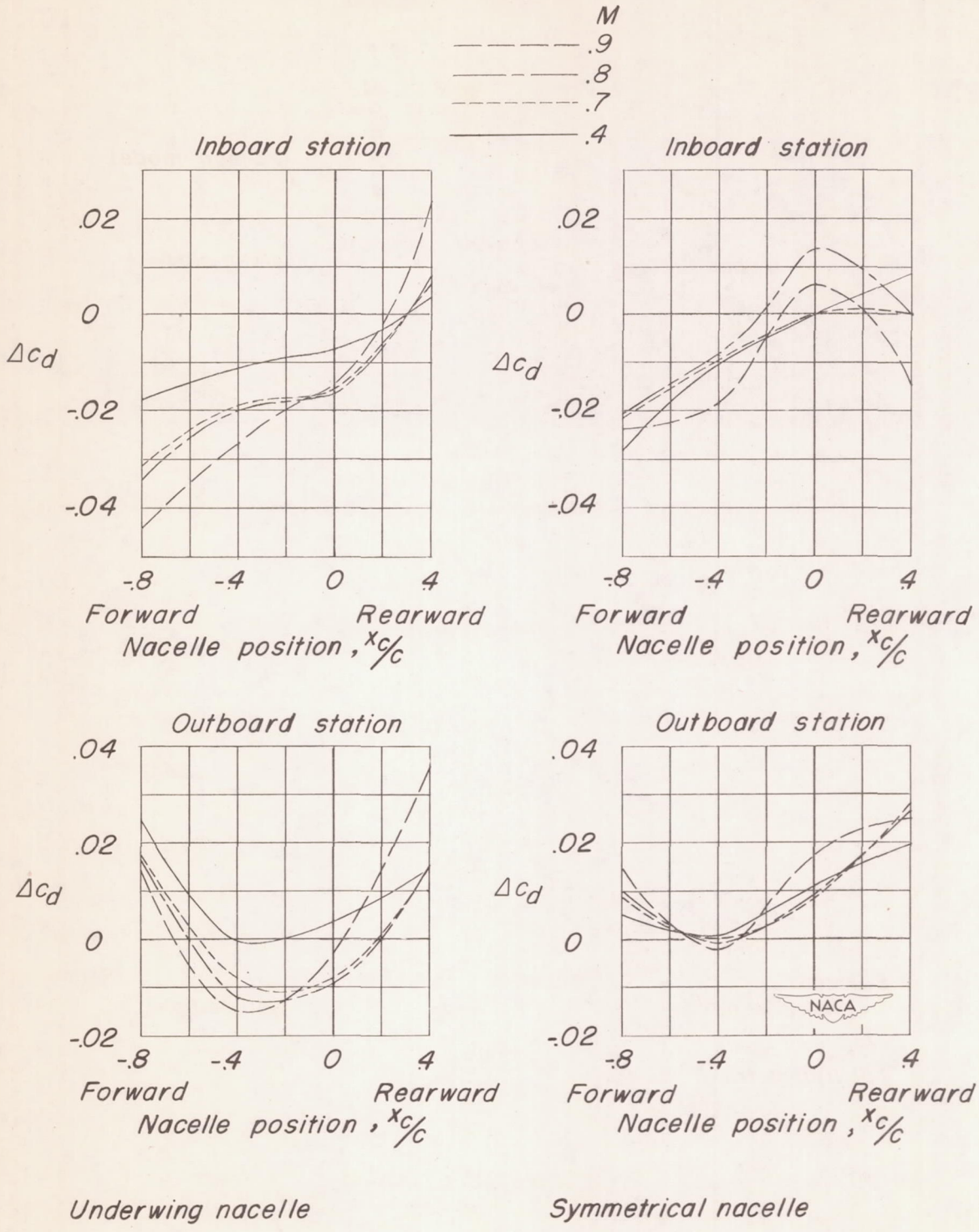

Figure 32.- Effect of nacelle position at various Mach numbers on the incremental section pressure drag coefficient due to nacelle at two spanwise juncture stations of a 45° sweptback wing and a fuselage of fineness ratio 10 with a nacelle of fineness ratio 5. $\alpha = 5.3°$.